



EXPANDING SENSORIMOTOR CAPABILITIES OF HUMANOID ROBOTS THROUGH MULTISENSORY INTEGRATION:

*A STUDY ON THE IMPLEMENTATION OF
PERIPERSONAL SPACE ON THE ICUB*

Alessandro Roncone

Thesis submitted in partial fulfillment
of the requirements for the degree of
DOCTOR OF PHILOSOPHY

iCub Facility– Istituto Italiano di Tecnologia

Università degli studi di Genova

April 2015

Alessandro Roncone: *Expanding sensorimotor capabilities of humanoid robots through multisensory integration;* A study on the implementation of peripersonal space on the iCub.

DOCTORAL SCHOOL:
Life and Humanoid Technologies (xxvii cycle)

DOCTORAL COURSE:
Robotics, Cognition and Interaction Technologies

SUPERVISORS:
Giorgio Metta
Luciano Fadiga
Ugo Pattacini
Matej Hoffmann

LOCATION:
Genova

TIME FRAME:
April 2015

Dedicated to the loving memory of *Luigi Carli*.

1930-2012

DECLARATION

This work has been carried out by Alessandro Roncone during his Ph.D. course in *Robotics, Cognition And Interaction Technologies*, from January 2012 to February 2015 at the Italian Institute of Technology, Genova, Italy. He was under the joint supervision of Prof. Giorgio Metta and Prof. Luciano Fadiga, and the additional supervision of Dr. Ugo Pattacini and Dr. Matej Hoffmann. The work has been fulfilled initially at the *Robotics, Brain and Cognitive Sciences Department*, directed by Prof. Giulio Sandini, and subsequently at the *iCub Facility*, directed by Prof. Giorgio Metta. His Ph.D. has been financially supported by the Italian Ministry of Education, University and Research (MIUR), the Fondazione Istituto Italiano di Tecnologia (IIT), and the European FP7 ICT project No. 270273 (Xperience).

Genova, April 2015

Alessandro Roncone,

April 9, 2015

ABSTRACT

The new generation of robotic devices will require machines able to adequately perform rich interactions with objects – and eventually humans – in their environment. This aspect will prove fundamental in the context of moving robots from the controlled domains typical of a factory environment toward our – much less structured – everyday life. To this end, robots need the ability to express some sort of awareness of their body and their surroundings: instead of focusing exclusively on the end-effector as the only part that interacts with the environment, the robotic field needs to move toward a more distributed, decentralized representation of the self and the nearby space. More importantly, albeit a consistently improving technology, robotic systems are equipped with inherently faulty systems characterized by calibration and systematic errors that need to be effectively coped with.

This thesis deals with the formalization and the development of a system able to let a humanoid robot learn a multisensory representation of the space around its body (or peripersonal space). The robot is equipped with a whole-body artificial skin and learns the consequences of its interaction with the self and the environment by means of a multisensory (tactile-motor and tactile-visual) representation. This results in the extension of the robot's tactile domain toward the nearby space, in such a way that it lets the robot to implicitly cope with modeling or calibration errors. Further, this representation is put under testing with a sensory-based guidance of the motor actions performed by the robot: that is, an avoidance and catching controller capable of using any body part in order to either prevent collision with or come into contact with incoming objects.

PUBLICATIONS

This work has been carried out during my Ph.D. course in *Robotics, Cognition and Interaction Technologies*, from January 2012 to February 2015. This three-year project resulted in the following publications (at the time of writing):

- Alessandro Roncone, Matej Hoffmann, Ugo Pattacini, Luciano Fadiga, and Giorgio Metta. Peripersonal space and margin of safety around the body: learning tactile-visual associations in a humanoid robot with artificial skin. Manuscript, 2015
- Alessandro Roncone, Matej Hoffmann, Ugo Pattacini, and Giorgio Metta. Learning peripersonal space representation through artificial skin for avoidance and reaching with whole body surface. Submitted to the 2015 IEEE/RSJ International Conference on Intelligent Robots and Systems (IROS), 2015
- Alessandro Roncone, Matej Hoffmann, Ugo Pattacini, and Giorgio Metta. Automatic kinematic chain calibration using artificial skin: self-touch in the iCub humanoid robot. In *Proc. IEEE Int. Conf. Robotics and Automation (ICRA)*, pages 2305–2312, 2014
- Matej Hoffmann, Alessandro Roncone, and Giorgio Metta. Modeling the development of human body representations. Submitted to the SMLC '13 Workshop on Synthetic Modeling of Life and Cognition: Open questions, 2013

This thesis will provide a structured discussion on top of these aforementioned papers, by providing a better understanding of the overall contribution of this Ph.D. project. As such, some ideas and figures have already appeared in those publications.

Some other publications that have not been included in this thesis are instead listed below:

- Alessandro Roncone, Ugo Pattacini, Giorgio Metta, and Lorenzo Natale. Gaze stabilization for humanoid robots: a comprehensive framework. In *2014 IEEE-RAS Int. Conf. on Humanoid Robots - HUMANOIDS '14*, 2014
- Sean Ryan Fanello, Ugo Pattacini, Ilaria Gori, Vadim Tikhanoff, Marco Randazzo, Alessandro Roncone, Francesca Odone, and

Giorgio Metta. 3D stereo estimation and fully automated learning of eye-hand coordination in humanoid robots. In *2014 IEEE-RAS Int. Conf. on Humanoid Robots - HUMANOIDS '14*, 2014

ACKNOWLEDGEMENTS

You will never walk alone.

— Rodgers and Hammerstein [70]

*I'm not strange, weird, off, nor crazy,
my reality is just different from yours.*

— Charles L. Dodgson [8]

There are a lot of people without which I would not be here. They made me what I am now, whatever that means. They are countless, and I will forget some of them on my way down the list, but nonetheless I'll do my best.

First of all, I would like to thank my supervisor Giorgio Metta. He was a great mentor (despite his superhuman schedules and the difficulties I had to cope with them), and gave me the opportunity to professionally grow up to the point in which I can call myself a robotic engineer. More importantly, this growth would not have even been put in place without two of my colleagues (and friends), Ugo Pattacini and Matej Hoffmann, who tutored me during these years. They have different background and expertise, and they both contributed in different ways to my growth. Ugo taught me the beauty of engineering. As only a senior engineer is capable of, he looks at any problem with pragmatism and says, *"I don't know exactly what the problem is, but I know where to look to understand it"*, and begins to dig into the data. He indoctrinated me into how to carry out a well-executed engineering project with an eye to clean, scalable code deployment and making things – really – work. On the other side, Matej is the type of researcher the academic community would need more. His deep knowledge of the field, his strong motivation as well as his sense of inquisitiveness have without any doubt helped me in directing my research towards what was most interesting to me, and pursuing my goals despite the obstacles I found down the path. I truly think that they both gifted me with a set of invaluable tools that I will bring with me for the years to come. The three of us form a team I'm really proud of.

The friends I've made over the time in IIT contributed to create the welcoming workplace I still love to go to every single day. Thanks to

Carlo, Randaz, Vadim, Luca, Ali for having answered my many questions and contributed in different parts to my work. Thanks to Fra, Silvio and Cammo for having patiently tolerated my morning enthusiasm and endless talking at 8am during our trips to work. Thanks to Castina and Sara for the countless number of lunches and jokes we shared together. Thanks to Andre, Ila and Sean that left the lab early on but were the best desk mates I will ever have. You all became true friends with which I shared a lot of quality time during these years.

Incredibly, during these years I even managed to keep a seemingly normal social life outside the lab. Mari, Olli, Jo, Daddy, Matte, Raffy, Teku, Giachi are the friends I've grown up with and that "dealt" with me every single day in the past 15 years. They know me better than anyone else, and I will always come back home to hang out with them whenever I have time. Some new friends joined this list as well. In particular, Ale and Jorh are the two outsiders worth mentioning: despite our different backgrounds, we share so many things in common that it seems we know each others since decades; they're the ones I will keep loving to hang out with wherever they (and I) will end up living. Massi and Ele have been my family for the two years I lived alongside with them, and that will be a period of my life I will never forget.

Finally, I will try to not degrade this document with that kind of overemotional sentences that are not suited for a Ph.D. thesis, but the biggest thank goes to you, Giorgia. I will carefully measure my words here, but still, I would like to underline how much you have been important to me – and to my project – during these years. You have been my past, you are my present, and I'm looking forward to a future with you.

In conclusion, I would like to thank the following "entities" that supported me during these years, and without which I could not be here: (i) my lovely dog *Pepe*, for relentlessly being at my side since her birth; (ii) my beloved old laptop, that died in a car accident without even a name (for the record, no any other object was injured); (iii) my new, blazingly fast, and shockingly slim ultrabook – called *Boris the blade*¹ – that let me write this thesis as well as implement ~ 40% of the work presented in it; (iv) the two pairs of running shoes I overused during these three years, without which I wouldn't be able to release the physical and mental pressure a Ph.D. comes with; (v) my body, that let me release the aforementioned pressure by running thousands of kilometers with only minor hitches.

I would also undermine the seriousness of this document by declaring that in this thesis there is one, single, adorable *easter egg*. If you

¹ Any resemblance to the character present in *The Snatch* movie is purely coincidental.

find it, feel free to contact me: I will be glad to offer you a beer. As a disclaimer, it is far from being difficult to find – it's rather an excuse to drink some beer. Thus, start reading and good luck!

CONTENTS

| | | |
|----------|--|-----------|
| 1 | INTRODUCTION | 1 |
| 1.1 | Motivations: toward a new generation of internal models for robotics | 1 |
| 1.2 | Contribution and outline | 3 |
| 2 | THE PERIPERSONAL SPACE | 5 |
| 2.1 | PeriPersonal Space in humans and animals | 5 |
| 2.2 | PeriPersonal Space in robotics | 7 |
| 2.2.1 | The iCub Humanoid Robot as a platform for developing peripersonal space and mar- gin of safety representations | 9 |
| 3 | THE ICUB HUMANOID ROBOT (AND SOME OF ITS KEY COMPONENTS) | 10 |
| 3.1 | Hardware | 10 |
| 3.1.1 | Arms and Hands | 10 |
| 3.1.2 | Joint angle sensing | 12 |
| 3.1.3 | Artificial Skin | 12 |
| 3.1.4 | Head and eyes | 13 |
| 3.2 | Software | 14 |
| 3.2.1 | YARP | 14 |
| 3.2.2 | Kinematic Model and coordinate transfor- mations | 14 |
| 3.2.3 | Visual Processing | 14 |
| 3.2.4 | Cartesian Control for arms and gaze | 16 |
| I | THE PERIPERSONAL SPACE ON THE ICUB | 17 |
| 4 | PROPOSED APPROACH: MILESTONES FOR THE DE- VELOPMENT OF PERIPERSONAL SPACE IN HUMANS AND ROBOTS | 18 |
| 4.1 | Basic behaviors that lead to the development of higher level multimodal associations | 19 |
| 4.1.1 | Motor-proprioceptive associations: the spi- nalized frog's wiping reflex | 19 |
| 4.1.2 | The self-touch in the early infancy | 20 |
| 4.2 | Milestones for the development of PPS in humans | 21 |
| 4.2.1 | "Bare" or "Blind" double touch | 22 |
| 4.2.2 | Invariance with respect to the configura- tion of the passive arm | 22 |
| 4.2.3 | Double touch with vision | 22 |
| 4.2.4 | Invariance with respect to the configura- tion of the passive arm | 23 |

| | | |
|-----------|--|-----------|
| 4.2.5 | Invariance with respect to the configuration of the head plant | 23 |
| 4.2.6 | From the self to the external world: adaptation of the model to external stimuli in order to create a margin of safety around the body | 23 |
| 4.2.7 | Exploitation of the learned associations: avoidance behaviors | 24 |
| 4.2.8 | Exploitation of the learned associations: reaching / catching behaviors | 24 |
| 4.3 | Milestones for the development of PPS in robots | 24 |
| 4.3.1 | “Bare” or “Blind” double touch + invariance with respect to the configuration of the passive arm | 26 |
| 4.3.2 | Double touch with vision + invariance with respect to the configuration of the passive arm and the head plant | 28 |
| 4.3.3 | From the self to the external world: adaptation of the model to external stimuli in order to create a margin of safety around the body | 29 |
| 4.3.4 | Exploitation of the learned associations: avoidance and catching behaviors | 29 |
| II | THE DOUBLE TOUCH PARADIGM AS A BASIC BEHAVIOR FOR THE DEVELOPMENT OF PERIPERSONAL SPACE | 30 |
| 5 | THE DOUBLE TOUCH IN THE ICUB HUMANOID ROBOT | 31 |
| 5.1 | Introduction | 31 |
| 5.2 | Experimental protocol | 31 |
| 5.3 | Classical approach to self-collision | 33 |
| 5.4 | Kinematic chain reformulation | 34 |
| 5.4.1 | The reversion of the kinematic chain | 34 |
| 5.4.2 | Inverse Kinematics solver | 38 |
| 5.4.3 | Controller | 40 |
| 6 | AUTOMATIC KINEMATIC CHAIN CALIBRATION | 41 |
| 6.1 | Introduction | 41 |
| 6.2 | Methods and experimental setup | 44 |
| 6.2.1 | Data collection and optimization | 45 |
| 6.3 | Experimental results | 47 |
| 6.3.1 | Exp. 1 - Optimization of parameters from CAD model | 47 |
| 6.3.2 | Exp. 2 and 3 - Optimization with 10% and 30% noise on initial values | 48 |
| 7 | PART II: DISCUSSION AND CONCLUSIONS | 51 |

| | |
|---|-----------|
| III PERIPERSONAL SPACE AND MARGIN OF SAFETY AROUND THE BODY | 53 |
| 8 LEARNING TACTILE-VISUAL ASSOCIATIONS ON A HUMANOID ROBOT WITH ARTIFICIAL SKIN | 54 |
| 8.1 Introduction | 54 |
| 8.2 Representation of space around the body | 55 |
| 8.2.1 Data collection for learning | 56 |
| 8.2.2 Internal representation | 59 |
| 8.3 Monte Carlo simulation of a single taxel model | 61 |
| 8.4 iCub humanoid robot and key modules | 63 |
| 8.4.1 Artificial skin | 63 |
| 8.4.2 Kinematic model and coordinate transformations | 65 |
| 8.4.3 Visual processing and gaze control | 66 |
| 8.5 Results | 68 |
| 8.5.1 Learning in a single taxel model | 69 |
| 8.5.2 Tactile-motor learning: double touch | 73 |
| 8.5.3 Tactile-visual learning | 73 |
| 9 APPLICATIONS OF THE MARGIN OF SAFETY IMPLEMENTATION: AVOIDANCE AND CATCHING BEHAVIORS | 81 |
| 9.1 Introduction | 81 |
| 9.2 Avoidance and catching controller | 82 |
| 9.3 Exploitation of the learned associations | 82 |
| 9.3.1 Margin of safety: Avoidance behavior demonstration | 83 |
| 9.3.2 “Catching” with arbitrary body parts | 85 |
| 10 PART III: DISCUSSION AND CONCLUSIONS | 88 |
| IV CONCLUSIONS AND FUTURE WORK | 90 |
| 11 CONCLUSIONS AND FUTURE WORK | 91 |
| 11.1 Summary | 91 |
| 11.2 Discussion and Future Work | 92 |
| V APPENDIX | 95 |
| A THE KINEMATIC PROBLEM AND THE DENAVIT-HARTENBERG CONVENTION | 96 |
| A.1 Direct and inverse kinematics of a serial robotic arm | 96 |
| A.1.1 Kinematic model of a robot | 96 |
| A.1.2 Kinematics of a serial robotic arm | 98 |
| A.2 The Denavit-Hartenberg notation | 99 |
| BIBLIOGRAPHY | 102 |

ACRONYMS

| | |
|-------|---------------------------------------|
| PPS | PeriPersonal Space |
| RF | Receptive Field |
| FoR | Frame of Reference |
| DoF | Degree of Freedom |
| DH | Denavit–Hartenberg (convention) |
| PDF | Probability Density Function |
| Taxel | Tactile Element |
| Root | Root FoR for the iCub kinematic model |
| PoC | Point of Contact |
| AI | Artificial Intelligence |
| HSV | Hue, Saturation, Value |

INTRODUCTION

*The main lesson of 35 years of AI research
is that the hard problems are easy
and the easy problems are hard.
— Steven Pinker [64]*

1.1 MOTIVATIONS: TOWARD A NEW GENERATION OF INTERNAL MODELS FOR ROBOTICS

It is a flourishing period for robotics in general: a number of top-notch companies are investing in the field, the first (working) robotic devices are showing up at exhibitions and populating our homes, and the press is universally designating it as the latest trendsetting discipline in the engineering world. On the other side, a number of widely esteemed science celebrities not belonging to the field are demonizing it with a series of questionable opinions^{1,2}. Overall, it is conservative to conclude that robotics has seen a significant increase in popularity and widespread attention in the past few years. The established consensus is that, sooner or later, robots will pervade our life, replacing us in some – if not most – of our everyday duties.

A number of issues are preventing these dystopian forecasts to happen – at least in the short term. It will be not matter of debate here, but in general, a key element in the pursuing of this goal is related to the development of truly autonomous systems. Autonomy is, unquestionably, what impresses us the most; still, autonomous cars, autonomous vacuum cleaners, autonomous flying drones are only the tip of the iceberg in the wide area of autonomous systems. As of now, any approach that backed this kind of devices is falling into the classical AI paradigm, in which a sufficient enough set of sensors helps in contextualizing a narrow (and solvable) problem in order to provide the device with a sufficient enough autonomy. That is, autonomy, for how big its meaning may represent, is no way tied in with

¹ Elon Musk Compares Rogue Artificial Intelligence to Demons. Yes, Really: <http://mashable.com/2014/10/26/elon-musk-artificial-intelligence-demons/>

² Stephen Hawking warns artificial intelligence could end mankind: <http://www.bbc.com/news/technology-30290540>

a *perceptual system capable of achieving autonomy*. But perceptual systems – even humans’ – are inherently faulty and poor in their measurement of the outside world. Any sensor the subject is provided with will prove inadequate in some circumstances, especially in the case of artificial systems: this is a fundamental constraint a generic subject (either biological or robotic) has to cope with.

The way humans are dealing with this issue is by integrating the information coming from different sources into a single, coherent view of their perceptual world³. By its very nature, a biological agent has a set of constraints to cope with, such as complexity, timing, energy, computational resources, and many more. Consequently, it chooses to maximize the amount of information it is provided with by melding different modalities one another. Further, this optimization proceeds also in the direction of filtering out whatever is irrelevant to the subject in a specific instant of time. This provides the subject with a maximization of the trade-off between the amount of information and the amount of resources needed to process that information.

This approach is best exemplified by the *peripersonal space* (PPS) representation, a model of the nearby space that holds a central role in the perception of humans and animals. Peripersonal space is the space surrounding our bodies, which can be reached by our limbs. In this region, there is evidence of multisensory-motor integration (see di Pellegrino and Ládavas [20] for a recent review on the topic). Further, it is implicitly focusing the processing power in the region of most relevance, i.e. the space surrounding the body. PPS representations are probably best described as multisensory and sensorimotor interfaces, with a fundamental role in the sensory guidance of actions. Owing to them is the ability to perform timely and appropriate actions toward objects located in the nearby space, which is critical for the survival of every animal. Depending on context, these actions may constitute an approaching or an

³ It is worth noting that many of the concepts mentioned in this preliminary section have been not properly introduced to the reader. This is because a proper dissertation of concepts like “autonomy”, “perceptual world”, “intelligence” probably deserves a whole thesis on its own. In this case, with “perceptual world” we mean whatever is mediated by the perceptual system, i.e. we are not constraining ourselves to the external world alone but we are considering also the proprioception and any estimation of the internal state of the subject. Accordingly, as we will clarify later on, there is no reason to limit our concept of “perceptual world” to the purely “sensory” modalities (such as vision or touch): the motor system is an important carrier of information on its own, not only regarding the internal state of the system, but also in relation with the interaction of the system with its environment.

avoidance behavior. In the case of defensive behavior, this creates a “*margin of safety*” around the body, such as the flight zone of grazing animals or the multimodal attentional space that surrounds the skin in humans [33].

Analogous behavior is desirable in robots as well. However, to date, robot controllers largely concentrate on the end-effector as the only part that interacts with the environment. The rest of the body is typically represented as a kinematic chain, the volume and surface of the body itself rarely taken into account. Sensing is dominated by “distal” sensors like cameras, whereas the body surface is “numb”. As a consequence, reaching in cluttered, unstructured environments poses a severe problem, as the robot is largely unaware of the full extent of its body, limiting the safety to the robot itself and the surrounding environment. That is one of the key bottlenecks that prevents robots from working alongside with human partners.

The robotic platform used in this thesis, the iCub humanoid robot [55], is provided with a set of sensors and capabilities comparable to humans’ and, more importantly, an artificial skin on most of its body. This gives us the unique opportunity to learn how these representations can be developed on a robotic platform, and let the robot build up its own representation of the self and the nearby space. Our work does not attempt at providing a functional model of peripersonal space representations, but rather a practical implementation that supports the relevant behaviors. Nonetheless, the road is open to further grounding of the architecture in putative brain mechanisms.

1.2 CONTRIBUTION AND OUTLINE

This thesis presents to our knowledge the first architecture capable of providing a humanoid robot with a distributed, decentralized representation of the space around its body. Starting from an initially blank state, the robot learns a multisensory (tactile-motor and tactile-visual) representation of the outside world by means of a whole-body skin and through interaction with the environment. Further, this multimodal representation is put under testing with a sensory-based guidance of the motor actions performed by the robot: that is, an avoidance and catching controller capable using any body part in order to either prevent collision with or come into contact with incoming objects.

In our view, this work paves the way for robots to enter new application domains. Robots capable of detecting and locating contact on any body part and also able to reach and avoid with any body part can be said to possess whole-body awareness, making them intrinsically safe not only for themselves (as demonstrated here), but also for their environment, possibly a humanly populated one. This is certainly one of the overarching goals and future measure of success of humanoid robotics.

In the following, an introduction to the peripersonal space problem in humans and animals is provided ([Section 2.1](#)), as well as the state of the art in the robotics field ([Section 2.2](#)). [Chapter 3](#) describes the robotic platform this thesis is based upon, whereas the subsequent chapters detail the proposed approach. To summarize, we list here the main contributions of this thesis:

- the first, to our knowledge, attempt at approaching the problem of building up a complex, multisensory representation of the nearby space that bridges the gap between biological and robotic agents [[Chapter 4](#)];
- a method for performing double touch and self-exploratory behaviors on an humanoid robot [[Chapter 5](#)];
- an application of the double touch paradigm in the context of autonomous closed-loop calibration [[Chapter 6](#)];
- an architecture able to build up an integrated representation of the nearby space of a robot through interaction with the self and the environment [[Chapter 8](#)];
- an exploitation of such a representation by means of a distributed avoidance and catching controller [[Chapter 9](#)].

2

THE IMPORTANCE OF PERIPERSONAL SPACE IN HUMANS AND ROBOTS

2.1 PERIPERSONAL SPACE IN HUMANS AND ANIMALS

The *peripersonal space* (PPS) is of special relevance for every animal. It is defined as the space immediately surrounding our bodies [67], within which objects can be reached for and manipulated. It acts as an interface between the body and the outside world, for defensive and/or purposeful actions toward objects: for this reason, items situated in peripersonal space (or moving rapidly toward it) benefit a different representation from those in extrapersonal space [12]. In the interpretation given by Graziano and Cooke [33], the PPS encodes the space near the body, computes a margin of safety, and helps to coordinate movements in relation to nearby objects with an emphasis on withdrawal or blocking movements. Deeply intertwined with the concept of *body schema* (or body image), the PPS is thought to play a central role in the construction and development of a rich internal model of the interrelations between the body structure and the nearby space [32]. Furthermore, the neurons that encode PPS may also provide a neuronal basis for the psychological phenomenon of *personal space* [33], the flexible bubble of space around each person that is protected from intrusion by other people [36].

This space thus deserves special attention and probably justifies specific neural circuitry devoted to its representation, which has to dynamically integrate information from several modalities (motor, visual, somatosensory and auditory). At this point, it is worth noting that this aspect has been historically studied by two distinct disciplines: the neurophysiology field on one side, and all the disciplines related to neuropsychology and behavioral psychology on the other. Not surprisingly, they followed two very distinct paths that resulted in different outcomes – the former being used to a bottom-up approach while the latter attacking the problem from a more top-down perspective. The neurophysiological approach focused on empha-

sizing the proprioceptive modality and its interplay with the motor modality (i.e. its role in the control of movement); conversely, the psychological field was generally highlighting the multisensory aspect of this representation, that is how the different modalities were combined and cross-referenced in order to build up a coherent representation of the body and the nearby space. Luckily, in the recent years the two fields have begun to converge toward a common ground: whilst the neurophysiological studies were shifting their focus on how purely “sensory” modalities such as vision and touch were integrated in the parietal lobe and the premotor cortex, the psychological experiments were trespassing their comfort zone by studying how this multisensory representation interfaces with the motor system.

In primates, evidence coming primarily from recordings in macaque monkeys is pointing to a parieto-frontal network as to the key circuitry supporting this functionality (e.g. [33, 44]). The key area in the frontal lobe seems to be area *F4* of ventral premotor cortex [25, 67] including the region of the spur of the arcuate sulcus (see Graziano and Gandhi [34]). In the parietal lobe, the area more strongly connected with area *F4* is area *VIP* (Ventral Intra-Parietal). Despite the fact that some observations report the presence of auditory-somatosensory responses as well, in this thesis we will leave the auditory modality aside and focus in particular on the integration of visual and tactile inputs.

Neurophysiological studies in monkeys [7, 22, 35, 31, 68, 11, 25, 30, 66], as well as neuropsychological [21, 48], behavioural [80, 82, 4], neuroimaging [7, 53] and electroencephalography [76] studies in humans, have revealed that the neural representation of peripersonal space is built up through a network of interacting cortical and subcortical brain areas. A key part of peripersonal space coding can presumably be attributed to populations of *polymodal neurons* that, in addition to motor discharge, have tactile and visual receptive fields (RFs) extending from the tactile one around the respective body part (e.g., [29, 25] - for a review, see Graziano and Cooke [33] and Holmes and Spence [44]). Furthermore, the visual RFs are often coded in the same frame of reference (FoR) of the respective body part and thus, during active or passive mobilization, follow the body part in space. This suggests that motor and proprioceptive information are probably integrated in such a body-centered encoding. A good part of the evidence coming from monkeys is presumably informative in the case of humans as well [7].

The adaptivity of these transformations is evident in a great number of psychophysical experiments – like the prism adaptation experiment, and the “rubber hand” experiments [5, 14] – and, more importantly, in all those experiments that involve the use of tools. For example, it has been shown that after some practice with a tool the monkey integrates it into his body schema, expanding *de facto* the somatosensory receptive field of given neurons [46].

Collectively, these results demonstrate that representations of peripersonal space are body centered or body-part centered (and the brain seems to use the reference frame most appropriate to the information being encoded), are restricted to the space immediately surrounding the body (extending to about 20 – 40 cm from the skin surface in monkeys, and up to perhaps 70 cm in humans), and involve the integration of information from multiple modalities (somatosensory, proprioceptive, visual, auditory and motor).

2.2 PERIPERSONAL SPACE MODELING AND ITS APPLICATIONS IN ROBOTICS

There are a number of models addressing phenomena related to peripersonal space representations. A major component are coordinate transformations, which seem inevitable in order to support the coding of information coming from the visual modality in body-part centered FoR; this has been investigated extensively and several connectionist models have been proposed (e.g. [3, 65, 87]). On the other hand, Magosso et al. [51] took these transformations for granted and focused on the mechanisms of tactile and visual interaction. They proposed a neural network that models unimodal (visual and tactile) and bimodal representations of an imaginary left and right body part and demonstrated a number of phenomena reported in humans (e.g., tactile extinction).

While individual components that presumably compose the representations of space around the body can be studied in isolation using computational models in simplified (for example 2-dimensional) scenarios, their interplay are difficult to model without an articulated body with corresponding sensorimotor capacities and interaction with the environment. Indeed, in animals and humans, these representations are gradually formed during interaction with the environment and in a complex interplay of body growth and neural maturation processes. One of the key behaviors that is relevant to the formation of the

multimodal body representations is presumably self-touch or double touch. For example, “*by 2-3 months, infants engage in exploration of their own body as it moves and acts in the environment. They babble and touch their own body, attracted and actively involved in investigating the rich intermodal redundancies, temporal contingencies, and spatial congruence of self-perception*” [69]. Such behaviors may initially be reflexive and controlled by spinal circuitry – the wiping/scratch reflex has been demonstrated in frogs [27, 6], though its existence is debated in humans [50] – but progressively become more complex and voluntary.

In order to model multimodal and nontrivial 3D spatial relationships, such as the one that arises from self-touching behaviors, robots qualify as a powerful modeling substrate. Some of the studies targeting body schema and peripersonal space representation models were reviewed in Hoffmann et al. [40]. Since platforms with tactile sensing are rare, most of the work has focused on the interaction of visual and proprioceptive information (in robotics typically equated with joint angles from encoders). For example, Antonelli et al. [2] developed a model in the Nao humanoid robot that adaptively codes the space that can be reached by the robot. A number of embodied models were also developed by Asada and colleagues. Hikita et al. [38] used a humanoid robot and employed a bio-inspired architecture (self-organizing maps, Hebbian learning, and attention module) to learn the visual receptive field around the robot’s hand and its extension when using a tool – inspired by the behavior of the “distal” type neurons reported by Iriki et al. [46]. Touch was only emulated and used to trigger the visuo-proprioceptive association. Finally, most related to our approach, Fuke et al. [26] used a simulated robot touching itself on the face to model the putative mechanism leading to the visual and tactile response properties of neurons in the ventral intraparietal area. A hierarchical architecture with visual, proprioceptive and tactile modality was used. After learning, as the robot’s hand was approaching its face, contact with the skin could be anticipated.

Pushed by the needs of safe interaction of robots with their environments and, in particular, humans, there is a need for technologies that allow robots to acquire some form of “whole-body awareness”. However, a bottleneck of robotics research along these lines has been the absence of appropriate platforms: although diverse tactile sensing technologies have been developed (see Dahiya and Valle [15] for a review), robots with whole-body tactile sensing have been – to our knowledge – unavailable. Alternative solutions mostly relied on force/torque sens-

ing and impedance control schemes that ensure compliant behavior of the platform on contact (e.g. Albu-Schaffer et al. [1]). Shimizu et al. [81] used force/torque feedback together with encoder information to develop self-protective reflexes and global reactions for the iCub robot. Distributed sensing over the whole surface of a robotic manipulator was used by Mittendorfer and Cheng [57]. Utilizing information from accelerometers from their multimodal “skin” during a motor exploration phase, the direction of movement of every sensory unit in response to every motor could be learned. Activations of infra-red distance sensors on the same sensory unit could then be used to trigger local avoidance reflexes to approaching objects. Finally, Jain et al. [47] devised a controller that allows for reaching in clutter while taking into account multiple contacts and keeping the forces within set limits. The solution was verified on a robot featuring a tactile-sensitive forearm.

2.2.1 THE ICUB HUMANOID ROBOT AS A PLATFORM FOR DEVELOPING PERIPERSONAL SPACE AND MARGIN OF SAFETY REPRESENTATIONS

The iCub humanoid robot [55] has a human-like morphology and a subset of the sensory capacities present in humans. It has been recently equipped with a whole-body skin [52] giving us the opportunity to address the problem of peripersonal space development in a biomimetic way. We are indeed in the unique position to learn how the proprioceptive-tactile and visuo-tactile associations are generated and let the robot autonomously establish a margin of safety through interaction with the environment.

In this thesis, we present a solution to this problem by proposing an architecture that achieves this functionality thanks to a “spatial” receptive field anchored to each taxel (tactile element) on the robot skin. By exploiting a temporal and spatial congruence between a purely visual event (e.g. an object approaching the robot’s body) and a purely tactile event (e.g. the same object eventually touching a skin part), a representation will be learned that allows the robot to autonomously establish a margin of safety around its body through interaction with the environment - extending its cutaneous tactile space (the artificial skin) into the space surrounding it.

THE ICUB HUMANOID ROBOT (AND SOME OF ITS KEY COMPONENTS)

In this chapter, an overview of the iCub humanoid robot is provided. The description reported here will not cover all the aspects about the design of the iCub's hardware and software architecture, but it will rather focus on the core elements that have been proven essential for the fulfillment of this work. As such, they will be generically referenced by any of the chapters in this thesis; if needed, some other aspects of the iCub platform will be detailed in the corresponding sections.

The iCub (Fig. 1) is an open-source platform for research in cognitive robotics. The following sections will describe the key components relevant for this work, divided into [Section 3.1](#) about the hardware (arms and hands mechanics, artificial skin, joint angle sensing, eye and camera setup), and [Section 3.2](#) about the software (YARP middleware, model of the robot's kinematics, visual processing, and finally cartesian control for arms and gaze).

3.1 HARDWARE

3.1.1 ARMS AND HANDS

The iCub is equipped with 7 and 9 degrees of freedom for arms and hands respectively. Four brushless motors control the upper part (three command the shoulder and one the elbow), whereas the three motors of the wrist are brushed. For the purposes of this thesis (see Chapter 5), it is worth noting that the shoulder joint presents a non-standard design: it is characterized by a cable differential mechanism with a coupled transmission system. Three coaxial motors housed in the upper torso move pulleys to generate the spherical motion of the shoulder [59].

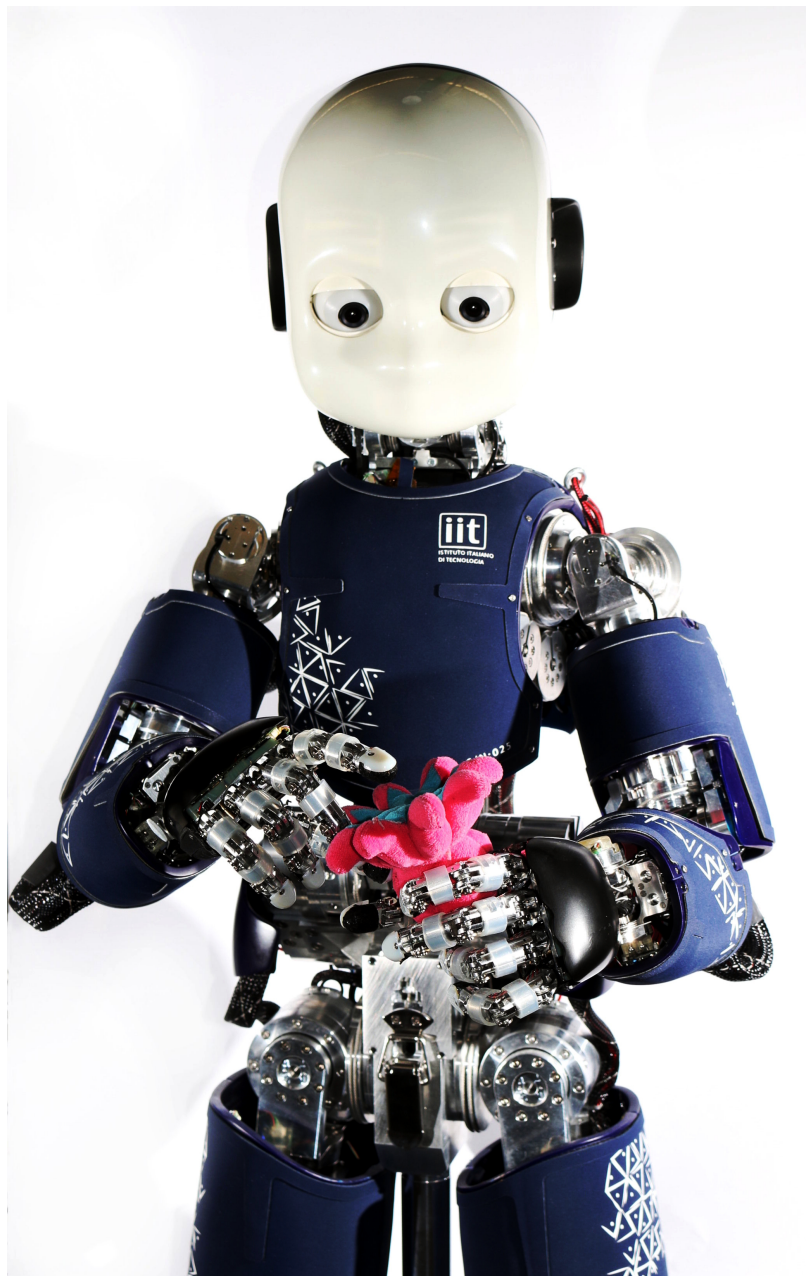


Figure 1: The *iCub* humanoid robot. It is composed by 53 degrees of freedom, a set of two independently moving cameras, and an artificial skin that covers most of its body.



Figure 2: Pressure-sensitive skin of the iCub. iCub forearm with exposed skin patches.

3.1.2 JOINT ANGLE SENSING

Proprioceptive inputs in the iCub simply consist in angular position measurements in every joint. For most joints, they are provided by absolute 12bit angular encoders (see Parmiggiani et al. [60] for details).

3.1.3 ARTIFICIAL SKIN

The iCub was recently equipped with an artificial pressure-sensitive skin covering most of its body parts [52]. The latest iCub version contains approximately 4000 tactile elements (taxels) – in the fingers, palms, forearms and upper arms, torso, and lately also in the legs and feet. The iCub forearm and hand with exposed skin is shown in [Figure 2](#).

A spatial calibration of the skin of the forearm with respect to the iCub kinematic model has been performed in Del Prete et al. [18] – the pose of each taxel in the reference frame of the corresponding link is available.

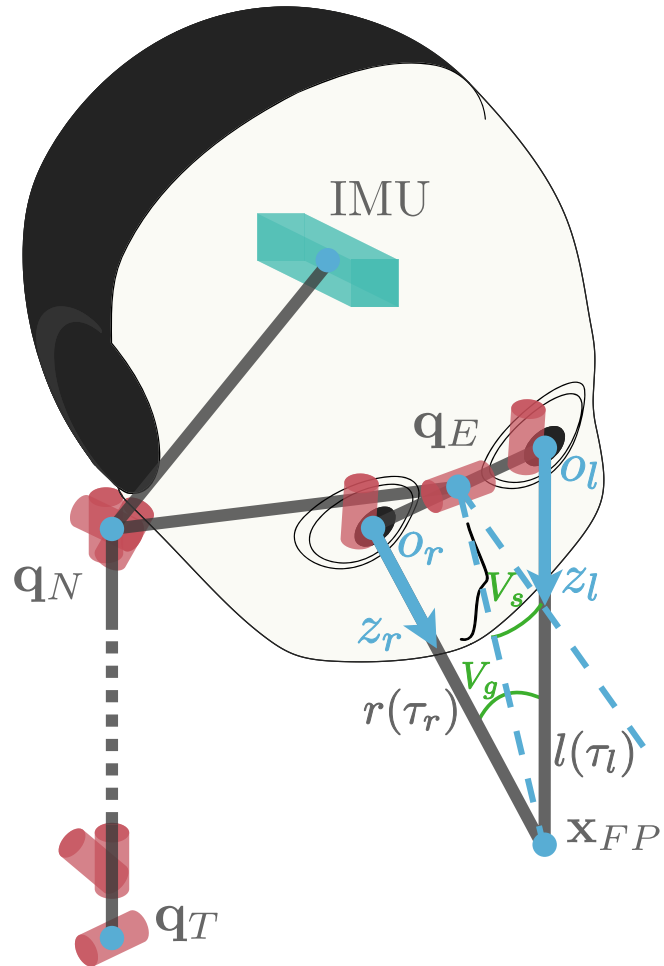


Figure 3: Kinematics of the iCub’s torso and head. The upper body of the iCub is composed of a 3 DoF torso, a 3 DoF neck and a 3 DoF binocular system, for a total of 9 DoFs. Each of these joints, depicted in red, are responsible for the motion of the fixation point. An Inertial Measurement Unit (IMU) is present in the head (the green rectangle in figure); its motion is not affected by the eyes.

3.1.4 HEAD AND EYES

Vision on the iCub is provided by two cameras contained inside the robot’s eyeballs. The neck of the robot has three degrees of freedom (DoFs) and there are three additional DoFs in the eyes allowing for tracking and vergence behaviors. The movement of the eyes is coupled, following an anthropomimetic arrangement. With appropriate calibration, depth information can be extracted from binocular disparity.

3.2 SOFTWARE

3.2.1 YARP

YARP (*Yet Another Robot Platform*) [24] is the middleware the iCub comes equipped with. It is a set of open-source libraries that support distributed computation under different operative systems¹. YARP facilitates code reuse and modularity by decoupling the software from the specific hardware (using *Device Drivers*) and operative system. Moreover, it provides an intuitive and powerful way to handle inter-process communication (using *Port* objects). Furthermore, YARP provides mathematical and image processing libraries.

3.2.2 KINEMATIC MODEL AND COORDINATE TRANSFORMATIONS

The iCub software² is another set of libraries and tools that have been used extensively in this work. Most important for the pursuance of the goals of this thesis is *iKin* [63], a library that provides a kinematic modeling for the iCub robot. It is based on the Denavit-Hartenberg convention [19], and is schematized in Figure 4³. Each joint is modeled as a rotational joint with a quadruplet of parameters $\Phi = \{a, d, \alpha, \vartheta\}$; for any joint configuration $q = \hat{\vartheta}$, this corresponds to a fixed rototranslation matrix from one link to its subsequent, up to the end effector.

3.2.3 VISUAL PROCESSING

The work presented in Part III has taken advantage of a series of software tools available in the iCub repository for visual processing. They are listed below:

- *2D Optical Flow (motionCUT)* [9]: it modifies the pyramidal Lucas-Kanade algorithm [49] to detect independent moving points over a selectable grid of nodes. It is designed to work with moving cameras, such as those available on the iCub.
- *2D Particle Filter Tracking* [83]: it is a single-object tracker that uses a color histogram-based observation model. The particle filtering algorithm keeps track of the object by

¹ The YARP source code is available at www.github.com/robotology/yarp

² Most of the iCub software is available at this link: www.github.com/robotology/. The core software modules are available at www.github.com/robotology/icub-main.

³ An in-depth analysis of the standard DH notation is available in Appendix A.

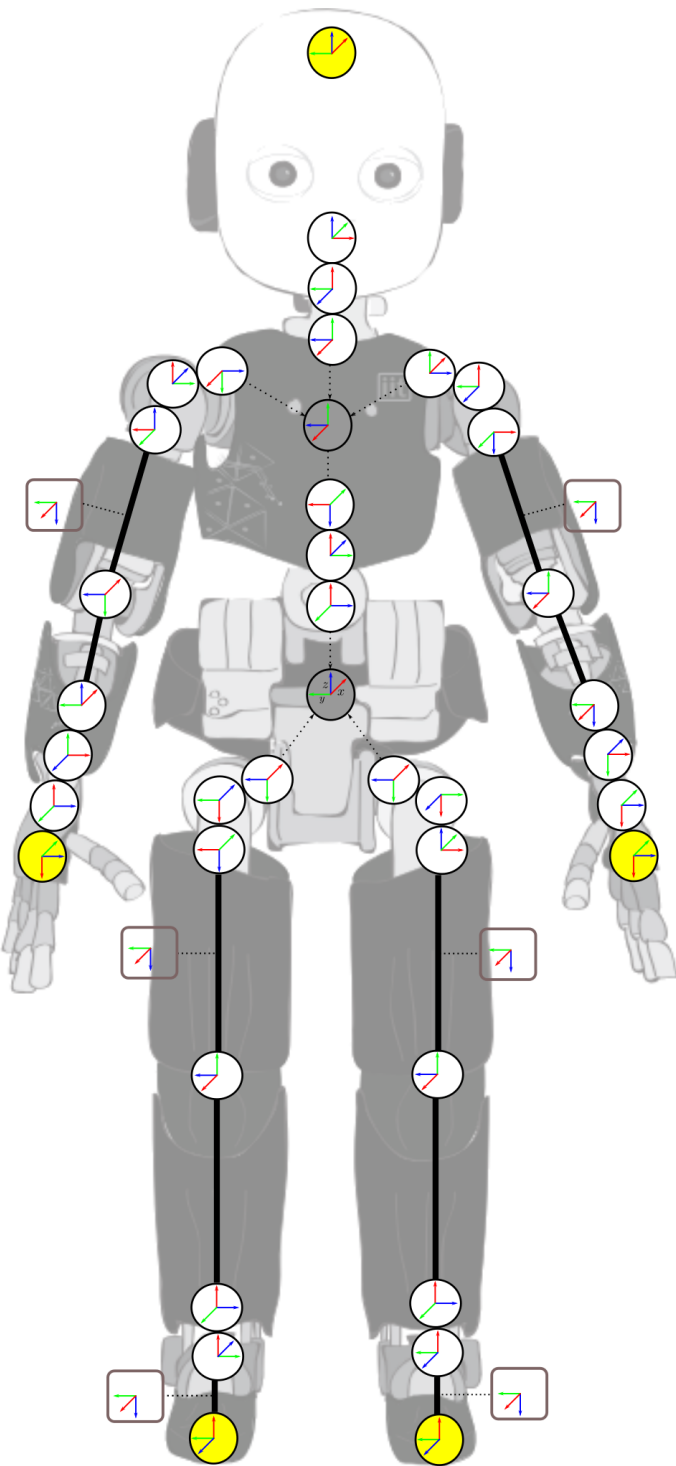


Figure 4: A schematics of the kinematic model of the iCub. With the exception of the hands and the head, each joint is visualized as a reference frame centered in its axis of rotation. Image courtesy of Laura Taverna and Jorhabib Eljaik.

maintaining a probability distribution over the state of the system it is monitoring, in this case the object.

- *Stereo Disparity Module* [23]: it wraps the Hirschmüller [39] algorithm in order to build a depth map on top of the iCub’s stereo vision system. It has been made robust to head and eyes movement by exploiting the encoders information and updating the camera reference system.

3.2.4 CARTESIAN CONTROL FOR ARMS AND GAZE

The iCub is provided with a *cartesian controller* for the arms and a *gaze controller* for the head and the vision system. They provide an interface that exploits an inverse kinematics solver in order to control the arms and the head directly in the operational space, by querying 3D points instead of configurations at the joint level. Both have been developed by Pattacini et al. [62] in conjunction with the *iKin* library [63].

Part I

THE PERIPERSONAL SPACE ON THE ICUB

In this part, we provide an overview of the proposed approach. It draws inspiration from human development, capitalizing above all on the role of movement toward own body (self-touch or double touch) that gives rise to unique cross-modal contingencies that allow the agent to learn about the spatial properties of its body and the space around it. The robotics implementation departs in many respects from the mechanisms that presumably operate in primate brains. Instead, the correspondence is often established on a behavioral level, while modules that were engineered for the robot are exploited to support the functionality needed. We are referring in particular to a complete model of the robot's kinematics and availability of coordinate transformations that map all information into a common reference frame. The implementation of the double touch itself (from Roncone et al. 2014) is taken as a primitive even if its workings were not biologically motivated. It is the learning/calibration of the spatial receptive fields around individual taxels that is primarily addressed in its thesis and related to biology.

Reference paper: Alessandro Roncone, Matej Hoffmann, Ugo Pattacini, Luciano Fadiga, and Giorgio Metta. Peripersonal space and margin of safety around the body: learning tactile-visual associations in a humanoid robot with artificial skin. Manuscript, 2015.

4

PROPOSED APPROACH: MILESTONES FOR THE DEVELOPMENT OF PERIPERSONAL SPACE IN HUMANS AND ROBOTS

In this chapter we describe our approach, which proposes a putative gradual development of peripersonal space in humans as well as in robots. We assume the availability of basic behaviors (that will be therefore considered “innate” – [Section 4.1](#)), and we suggest a series of milestones throughout which a generic biological “agent” (human or animal) has to go through in order to succeed in developing a peripersonal space representation ([Section 4.2](#)). In [Section 4.3](#) we will go through the description of the software modules that need to be implemented in order to build up behaviors that are correspondent to the putative neurophysiological correlates described in [Section 4.2](#).

The scenarios investigated in [Section 4.3](#) are parallel to those experienced by humans and animals – thanks to the anthropomorphic nature of the iCub – and should thus speak directly to the mechanisms of peripersonal space representations in primates that have been subject of intensive investigations in cognitive psychology as well as the neurosciences over decades. Importantly, the developmental trajectory leading to the acquisition of these representations is largely unknown. The development of reaching may constitute one key factor in this mechanism (e.g. Sclafani et al. [79]); the exploration of own body may be another (e.g. Rochat [69]). In the work presented here, we mimicked the latter trajectory by considering first the self-touch behaviors and adding encounters with external objects later on.

This chapter will act as a scaffold for the rest of this thesis. In particular, in [Part II](#) we investigate aspects related to the implementation of the innate capabilities described in [Section 4.3.1](#), whereas in [Part III](#) we detail the core contribution of this thesis, that is the first, to our knowledge, attempt at building a tactile-visual representation on a humanoid robot.

4.1 BASIC BEHAVIORS THAT LEAD TO THE DEVELOPMENT OF HIGHER LEVEL MULTIMODAL ASSOCIATIONS

In order for a subject to develop the necessary tactile-motor-proprioceptive-visual associations needed for it to build up a peripersonal space representation, we speculate it already masters a set of basic motor behaviors. We can harmlessly assume these behaviors to be “innate” to the agent under consideration, in the sense that they can be either already available to the subject at birth, or that they have been developed during earlier stages of growth.

Hereafter, two test cases are described, with both the purpose of showcasing useful examples for the subsequent overall discussion, and the goal of fostering the idea that this kind of behaviors is vital for the development of the peripersonal space in humans as well as in animals.

4.1.1 MOTOR-PROPRIOCEPTIVE ASSOCIATIONS: THE SPINALIZED FROG’S WIPING REFLEX (FROM SCHMIDT AND LEE [77])

Early in the thinking about motor control, the spinal cord was viewed as a “freeway” that simply carried impulses back and forth from the brain to the peripheral receptors and muscles. Gradually, evidence that the spinal cord contains central pattern generators for gait and other movements pointed toward the cord as a complex organ where much of motor control is structured. Further evidence suggests that the spinal cord is responsible for considerable integration and processing of sensory and motor information.

The *hindlimb wiping reflex* of the frog is an example of a basic behavior that is organized at the spinal level. [Figure 5](#) shows a frog making a wiping response as a consequence of either an electric or a chemically noxious stimulus placed on its forelimb. Fukson et al. [27] and Berkinblit et al. [6] showed that the frog is capable of performing these hindlimb responses when spinalized (i.e. with a transection that separates the cortex from the intact spinal cord). The response always begins with a movement of the hindlimb toe to the region of the shoulder area, followed by a rapid wiping action that is aimed at the elbow.

Interestingly, the animal can use sensory information from one part of the body (the elbow) to trigger an action pattern

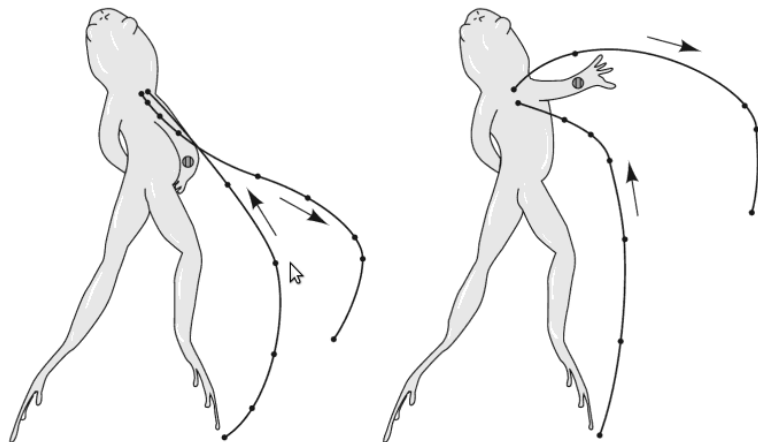


Figure 5: In the spinalized frog, the hindlimb response to wipe an acid stimulus from the elbow is aimed to various elbow positions without the involvement of voluntary control from the cortex. This reflex was found to have two stages. During the first, the frog fixed the hindlimb in an intermediate posture irrespective of forelimb position. In the second, the movement depended on the forelimb position, which determined the final posture of the hindlimb [27].

in some other part (the ipsilateral hindlimb), even when deafferentated (and thus with neither cortical involvement nor awareness of the limbs' actions). Furthermore, the animal produces different wiping movements depending on the location of the elbow at which the response is aimed. That is, the generator for this response appears to modify its action depending on the sensory information from the forelimb indicating the position of the stimulus – the cord knows where the limbs are. Suggestions that these behaviors also operate in humans have sparked considerable debate, and to date the evidence is not entirely clear on the issue [50]. We might expect that they likely would operate in humans to some extent.

4.1.2 TACTILE-MOTOR-PROPRIOCEPTIVE-VISUAL ASSOCIATIONS: SELF-TOUCH IN THE EARLY INFANCY

From birth, newborns are subject to contrasting perceptual and sensorimotor events. These events potentially inform them about their own body as well as their interaction with the nearby space. It is believed that young infants' propensity to engage in self-perception and systematic exploration of the perceptual consequences of their own actions plays an important role in the intermodal calibration of the body and the space surrounding it. The process of *self* (or *double*) touch provides correspondences between different forms of sensory information which

may underpin a basic structural model of the body as a physical object distinct from the outside world. Rochat [69] showed that by 2–3 months infants appear to be attracted to and actively involved in investigating the rich intermodal redundancies, temporal contingencies, and spatial congruence of self-perception. They engage in intermodal calibration of their own body, in order to detect invariants and regularities in their sensorimotor experiences.

Moreover, studies on patients with unilateral lesions showed that self-touch can enhance sensory processing. Weiskrantz and Zhang [86] reported a patient who could feel tactile stimulation on the contralateral hand when she delivered them with her ipsilesional hand, but not otherwise. Valentini et al. [84] reported similar findings in a large sample of left and right hemisphere stroke patients. Coslett and Lie [13] found that extinction of a left-sided tactile stimulus in two patients with right hemisphere damage was ameliorated when the patients touched the stimulated left part of the body with the right hand. They suggested that the right hand could function as an ‘attentional wand’, increasing the salience of events on the left side of the body. However, their result could also be attributed to integration between the experiences of the two hands as a result of self-touch. If stimuli delivered to joined hands become in some sense inseparable, then an undetected stimulation of the left hand might benefit from summation with a detectable stimulus on the right hand.

4.2 MILESTONES FOR THE DEVELOPMENT OF PERIPERSONAL SPACE IN HUMANS AND ANIMALS

In the following, we will investigate a set of stages in which the agent is most likely to go through in order to develop more complex forms of perception of its own body and the nearby space. Our premise is to assume the availability of the basic motor capabilities described in [Section 4.1](#): that is, the subject is able to independently execute a set of reflexive actions that let it perform a *double-touch* scenario. For the purposes of this thesis, with double touch we simply define an action directed toward the self which is characterized by the concurrent activation of two different skin parts, i.e. the skin part of the *active* arm (the one that touches) and the one belonging to the *passive* arm (namely, the arm to be touched).

4.2.1 “BARE” OR “BLIND” DOUBLE TOUCH (*tactile-motor associations*)

In this scenario, the subject is equipped with a series of low-level capabilities (the scratch reflex or a self-exploration mechanism described in [Section 4.1](#)) that generate purely reflexive movements. These movements can give rise to a new mapping which is not reflexive, but voluntary – in other words, the organism can learn to produce a specific tactile stimulation by voluntarily repeating the same movement that has been previously triggered by the reflex. This presumably corresponds to the shift from spinal control of reflexes to voluntary actions controlled by the cortex.

At this stage, the agent is focused toward the development of a pure tactile-motor representation (i.e. there is neither vision nor proprioception in the loop). The subject is “blindly” executing the self-touching movements, with the passive arm that is fixed and is simply recording an eventual contact coming from the active arm.

4.2.2 INVARIANCE WITH RESPECT TO THE CONFIGURATION OF THE PASSIVE ARM (*tactile-motor-proprioceptive associations*)

This step generalizes the framework of [Section 4.2.1](#) by achieving the double touch even if the passive arm changes its configuration in space (but remains static during the execution), similarly to the targeted trajectory showed by the spinalized frog in [Section 4.1.1](#). In this case, different motor commands will be sent to the active arm in order to succeed in the double touch. The representation is not purely tactile-motor anymore, because it involves the proprioceptive information coming from the passive arm in order to decode its position in space.

4.2.3 DOUBLE TOUCH WITH VISION (*tactile-visual associations*)

The developmental scenario here is similar to what the subject experiences into [Section 4.2.2](#), but now the visual system comes into place: the subject is able to visually perceive the active arm coming onto the passive one in its visual system.

In this milestone, both the head system (neck + eyes) and the passive arm are fixed: the subject is looking at the body part that is going to be touched, without changing its config-

uration over the course of the action. The agent can thus start building up a purely visuo-tactile association able to provide a prediction of the incoming contact based upon the visual stimulus. This step is crucial for the development of a peripersonal space representation, since at this stage the “motor” information about the position of the active arm is replaced by the “visual” information coming from the head system.

4.2.4 INVARIANCE WITH RESPECT TO THE CONFIGURATION OF THE PASSIVE ARM (*tactile-motor-proprioceptive-visual associations*)

At this stage, the tactile-visual association is generalized toward the inclusion of the proprioceptive modality into the representation, with a scenario similar to [Section 4.2.2](#): the passive arm is in an arbitrary configuration (but remains static during the intercourse of the self-touching behavior), and the proprioception of the passive arm’s position in space is needed in order to perform the double touch and keep record of where the movement will be heading to. The head plant is still not moving and is fixating the point to be touched.

4.2.5 INVARIANCE WITH RESPECT TO THE CONFIGURATION OF THE HEAD PLANT (*tactile-motor-proprioceptive-visual associations*)

In this scenario, the head system configuration has been freed, giving the agent the possibility of tracking the active arm coming onto the passive arm throughout the whole self-touching behavior. The proprioception is thus needed not only for coding the arbitrary position of the passive arm in space, but also for incorporating the different configurations of the neck and eyes plant into the representation.

4.2.6 FROM THE SELF TO THE EXTERNAL WORLD: ADAPTATION OF THE MODEL TO EXTERNAL STIMULI IN ORDER TO CREATE A MARGIN OF SAFETY AROUND THE BODY (*tactile-proprioceptive-visual associations*)

After a proper tactile-visual-proprioceptive association has been learned, this can be generalized and applied to external (i.e. not self-generated) stimuli as well - objects coming onto the skin. At this stage, the subject is able to perform a predictive behavior thanks to the skills acquired at the previous stages (the learned

representation can be also updated). This stage is purely perceptive.

At this stage, the goal is to create a visuo-tactile association for the external world, able to give a prior-to-contact activation of the visuo-tactile receptive fields when an incoming object is presented. It is the first step toward the building up of a “margin of safety” around the body: by developing a prediction of a forthcoming contact on the skin, the agent is building up a safety margin that will prove advantageous for its survival.

4.2.7 EXPLOITATION OF THE LEARNED ASSOCIATIONS: AVOIDANCE BEHAVIORS

The representations learned at previous stages are purely passive, i.e. they don't implicate any active contribution of the taxel involved into their development. In this stage, they are instead used to generate *active* avoidance behaviors. These avoidance movements can either pertain to the own body (i.e. avoiding self-collisions) or to the external world (i.e. avoiding incoming potentially harmful objects). The consequence is to effectively exploit the margin of safety around the body that has been learned in the previous stage ([Section 4.2.6](#)).

It is worth noting that, at this step, the tactile information is not used anymore, because it was needed only at learning stage. Furthermore, activity – i.e. motor commands – for what was up to now the passive arm is needed, since it has to actively move away from an incoming event.

4.2.8 EXPLOITATION OF THE LEARNED ASSOCIATIONS: REACHING / CATCHING BEHAVIORS

One of the main goals of the peripersonal space has been to create a margin of safety around the body [[33](#)]. Nonetheless, the peripersonal space helps to coordinate movements regarding purposeful actions toward nearby objects as well. This latter stage is headed toward the development of movements that are directed toward the nearby object, rather than away from it. It effectively results in reaching with arbitrary body parts.

4.3 MILESTONES FOR THE DEVELOPMENT OF PERIPERSONAL SPACE IN ROBOTS

In this section, we list the steps needed for our robotics platform (i.e. the iCub, [Chapter 3](#)) to develop a series of capabil-

ties comparable to what described in [Section 4.2](#). Crucial for the pursuit of the road map presented in [Section 4.2](#) has been the implementation of a *double-touch* paradigm on the iCub humanoid robot¹. Such a paradigm, if implemented on a robot, presents the same key advantages found in humans, because it gives access to a more structured information. It provides a way to achieve multimodal integration, and the possibility to synchronize sensory feedback coming from different modalities. Furthermore, it can be used for the automatic self calibration of the robot, in order to comply with an ever evolving platform able to cope with changes in its structure – something that the robotics community strives for.

It is worth noting that we assume three basic premises:

- (i) the goal is not to create a software as similar as possible to its biological counterpart, but to extrapolate the salient points of interest of peripersonal space in biological systems. Hence, a PPS implementation on the iCub should potentially try to maximize a sort of *congruency* property, rather than a similarity property. Consequently, the architecture presented has not to be seen as a model of a particular brain network.
- (ii) we are going to rely heavily on a centralized Cartesian space representation where information from different modalities (proprioceptive, motor, visual, tactile) can be mapped into. To what extent this is the case for the brain is debatable, but this is one of the strengths of our approach.
- (iii) in pursuance of the previous points, and loosely inspired by neurophysiological and psychological findings, this results in our own interpretation of the concept of peripersonal space – one that fits suitably with a robotic platform. With reference to [Section 2.1](#), there is considerable debate on what peripersonal space ultimately means, how it interfaces with the body schema, and to what extent it relates to the motor system. In the following section, we will generally approach the more general problem of peripersonal space representations by focusing on the learning of a visuo-tactile representation of the nearby space, that will be then exploited on a later stage for reaching and avoiding with whole body surface.

¹ A paper related to this has been presented in Roncone et al. [72], and will be more thoroughly detailed in [Part II](#).

The following Sections describe a comparison between the milestones we listed in [Section 4.2](#) and the proposed approach on the real platform, i.e. the iCub. We will not go deep into the details of the implementation, but we will highlight the functional capabilities and the theoretical assumptions our implementation is based on.

4.3.1 “BARE” OR “BLIND” DOUBLE TOUCH + INVARIANCE WITH RESPECT TO THE CONFIGURATION OF THE PASSIVE ARM (*tactile-motor-proprioceptive associations*)

The double touch paradigm will be detailed in [Chapter 5](#); a depiction of the scenario is illustrated in [Figure 6](#). The desired behavior is analogous to the self-exploratory capabilities needed by the biological agent and described in [Section 4.2.1](#): that is, an action aimed at stimulating concurrently two different skin parts belonging to two different kinematic chains. Due to the physical constraints our robotic platform presents, we will focus on actions involving the distal parts of the upper limbs, i.e. forearms and hands.

To this end, we can take advantage from a set of existing software tools (see [Section 3.2](#) for details):

- *Forward Kinematics + Skin Calibration* for the passive arm, in order to compute the taxels’ (“skin receptor”) coordinates in the centralized Cartesian Space (Root FoR), and determine a point in space where to reach.
- *Inverse Kinematics* for the active arm, to compute the joint configuration needed to accomplish the task, given the target 3D cartesian point.

The double-touch scenario does not take into account any distinction between reflexes and voluntary action. Furthermore, everything is relying on the existing kinematic model of the robot (links’ lengths and joints’ orientations are known) and explicit mathematical coordinate transformations. Nothing is learned, even though we are planning to do that in the future (see [Chapter 10](#) for details). It is worth noting that, as shown in [Figure 6](#), this implementation lets us automatically adapt the behavior to different arm configurations, since current joint positions automatically enter forward kinematics. We can thus safely assume that once the step described in [Section 4.2.1](#) is implemented, we will be able to automatically abstract our framework in order for it to be invariant to the configuration of the passive arm.

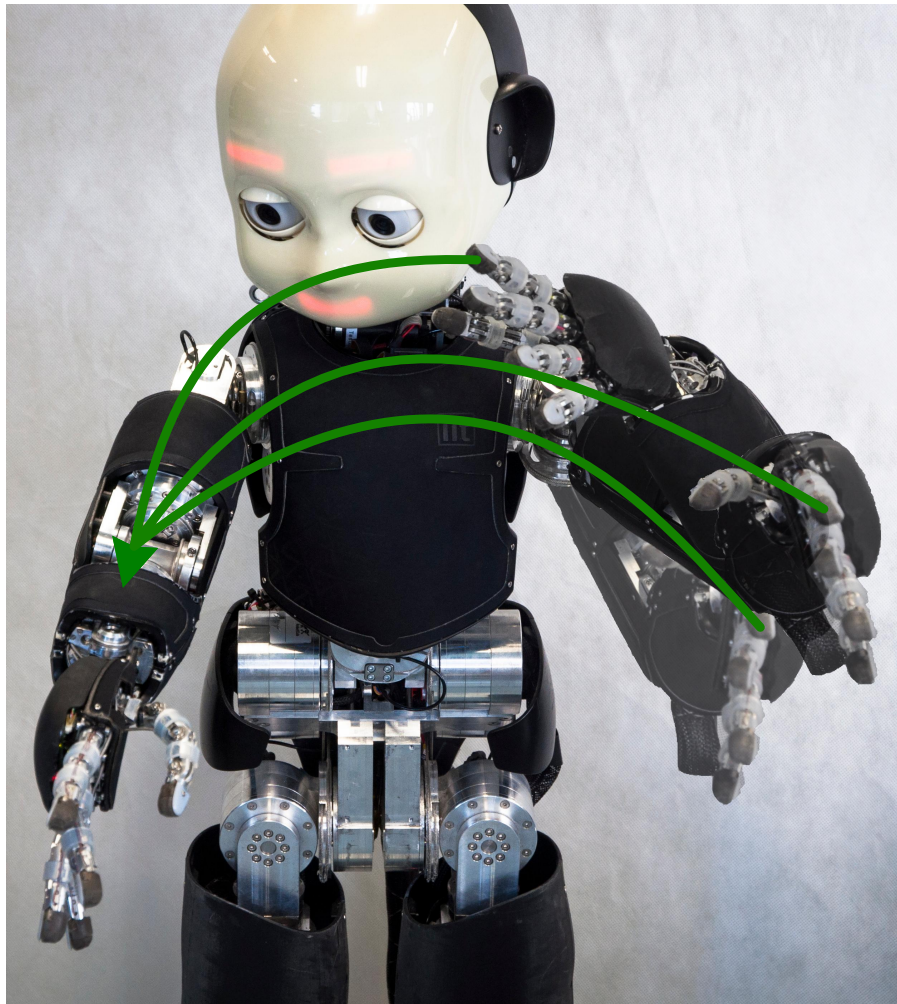


Figure 6: *Double Touch paradigm on the iCub humanoid robot.* By taking advantage of the forward and inverse kinematics model available on the iCub software repository, the double touch paradigm is able to automatically abstract from different passive and active arm configurations. See text for details.

At this stage, the robot can learn to associate the tactile stimulation occurring at the passive arm (i.e. activation of a skin patch) with the motor signal commanded at the active arm (via a convenient conversion into the robot's Root frame of reference). It will, in other words, build up a *tactile-motor-proprioceptive association* similar to what developed by the biological agent ([Section 4.2.2](#)).

4.3.2 DOUBLE TOUCH WITH VISION + INVARIANCE WITH RESPECT TO THE CONFIGURATION OF THE PASSIVE ARM AND THE HEAD PLANT (*tactile-proprioceptive-visual associations*)

The experimental scenario is the same as the one described in [Section 4.3.1](#), but now instead of taking into account the "motor signal" issued to the active arm in order to perform the double touch movement, visual information is used. The end effector belonging to the incoming arm (in our case, the tip of its index finger) will be visually detected thanks to a marker placed onto it.

At this stage, crucial is the knowledge of a *complete kinematic model* of the robot: in particular, the forward kinematics relative to the head plant that is used to transform the visual input into the Root FoR. Furthermore, a *visual tracking system* is needed in order for the robot to successfully track the active arm during the experimental session. This will be composed by a 2D tracker (see [Section 8.4.3](#) for details) and an existing gaze controller (cf. [Section 3.2.4](#)).

This milestone is crucial in the development of a *tactile-proprioceptive-visual association* able to provide a prediction of the incoming contact based upon the visual stimulus alone. It is worth noting that this representation needs to proficiently compensate for errors in the kinematic model, even though the kinematic model is still required to perform the necessary transformations. As highlighted [Section 4.3.1](#), also in this case our approach lets us automatically adapt the behavior to different neck + eye configurations, as well as different postures of the passive arm.

4.3.3 FROM THE SELF TO THE EXTERNAL WORLD: ADAPTATION OF THE MODEL TO EXTERNAL STIMULI IN ORDER TO CREATE A MARGIN OF SAFETY AROUND THE BODY (*tactile-proprioceptive-visual associations*)

At this stage, the experimental scenario described in Section 4.3.1 and 4.3.2 will be provided with the possibility to visually track not only internal, self-generated movements, but also any external object present in the nearby space and coming toward the robot. This scenario envisages the development of a *general-purpose tracker* in order to perceive potentially harmful objects coming toward the body. The representation learned in the previous step can be abstracted from the self to the external world, in order to provide a prior-to-contact activation of the tactile-visual RFs that fires not only with a self-generated incoming stimulus, but with an external source as well. That is, regardless of the source of information the robot is relying on, the tactile system is provided with a representation that is able to activate a specific part of the skin based upon an estimation of the probability of that skin part of being eventually touched by an incoming event.

4.3.4 EXPLOITATION OF THE LEARNED ASSOCIATIONS: AVOIDANCE AND CATCHING BEHAVIORS

In this step, the representation that have been gradually built up during previous stages is exploited in order to demonstrate its suitability in the construction of a margin of safety around the body. Furthermore, as described in Section 4.2.8, the same exact representation can be similarly used for the dual purpose of reaching with arbitrary body parts for objects in the nearby space. To this end, a proper *avoidance/catching controller* needs to be implemented. The – either avoidance or catching – motion is achieved thanks to a motor control placed onto the taxel that is firing: if an incoming event is activating a specific taxel, the effect will be that the taxel will either push the arm away from the incoming object (during the avoidance behavior), or pull it toward it (in the case of catching behavior). The implementation will be detailed in Part III.

Part II

THE DOUBLE TOUCH PARADIGM AS A BASIC BEHAVIOR FOR THE DEVELOPMENT OF PERIPERSONAL SPACE

Reference paper: Alessandro Roncone, Matej Hoffmann, Ugo Pattacini, and Giorgio Metta. Automatic kinematic chain calibration using artificial skin: self-touch in the iCub humanoid robot. In *Proc. IEEE Int. Conf. Robotics and Automation (ICRA)*, pages 2305–2312, 2014.

THE DOUBLE TOUCH IN THE ICUB HUMANOID ROBOT

5.1 INTRODUCTION

From a robotic perspective, double-touch can be viewed as the closure of an open kinematic chain. Clearly, robotic manipulators are designed with a different goal in mind – reaching in the operational space – and self-collisions are typically not desirable in the first place. In what follows, we will be specifically concerned with the case of self-collision, or double-touch, of two manipulators whose operational spaces are overlapping – like two arms of a humanoid robot. In order for the two end-effectors to collide, standard techniques could be used: a dual inverse kinematics task for each of the arms with the target set to any point of the shared operational space. However, a very accurate model is necessary to achieve contact. In addition, we are interested in achieving successful contacts between different parts of the manipulators, not only their the end-effectors. Hence, other parts of the body (in this paper the forearm) need to be touched by the contralateral arm.

This chapter is structured as follows: [Section 5.2](#) describes the experimental protocol used for the accomplishment of this task. [Section 5.3](#) introduces the problem as seen from a classical point of view, whereas [Section 5.4](#) presents our proposed solution to the problem. An application of this method is then performed in [Chapter 6](#).

5.2 EXPERIMENTAL PROTOCOL

The experimental protocol is schematically illustrated in [Figure 7](#). The experimenter touches the robot on a skin part (the left forearm in the picture). This is detected by the robot's tactile system; as described in [Chapter 3](#), a skin calibration (Del Prete et al. [18]) and the kinematic model of the iCub (Pattacini [63]) let us locate the position of the contact in the Root FoR. The position of the active taxel (in fact the average position of all the taxels that are stimulated) is then recorded to be used later by the inverse kinematics solver. The arms start moving toward

the self-touch configuration. The session is considered successful if a double touch actually occurs on the robot, i.e. if a contact is detected by the robot on both the arms (namely, the skin part that has been stimulated by the experimenter and the tip of the index finger of the contralateral arm, cf. [Figure 7b](#)).

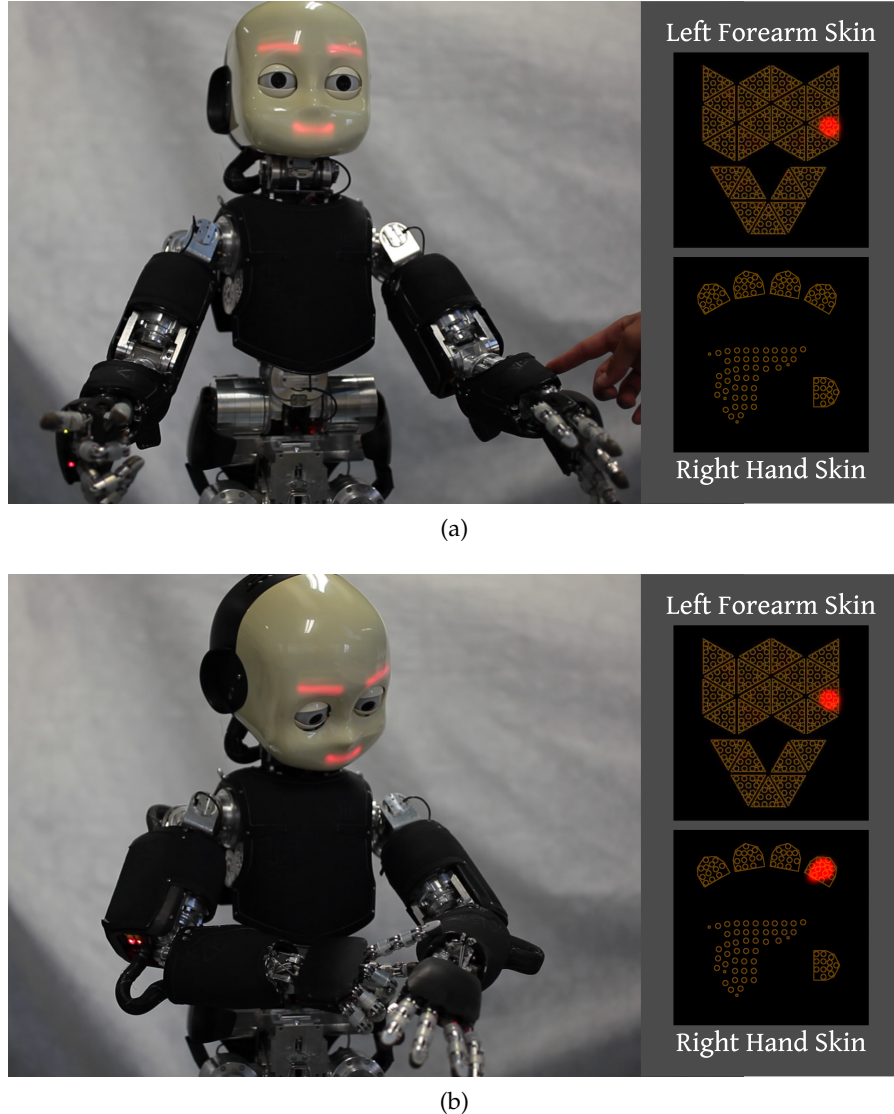


Figure 7: Self-touch experiment. (a) The iCub touched on its left forearm by the experimenter; corresponding skin activation of the forearm shown on the top right. (b) The iCub touching the previously stimulated point using the index finger of the contralateral arm. In this case, a concurrent activation of both the left forearm (top right) and the right hand's index fingertip (bottom right) is present.

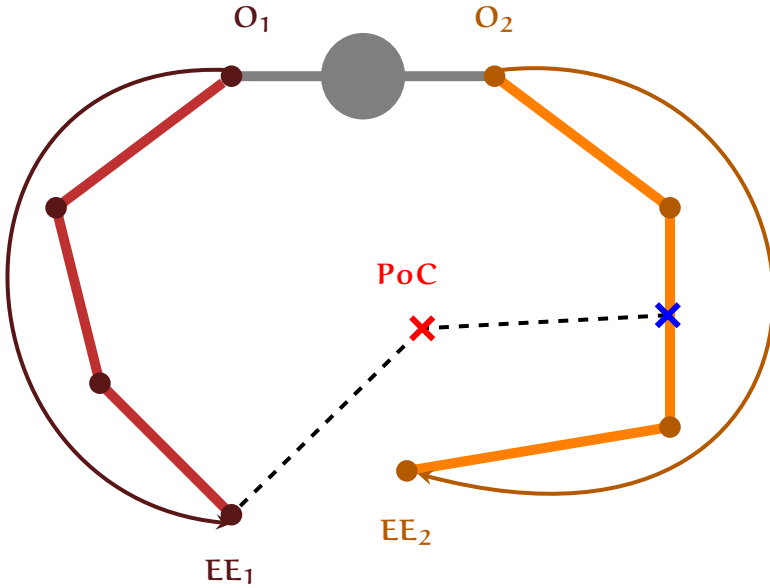


Figure 8: *Classical Approach to self collision.* The two arms, with origins O_1 and O_2 , corresponding to the shoulders of the iCub, and end-effectors EE_1 and EE_2 located in the palms of its hands, are controlled in parallel. The blue cross is the point to be touched (left forearm), whereas the red one is the final Cartesian point in which the two arms get in contact (PoC); the grey links are either not controlled or fixed.

5.3 DIFFICULTIES OF CLASSICAL APPROACH TO SELF-COLLISION OF TWO ROBOTIC MANIPULATORS

A schematic illustration of this situation is depicted in Figure 8: without loss of generality, we can assign the point to be touched (blue cross) to the left forearm; thus, the goal is to reach this point with the end-effector EE_1 of the contralateral arm (the DoFs in the schematics do not match those of the real robot). In this case, we are facing the following difficulties:

- i *Limited number of Degrees of Freedom (DoFs) for the task and kinematic constraints.* The closer the desired point of contact to the base of its kinematic chain (i.e. O_2 in Figure 8), the smaller number of DoFs are usable to position the manipulator in a suitable configuration for being reached by the contralateral arm. In addition, the operational space of a manipulator is generally bigger at a certain distance from the base and shrinks as one moves toward the origin of the kinematic chain. However, since many self-touch

configurations are located closer to the origin of the chain, this results in poor reachability/manipulability measure.

- ii *Defining the point-of-contact (PoC) in operational space.* In view of point i), there is only a limited number of configurations that succeed in achieving a self-touch and sometimes no solution exists. Moreover, the coordinates of the solution are unknown. Therefore, a suitable heuristics would be needed in order to find the common solution of two inverse kinematics problems.
- iii *Undesired self-collisions.* Apart from the specifically requested contact point, collisions between other parts can occur. Some body parts are not covered by skin (e.g., joints) and some parts, like fingers, are very fragile.

5.4 REFORMULATING THE KINEMATIC CHAIN: FROM TWO FIXED-BASE PARALLEL CHAINS TO A SINGLE FLOATING-BASE SERIAL CHAIN

The above mentioned difficulties can be significantly mitigated if the problem is reformulated: instead of parallel control of two kinematic chains, the task can be transformed into the control of a single chain that spans from the point to be touched to the contralateral end-effector. The new situation is schematically depicted in [Figure 9](#). Under this reformulation, the task is to move the end-effector EE to the origin O of the kinematic chain.

Compared to the previous situation, this brings about one key advantage, i.e. the final Cartesian PoC of the two arms is defined *implicitly* since the base of the kinematic chain is floating. The inverse kinematic solution will move both the base and the end-effector in order to make them converge at a specific point of the 3D operational space. To this end, first, one part of the kinematic chain is “reversed” – because it has to be traversed “upside down”, from the point to be touched up to the shoulder (O_2 in [Figure 8](#)). Second, an inverse kinematic solver has to be employed to get the solution to this task. The next section describes the reversal of the kinematic chain, whereas the design of the solver and the controller will be detailed in the next Sections [5.4.2](#) and [5.4.3](#).

5.4.1 THE REVERSION OF THE KINEMATIC CHAIN

The description of the kinematics is typically based on the *Denavit–Hartenberg* (DH) convention [[19](#)] with four parameters for

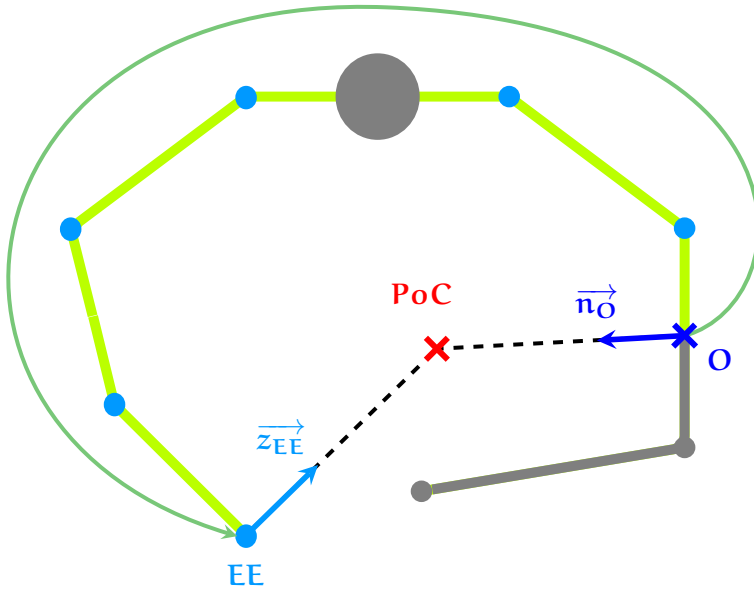


Figure 9: *Proposed Approach to self-collision.* The problem has been reformulated into a single floating-base serial chain, with origin O in the point to be touched and end-effector EE in the contralateral arm. Similarly to Figure 8, the blue cross is the point to be touched, whereas the red one is the final PoC; the grey links are either not controlled or fixed.

each joint i belonging to the chain: $\Phi_i = \{a_i, d_i, \alpha_i, \vartheta_i\}$. With an initial choice of axes, it is subsequently possible to compute a homogeneous transform matrix to describe each relative roto-translation from one joint to the next one. However, although these matrices have an inverse, they cannot be transformed into a set of valid DH parameters suitable for the reversed kinematic chain. In the following, we propose a method to compute a DH-compatible set of parameters.

Figure 10 and Figure 11 depict a comparison between the original DH convention for the forward chain and the proposed approach for its reversed version. Figure 10 illustrates the reference frames' attachment for a generic joint i belonging to a chain pointing from left to right, whereas Figure 11 describes the proposed solution for the reversed chain (traversed from right to left).

In order to reverse the chain, we changed the order of the joints such that the end-effector of the original direct chain becomes the origin of the new one. However, the placement of the reference frames has been kept the same. This requires a cor-

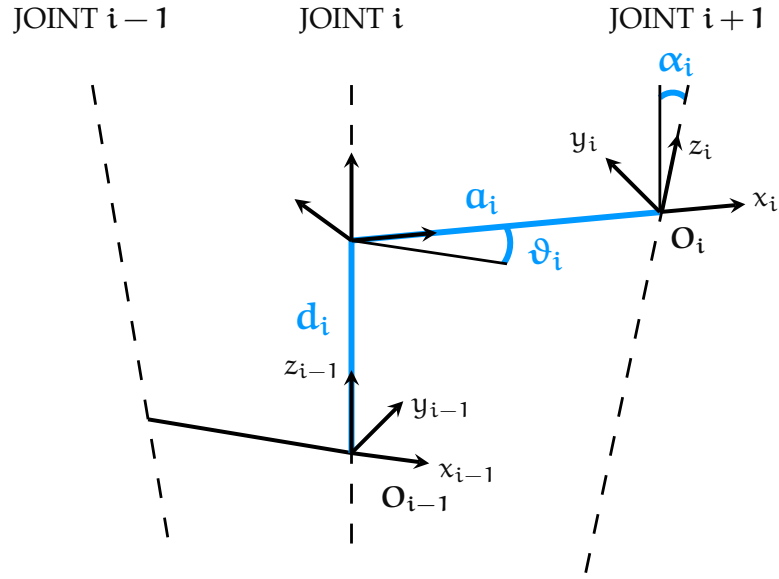


Figure 10: *Original Denavit–Hartenberg convention.* The homogeneous roto-translation matrix between the two frames of reference O_{i-1} and O_i is defined by a set of four parameters $\Phi_i = \{a_i, d_i, \alpha_i, \vartheta_i\}$. An in-depth analysis of the standard DH notation is available in [Appendix A](#).

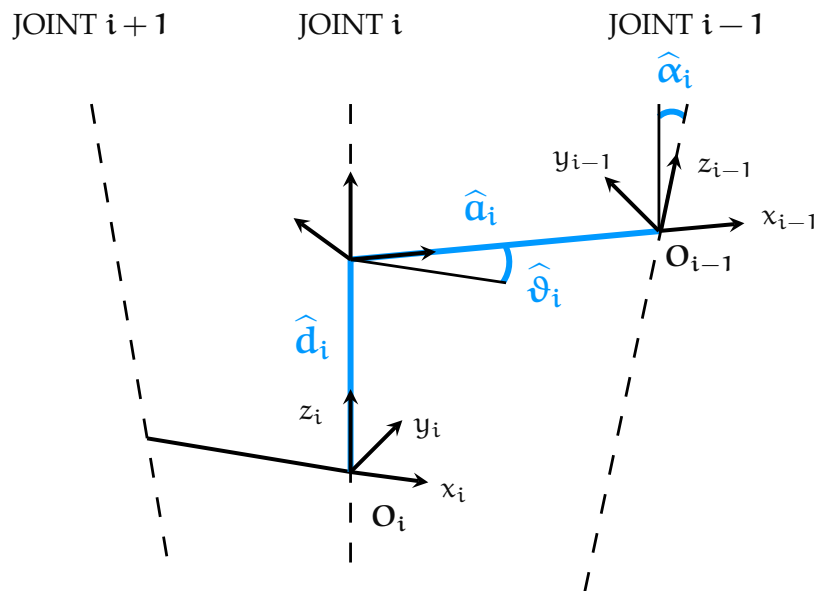


Figure 11: *Proposed solution for the reversion of a kinematic chain expressed in DH notation.* In order to “reverse” the original kinematic chain, the reference frames for the links have been kept coincident with the original ones.

responding change of the parameters of every joint. The new parameters, $\widehat{\Phi}_i = \{\widehat{a}_i, \widehat{d}_i, \widehat{\alpha}_i, \widehat{\vartheta}_i\}$, are calculated as:

$$\begin{aligned}\langle \widehat{a}_0, \widehat{a}_1, \dots, \widehat{a}_n \rangle &= \langle -a_n, -a_{n-1}, \dots, -a_0 \rangle \\ \langle \widehat{d}_0, \widehat{d}_1, \dots, \widehat{d}_n \rangle &= \langle -d_n, -d_{n-1}, \dots, -d_0 \rangle \\ \langle \widehat{\alpha}_0, \widehat{\alpha}_1, \dots, \widehat{\alpha}_n \rangle &= \langle -\alpha_n, -\alpha_{n-1}, \dots, -\alpha_0 \rangle \\ \langle \widehat{\vartheta}_0, \widehat{\vartheta}_1, \dots, \widehat{\vartheta}_n \rangle &= \langle -\vartheta_n, -\vartheta_{n-1}, \dots, -\vartheta_0 \rangle,\end{aligned}\tag{1}$$

where $\Phi_i = \{a_i, d_i, \alpha_i, \vartheta_i\}$ is the original set of DH parameters for the i -th link.

The standard transform matrix for the direct chain dDH is shown below:

$$dDH = \begin{bmatrix} c_\vartheta & -s_\vartheta c_\alpha & s_\vartheta s_\alpha & ac_\vartheta \\ s_\vartheta & c_\vartheta c_\alpha & -c_\vartheta s_\alpha & as_\vartheta \\ 0 & s_\alpha & c_\alpha & d \\ 0 & 0 & 0 & 1 \end{bmatrix}\tag{2}$$

Under the convention defined above, the transform matrix for the reversed chain, rDH corresponds to the inverse of the standard transform matrix (i.e. dDH^{-1}), but with the new set of parameters $\widehat{\Phi}_i$. Substituting Φ_i with $\widehat{\Phi}_i$ in dDH^{-1} thus gives the following form for rDH:

$$rDH = \begin{bmatrix} c_{\widehat{\vartheta}} & -s_{\widehat{\vartheta}} & 0 & \widehat{a} \\ s_{\widehat{\vartheta}} c_{\widehat{\alpha}} & c_{\widehat{\vartheta}} c_{\widehat{\alpha}} & -s_{\widehat{\alpha}} & -\widehat{d} s_{\widehat{\alpha}} \\ s_{\widehat{\vartheta}} s_{\widehat{\alpha}} & c_{\widehat{\vartheta}} s_{\widehat{\alpha}} & c_{\widehat{\alpha}} & \widehat{d} c_{\widehat{\alpha}} \\ 0 & 0 & 0 & 1 \end{bmatrix}\tag{3}$$

Under this approach, the parameters lose their physical meaning (those related to lengths, such as \widehat{a}_i and \widehat{d}_i , become negative), but the geometrical representation is correctly preserved. In addition, the existing machinery for the kinematic computation (e.g. the differential kinematics) can be maintained, because the Jacobians are still dependent on the same parameter (i.e. $\widehat{\vartheta}_i$ for revolute joints)¹.

¹ In the case of differential and higher order kinematics, it is worth noting that with the proposed approach the axis of rotation of the i -th link is preserved, but the joint will rotate in opposite direction. Thus, each Jacobian matrix will carry opposite sign with respect to the Jacobian expressed in the original D-H notation.

5.4.2 INVERSE KINEMATICS SOLVER

The task – in the formulation proposed above – is an inverse kinematic resolution of a serial chain with a floating base. Hence, we consider the problem of computing the values of joint angles $\mathbf{q}^* \in \mathbb{R}^n$ such that the end-effector reaches a given position $\mathbf{x}_d \in \mathbb{R}^6$ (we are considering the desired position and orientation as a single 6D vector, rotations are described by the axis-angle representation). In addition, \mathbf{q}^* has to satisfy a number of constraints, expressed as a set of inequalities. Formally, the problem can be stated as follows:

$$\begin{aligned}\mathbf{q}^* &= \arg \min_{\mathbf{q} \in \mathbb{R}^n} \langle \mathbf{n}_O, \mathbf{z}_{EE} \rangle = \\ &= \arg \min_{\mathbf{q} \in \mathbb{R}^n} \left\{ \|\mathbf{n}_O\| \cdot \|\mathbf{z}_{EE}\| \cdot \cos(\alpha) \right\} \\ &\text{s.t. } \begin{cases} \|K_x(\mathbf{q}) - \mathbf{O}\|^2 < \varepsilon \\ \mathbf{q}_l < \mathbf{q} < \mathbf{q}_u \end{cases},\end{aligned}\quad (4)$$

where:

- \mathbf{O} is the origin of the kinematic chain (i.e. $[0 \ 0 \ 0]$);
- \mathbf{n}_O is a unit vector perpendicular to the first link of the kinematic chain and originating in \mathbf{O} ;
- \mathbf{z}_{EE} is the z -axis of the end-effector, as specified in [Figure 9](#);
- α is the angle between \mathbf{n}_O and \mathbf{z}_{EE} ;
- K_x is the forward kinematic function that represents the position of the end-effector;
- \mathbf{q}_l and \mathbf{q}_u are vectors describing the joints' lower and upper limits.

The optimization criterion is thus the minimization of the scalar product between the z -axis of the end-effector and a vector \mathbf{n}_O normal to the surface to be touched. Since both vectors are of unit length, the optimization boils down to the minimization of $\cos(\alpha)$, that is the normal of the target and the z -axis of the end-effector pointing in exactly opposite directions (where $\alpha = \pi$ and $\cos(\alpha) = -1$). Further, the solution to [Equation 4](#) has to satisfy a set of additional constraints: in particular, we require that the end-effector's position is coincident with the origin of the kinematic chain (up to a certain tolerance ε), and

that the solution lies between a set of lower and upper bounds ($\mathbf{q}_l, \mathbf{q}_u \in \mathbb{R}^n$) of physically admissible values for the joints. This description of the problem entails that the final position and joint limits are always satisfied (being a constrained optimization problem) whereas the orientation of the end-effector may have a residual error (the minimum cost may not be zero).

It is worth noting that the design choice of posing the inverse kinematics problem as a nonlinear constrained optimization task makes it intrinsically scalable to any number of degrees of freedom, i.e. it is possible to perform the task for any – suitable – kinematic chain without changing the software code base. Moreover, it becomes easy to add new constraints to the solver as linear or nonlinear inequalities either in task or joint space. This has proven useful in the moment in which the nonlinearities at the iCub shoulders were involved: similarly to what developed by Pattacini [63] for his cartesian solver, we have the need of constraining the solution to the configurations that do not break the tendons at the shoulder (see [Section 3.1.1](#) for details about the hardware). To this end, three linear inequalities are proficiently included into [Equation 4](#) in the following form:

$$\mathbf{l} \leq \mathbf{C} \cdot \mathbf{q}_s \mathbf{h} \leq \mathbf{L}, \quad (5)$$

where $\mathbf{q}_s \mathbf{h}$ is the vector describing the shoulder joints, \mathbf{C} is a proper coupling matrix, and \mathbf{l} and \mathbf{L} are the lower and upper limits [Equation 5](#) is imposing to the tendon lengths.

Kinematically, the inverse kinematics task presented in [Equation 4](#) can be explained as a reaching problem (the end-effector reaches the origin) with orientation normal to the surface of the touched point. The particular formulation of the problem (namely, a serial chain with a floating base) implies that both arms are automatically controlled in order to solve the task. Since the iCub arms are redundant, the solver has a certain freedom to impose the final configuration while satisfying the joint limit or collision constraints. Nonetheless, the solution we proposed has dramatically increased the redundancy of the task: the adoption of a single serial chain that spans from the point to be touched up to the contralateral end-effector has further increased the number of degrees of freedom available ².

In order to solve the problem described by [Equation 4](#), an interior point optimization technique is used, in particular we

² In our concrete case, where the point to be touched is located on the robot's left forearm, 12 DoF are used – 5 on the manipulator that is touched, 7 in the contralateral one.

employ *IpOpt* [85], a public domain software package designed for large-scale nonlinear optimization problems.

5.4.3 CONTROLLER

The motor control has been achieved by means of a simple position control in most of the joints. Two of them (namely, the shoulder yaw and the elbow of the left arm) have been controlled in impedance mode, in order to ensure more compliance and thus intrinsic safety during contact.

6

APPLICATIONS OF THE DOUBLE-TOUCH PARADIGM: AUTOMATIC KINEMATIC CHAIN CALIBRATION USING ARTIFICIAL SKIN

6.1 INTRODUCTION

Practically all robots performing manipulation or reaching tasks rely on models of their kinematics and dynamics. Their success is largely determined by the accuracy of such models. This is even more so if they operate with limited feedback, as it is often the case when we consider humanoid robots in real-time interaction with the environment. The models are typically based on mechanical design specifications (such as CAD drawings) of the robot. However, inaccuracies creep in in many ways as for example in the assembly process, in mechanical elasticity, or simply because of cheap design or components. Therefore, the actual model parameters of every robot exemplar have to be found by means of a calibration procedure.

In this chapter, we will be concerned with calibration of the standard *Denavit-Hartenberg* (DH) parameters that fully describe the robot's kinematics through a series of rotations and translations from the base of the robot up to the end-effector. If the configuration of every joint is known, the full pose (3D position and 3D orientation) of the end-effector can be obtained in the base reference frame. However, in order to calibrate the robot's parameters additional information is required. This can be obtained by observing the end-effector configuration (or several of its components) w.r.t. the base. The literature provides various examples of apparatuses that can measure one or more of the components of the end-effector pose employing mechanical, visual, or laser systems. An overview of these – so-called *open-loop calibration methods* – is presented in [43, 42]. Alternatively, physical constraints on the end-effector position or orientation can substitute for measurements (cf. [43, 42] again for an overview). As the robot is in contact for example with the ground, these methods are called *closed-loop*. In fact, the prob-

lem can be framed in such a way that the open- and closed-loop methods are mathematically equivalent – the external measurement systems can be modeled as additional joints and links that close a virtual loop; in both cases the excess of sensed over actual degrees of freedom is needed, as expressed by the calibration index [43], which at the same time defines the number of equations per pose that are available for calibration. Recently, apparatuses extending the kinematic chain using a laser pointer have become popular (e.g., [28, 45]). Different arrangements have different calibration indices, accuracy, requirements on the environment, and cost. Nevertheless, all of them invariably require to know beforehand a number of quantities from the robot’s environment (such as a measurement system with a known pose w.r.t. the robot base, a fixed contact point in the environment where the robot can be attached, a surface that is known to be planar on which the robot can slide, etc.). These conditions have to be present for recalibration to be performed.

This has motivated alternative solutions to the self-calibration problem that are also “*self-contained*” and can be performed autonomously by the robot. One option is self-observation using a stereo camera mounted on the robot. This has been shown in a humanoid robot in [37] and in [54] in a humanoid torso setup. The limit of these approaches is usually to be found in the accuracy of the pose observation from visual input. Special markers need to be used and attached to known positions on the robot, such as on the end-effector. Alternatively, inertial sensors can be used. Xsens for example developed a wearable setup for humans composed of several inertial measurement units (IMUs) [71], which, however, requires a specific *a priori* body model. Mittendorfer and Cheng [58] presented a method that uses data from accelerometers distributed on the surface of a robot (this matches the artificial skin they developed [56]) to calibrate the DH parameters. Other approaches that do not rely on an explicit given representation – like the DH parameters –, but that learn more implicit relationships between proprioceptive and visual variables, for example, have been also developed (see [40] for a review).

In the following, we present an approach that closes the kinematic loop in a completely new way: i.e. by self-touch. Our inspiration is in biology: infants do not have access to calibration chambers or ground truth measurements. In addition, in early infancy, the visual system is still immature, thus an unlikely source of accurate calibration information. A possible “*self-calibration*” strategy entails therefore self-stimulation: touching their own body gives rise to unique stimulation pat-

terns – tactile stimulation on the touching and the touched part, together with corresponding proprioceptive feedback [69, 78]. From a robotics point of view, this constitutes a compact calibration procedure that can be repeated at any given time and that does not incur any additional cost. Furthermore, not only the kinematic model, but also the geometry of the robot (its volume in space) can be learned. The new requirements induced by this approach are: (i) the availability of tactile arrays on the robot’s surface; (ii) a sufficient agility to permit self-touch (or self-collision) configurations; (iii) the availability of a controller – such as hybrid position-force control – that allows safe execution of the movements which generate self collisions. These three conditions are satisfied by the iCub humanoid robot – the experimental platform employed in this work. The method proposed is however applicable to a much wider set of platforms. First and foremost, solutions to robot tactile sensing are now numerous (see [16] for a survey) – many of them with the ambition of providing a portable solution that can be simply attached to robots of any shape. Second, any robot that possesses multiple limbs – especially humanoid robots – will be able to self-touch (apart from pathological cases). Third, many robots have force/torque sensing and corresponding controllers that can actively control impedance, thus allowing for safe interactions with the environment and with themselves (e.g., [17]).

We present a method for calibration using self-touch and describe its experimental validation. The theoretical contribution consists in an advantageous transformation of the problem of controlling two serial chains (like two arms of a humanoid robot) to self-collide at a certain point in space into a single floating-base serial chain that originates at the contact point and ends in the “end-effector” of the other arm – the point that is “touching”. Interestingly, this method (described in [Chapter 5](#)) encompasses both open- and closed-loop calibration. If different points on the robot’s skin are touched, an initial calibration of the skin serves as a “metrology” to observe the 3D position of the end-effector. This can be used for calibrating the DH parameters only, or, simultaneously, to improve the calibration of the tactile array. Alternatively, keeping the same contact point and varying the position of the joints constitutes a closed-loop calibration setup, where the end-effector is constrained in a known position. The advantage of our approach is that a large number of such points are automatically available corresponding to the skin sensors’ positions. The experimental validation in this work uses the first method: contact points are varied and corresponding joint configurations are recorded. Optimization

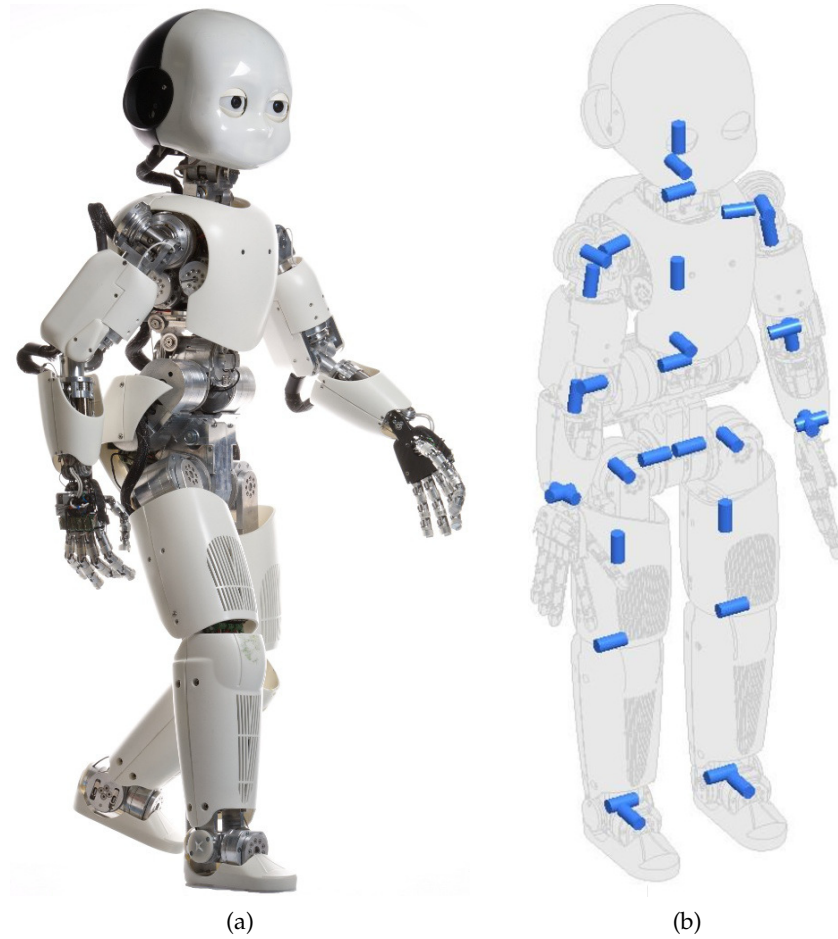


Figure 12: The iCub robot (left) and its kinematic structure (right).

of the DH parameters is then performed starting from different initial configurations.

This chapter is structured as follows. In [Section 6.2](#), the robot and the scenario are presented. The experimental protocol and the optimization problem are defined. The optimization experiments are presented in [Section 6.3](#), followed by Conclusions and Future work ([Chapter 7](#)).

6.2 METHODS AND EXPERIMENTAL SETUP

The experimental platform we used for this work is the iCub. The core elements crucial for the pursuit of this work have been extensively presented in [Chapter 3](#); please refer to [Section 3.2.2](#) and [Section 3.2.2](#) for a detailed description of the iCub artificial skin and its overall kinematic modeling. The theoretical analysis of implementation of movements that generate controlled self-collisions has been instead featured in [Chapter 5](#). In the

following, we present the data collection and optimization procedures for the update of the DH parameters.

6.2.1 DATA COLLECTION AND OPTIMIZATION

6.2.1.1 *Experimental protocol*

The experimental protocol is similar to what presented in [Section 5.2](#) and in [Figure 7](#). The double touch scenario is used to collect suitable samples in order to perform a closed-loop calibration. If the double touch is successful, the contact is detected by the robot (on the touched skin part and on the tip of the index finger of the touching arm). The coordinates of this point (relying on the skin calibration) are recorded together with the current joint configuration, and constitute one data point that is later used for subsequent optimization of the kinematic model. Due to inaccuracies in the initial model, not all attempts result in a final self-touch configuration – these trials are ignored. In total, 100 successful data points were collected in this way. Then, in order to speed up data collection (only the final configuration is important for the calibration), further 200 points were collected by setting the joints to idle and generating the self-touch configurations by the experimenters.

6.2.1.2 *Problem formulation*

Referring to Hollerbach et al. [42], a kinematic calibration has to optimize the vector of DH parameters for the chain under evaluation. It is given by:

$$\Phi_i = \{a_i, d_i, \alpha_i, o_i\} , \quad (6)$$

with:

- $i \in [1, n]$;
- a, d, α the first three parameters of the DH formulation ([Appendix A](#));
- o the offset that specifies the positioning of the encoders on the joints with respect to the DH representation. It is part of the model that should be subject to calibration and is therefore also included in the optimization (like in Hollerbach et al. [42]).

In the experimental setup presented here, the kinematic chain consists of 12 DoFs. With 4 parameters per joint, the number of

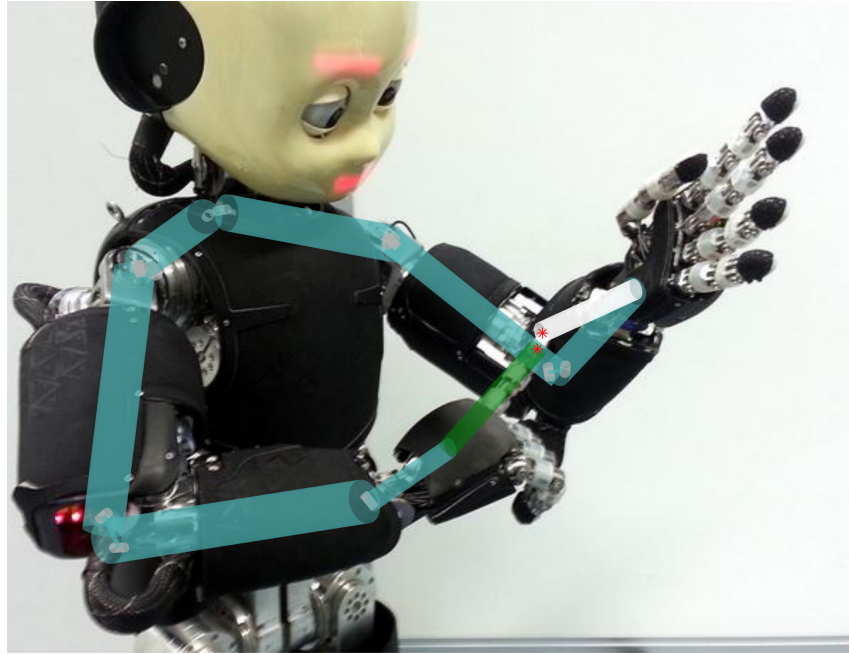


Figure 13: *Depiction of the kinematic chain optimization.* The chain is closed on one end through the skin (a fixed transformation from the taxel to the wrist) and through the index finger on the other end (another fixed transformation from the contralateral hand to the fingertip).

parameters to be optimized is thus 48 (see [Table 2](#), first column). A schematic illustration of this is depicted in [Figure 13](#). The kinematic chain is closed through two fixed transformations at its ends (skin – white in the figure; index finger – green in the figure). These transform matrices are kept constant and their parameters are not optimized.

The parameter calibration is obtained by using the same non linear optimizer described earlier (IpOpt – Wächter and Biegler [[85](#)]). The cost is set in order to minimize the total position error:

$$\Phi^* = \arg \min_{\Phi} \sum_{m=1}^M \|p_s - p_e(\Phi, \vartheta_m)\| \quad , \quad (7)$$

where:

- ϑ_m are the joint angles of the m -th sample as read from the joint encoders (for a total of $M = 300$ samples);
- p_e is the estimated position (as function of the joint angles and the current parameter values);
- p_s is the position of the end-effector as measured from the skin.

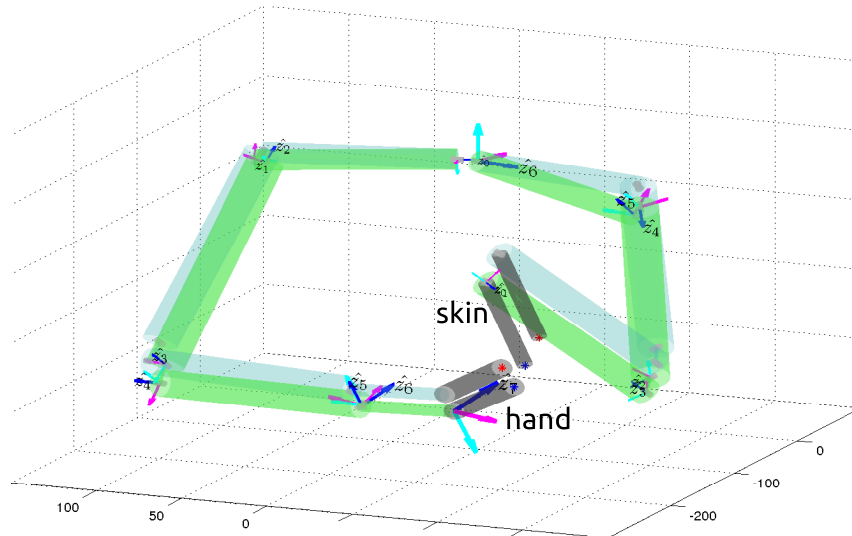


Figure 14: Initial vs. optimized kinematic chain. The initial parameters (CAD values) shown in blue, the optimized in green. The chain is closed through two fixed transformations: on one end through the skin and through the index finger on the other end.

6.3 EXPERIMENTAL RESULTS

Using the data set collected according to the procedure described in the previous section, we conducted three optimization experiments. They are described in the following sections.

6.3.1 EXP. 1 - OPTIMIZATION OF PARAMETERS FROM CAD MODEL

In this experiment, the initial values of the DH parameters are those from the CAD model. Assuming that the skin calibration is correct, these parameters can be used by the optimizer with the aim of minimizing the error of the forward kinematic function w.r.t. the position of the taxels. The result is shown in Figure 14. The values after optimization can be seen in the “*Exp 1*” column of Table 2.

The measure of performance is the error on the end-effector position – euclidean distance of the predicted position of the end-effector to the taxel position from the skin calibration – as shown in the first row of Table 1. As expected, here the improvement is small owing to the accurate initial estimate of the DH parameters derived from the CAD models. Nonetheless, the error in the task is reduced by 7.9%.

Table 1: Error at the end-effector before and after calibration. For each of the experimental sessions listed in the first column (i.e. optimization from CAD values, optimization with 10% noise and finally with 30% noise), a comparison between the error at the end-effector prior (second column) and after (third column) the calibration is provided. The improvement is between 7.9% (Exp. 1) and 65% (Exp. 3).

| | <i>Initial (m)</i> | <i>Optimized (m)</i> |
|-------------------|---------------------|----------------------|
| Exp 1 | 0.0226 | 0.0208 |
| Exp 2 (10% noise) | 0.0819 ± 0.0299 | 0.0377 ± 0.0139 |
| Exp 3 (30% noise) | 0.1919 ± 0.0301 | 0.0664 ± 0.0175 |

6.3.2 EXP. 2 AND 3 - OPTIMIZATION WITH 10% AND 30% NOISE ON INITIAL VALUES

The initial parameter values in [Section 6.3.1](#) are naturally already reasonable guesses of the real parameters. In order to further test our proposed method, we have conducted additional experiments with more noisy estimates of the initial parameters. Therefore, we perturbed the CAD parameters as follows:

$$\Phi_i^n = p * \text{uniform}[-1; 1] * \Phi_i + \Phi_i \quad (8)$$

$p = [0.1, 0.3]$

where:

- Φ_i^n is the new set of perturbed parameters;
- p is the amount of noise with a uniform distribution (effectively 10% or 30% of the parameter value);
- Φ_i is the original set of parameters.

The noise is thus proportional to the initial value of every DH parameter (angle or length), with a special consequence that parameters with an initial value of zero are not perturbed. All parameters – including the ones with zero values – are then subject to optimization.

Five different initial configurations were generated and the optimizer was run using the same data set (300 data points). The results can be seen in [Table 1](#) and [Table 2](#) (fourth and fifth column). In the 10% noise case, the reduction of error is substantial in all the tests that have been run (54% on average - [Table 1](#)). In Experiment 3, with 30% noise on the DH parameters, qualitatively similar conclusions can be drawn: the error on the task is reduced by 65% on average after optimization.

Table 2: *DH Parameters and optimization.* The first column lists all the 48 parameters that have been optimized during the experimental session (i.e. 4 parameters for each of the 12 joints under consideration). Second column shows their original DH value (extrapolated from the CAD model), whereas the third, fourth and fifth columns illustrate their value after Experiment 1, 2 and 3 respectively.

| <i>CAD</i> | | <i>Exp 1</i> (μ) | <i>Exp 2 – 10% noise</i> ($\mu \pm \sigma$) | <i>Exp 2 – 30% noise</i> ($\mu \pm \sigma$) |
|------------|---------|---------------------------|--|--|
| a_1 | 0 | 0 | 0 ± 0 | 0 ± 0 |
| d_1 | -0.1373 | -0.1373 | -0.1343 ± 0.0097 | -0.1477 ± 0.0206 |
| α_1 | -1.5708 | -1.5968 | -1.6292 ± 0.0787 | -1.7148 ± 0.1119 |
| o_1 | 1.5708 | 1.5887 | 1.5770 ± 0.1134 | 1.8133 ± 0.2217 |
| a_2 | 0.0150 | 0.0126 | 0.0129 ± 0.0027 | 0.0051 ± 0.0073 |
| d_2 | 0 | -0.0026 | -0.0020 ± 0.0028 | -0.0074 ± 0.0083 |
| α_2 | -1.5708 | -1.6014 | -1.5165 ± 0.0703 | -1.5658 ± 0.3268 |
| o_2 | 0 | -0.0040 | -0.0013 ± 0.0572 | 0.0194 ± 0.1127 |
| a_3 | -0.0150 | -0.0179 | -0.0166 ± 0.0029 | -0.0236 ± 0.0086 |
| d_3 | -0.1523 | -0.1604 | -0.1560 ± 0.0050 | -0.1963 ± 0.0187 |
| α_3 | 1.5708 | 1.5887 | 1.5848 ± 0.0526 | 1.6144 ± 0.2614 |
| o_3 | -1.3090 | -1.3360 | -1.3508 ± 0.0511 | -1.3663 ± 0.4323 |
| a_4 | 0 | -0.0064 | -0.0029 ± 0.0029 | -0.0195 ± 0.0164 |
| d_4 | 0 | -0.0060 | -0.0029 ± 0.0029 | -0.0190 ± 0.0168 |
| α_4 | -1.5708 | -1.5487 | -1.5295 ± 0.0496 | -1.4276 ± 0.3057 |
| o_4 | 1.5708 | 1.5841 | 1.5163 ± 0.1037 | 1.5072 ± 0.2475 |
| a_5 | 0 | 0.0216 | -0.0029 ± 0.0029 | -0.0162 ± 0.0232 |
| d_5 | -0.1077 | -0.1153 | -0.1099 ± 0.0042 | -0.1175 ± 0.0187 |
| α_5 | 1.5708 | 1.5841 | 1.5660 ± 0.1299 | 1.7101 ± 0.3909 |
| o_5 | -1.5708 | -1.6014 | -1.5712 ± 0.0439 | -1.7181 ± 0.3643 |
| a_6 | 0 | -0.0060 | -0.0029 ± 0.0029 | -0.0217 ± 0.0194 |
| d_6 | -0.1077 | -0.1119 | -0.1123 ± 0.0072 | -0.1222 ± 0.0288 |
| α_6 | 1.5708 | 1.5839 | 1.5609 ± 0.0982 | 1.5766 ± 0.1594 |
| o_6 | -1.5708 | -1.6024 | -1.6297 ± 0.0964 | -1.6054 ± 0.2078 |
| a_7 | 0 | -0.0069 | -0.0041 ± 0.0052 | 0.0166 ± 0.0479 |
| d_7 | 0 | -0.0030 | -0.0029 ± 0.0029 | -0.0155 ± 0.0203 |
| α_7 | -1.5708 | -1.5963 | -1.5644 ± 0.0352 | -1.5986 ± 0.2675 |
| o_7 | -1.5708 | -1.5963 | -1.5716 ± 0.0841 | -1.6173 ± 0.3691 |
| a_8 | -0.0150 | -0.0171 | -0.0172 ± 0.0029 | -0.0170 ± 0.0150 |
| d_8 | -0.1523 | -0.1605 | -0.1541 ± 0.0077 | -0.1176 ± 0.0496 |
| α_8 | -1.5708 | -1.5831 | -1.5748 ± 0.1046 | -1.6635 ± 0.2511 |
| o_8 | -1.8326 | -1.8618 | -1.8268 ± 0.1184 | -1.8297 ± 0.2338 |
| a_9 | 0.0150 | 0.0133 | 0.0129 ± 0.0030 | 0.0012 ± 0.0296 |
| d_9 | 0 | -0.0026 | -0.0028 ± 0.0028 | -0.0080 ± 0.0080 |

continued on next page

Table 2: continued from previous page

| <i>CAD</i> | | <i>Exp 1</i> (μ) | <i>Exp 2 - 10% noise</i> ($\mu \pm \sigma$) | <i>Exp 2 - 30% noise</i> ($\mu \pm \sigma$) |
|---------------|---------|---------------------------|--|--|
| α_9 | 1.5708 | 1.5891 | 1.5990 ± 0.1019 | 1.5853 ± 0.2720 |
| o_9 | 0 | -0.0040 | 0.0011 ± 0.0565 | 0.0095 ± 0.0985 |
| a_{10} | 0 | -0.0019 | -0.0025 ± 0.0037 | -0.0050 ± 0.0144 |
| d_{10} | -0.1373 | -0.1411 | -0.1410 ± 0.0093 | -0.1279 ± 0.0395 |
| α_{10} | 1.5708 | 1.5915 | 1.6521 ± 0.0582 | 1.6108 ± 0.2230 |
| o_{10} | -1.5708 | -1.5937 | -1.6092 ± 0.1299 | -1.6252 ± 0.3956 |
| a_{11} | 0 | 0.0008 | -0.0028 ± 0.0028 | -0.0045 ± 0.0148 |
| d_{11} | 0 | -0.0011 | -0.0029 ± 0.0029 | -0.0046 ± 0.0147 |
| α_{11} | 1.5708 | 1.5918 | 1.6273 ± 0.1152 | 1.5263 ± 0.2460 |
| o_{11} | 1.5708 | 1.5915 | 1.6771 ± 0.0766 | 1.5118 ± 0.3519 |
| a_{12} | 0.0625 | 0.0623 | 0.0579 ± 0.0038 | 0.0528 ± 0.0099 |
| d_{12} | 0.0160 | 0.0151 | 0.0136 ± 0.0026 | 0.0102 ± 0.0142 |
| α_{12} | 0 | -0.0012 | -0.0102 ± 0.0838 | -0.0244 ± 0.1054 |
| o_{12} | 3.1416 | 3.1842 | 3.1370 ± 0.1743 | 3.0448 ± 0.4766 |

PART II: DISCUSSION AND CONCLUSIONS

In the work described in [Chapter 5](#) and [Chapter 6](#), we presented a new method for robotic self-calibration that does not rely on any external measurement apparatus or on constraints arising from specific contact with the environment. Furthermore, no sensing at a distance (vision, laser) is needed. Instead, taking inspiration from early infant development and exploiting the artificial skin on the iCub robot, we exploited the correspondences between the tactile and proprioceptive modality – in our case tactile inputs and joint angle values – to calibrate the parameters of a kinematic chain. The data sets were collected using a novel self-touch behavior that is generated autonomously by the robot: the inverse kinematic solver was relying on an advantageous reformulation of the reaching problem for the two arms of the iCub into a single floating-base kinematic chain. Then, optimization of the DH parameters was performed through minimization of the distance between positions predicted by forward kinematics and known positions of the taxels on the robotic skin. An improvement over the CAD values was achieved. Furthermore, configurations with 10% and 30% noise on the initial DH parameters were also subject to optimization and resulted in an average improvement of 54% and 65% respectively.

As part of our future work we will investigate a variation on the self-touch scenario where the robot will keep a contact configuration for an extended period of time while varying the joint configurations. The utility of data sets originating from this “closed-loop” strategy will be compared with the data set used in this initial work. Furthermore, several additional sources of inaccuracy were not considered here. These include the skin calibration, the kinematics of the hand (from wrist to fingertip), or the precision of the joint measurements. These could be subject to optimization in the future as well. At the same time, while self-touch theoretically provides the means to come close to perfect accuracy when reaching for one’s own body, in the future, we want to investigate extrapolation of the calibration to the whole operational space. Finally, additional

loops can be closed by adding the visual modality. Using stereo vision and adding the head and eye kinematics while keeping the same methodology – that is the point where “double touch” occurs can be observed – will allow for calibration of all the remaining components, including camera projective maps. A theoretical analysis of the observability and identifiability with respect to the contributions of different data collection methods and individual sensory modalities will be performed.

Part III

PERIPERSONAL SPACE AND MARGIN OF SAFETY AROUND THE BODY

Reference paper: Alessandro Roncone, Matej Hoffmann, Ugo Pattacini, Luciano Fadiga, and Giorgio Metta. Peripersonal space and margin of safety around the body: learning tactile-visual associations in a humanoid robot with artificial skin. Manuscript, 2015.

Further, this part marginally draws inspiration from the following publication: Alessandro Roncone, Matej Hoffmann, Ugo Pattacini, and Giorgio Metta. Learning peripersonal space representation through artificial skin for avoidance and reaching with whole body surface. Submitted to the 2015 IEEE/RSJ International Conference on Intelligent Robots and Systems (IROS), 2015.

8

LEARNING TACTILE-VISUAL ASSOCIATIONS ON A HUMANOID ROBOT WITH ARTIFICIAL SKIN

8.1 INTRODUCTION

In this chapter, we present a solution to the problem of building a tactile-visual representation on the iCub humanoid robot through interaction with the self and the external world. In pursuance of this, we built a series of receptive fields anchored to each taxel of the iCub’s skin. Starting from an initially blank state, we exposed the iCub robot to objects coming onto its body surface. The objects are tracked and their trajectory recorded¹. In particular, the distance and velocity of every object entering this RF is recorded with respect to the taxel’s FoR, together with information whether the object has eventually contacted the particular skin area or not. If the objects eventually contact the body, respective taxels update their representation. This gives rise to a set of probabilities that are updated incrementally and that carry information about the likelihood of particular events in the environment physically contacting a particular set of taxels. We explore two modes of this “spatial” RF. First, the approaching object is the robot’s own body – its contralateral arm, for example. As described in [Chapter 5](#), the robot has been made able to execute self-touching behaviors that allow him to calibrate a tactile-proprioceptive representation of the space – essentially a self-collision space – around every taxel. Second, the objects are any oncoming objects in the environment that are perceived visually and hence tactile-visual associations are learned.

Coordinate transformations to the FoRs of individual taxels are indispensable – existing kinematic model and FoR transformation modules available for the iCub robot, together with current joint encoder values, will be used (cf. [Chapter 3](#)). However, these transformations are subject to numerous errors (in-

¹ Considering their general nature (i.e. a recorded trajectory can be either referred to the robot’s own arm or any external object), we will frequently refer to them as *events*.

accuracy of kinematic model, calibration of cameras, skin calibration, joint backlash etc.) that can amount to an error of a couple of centimeters. The representation that each taxel will learn from experience will automatically compensate for these inaccuracies and ensure more robust responses of the robot.

The properties of this architecture (described in [Section 8.2](#)) are first verified in simulation ([Section 8.5.1](#)) and then in the iCub robot ([Section 8.5.2](#) and [Section 8.5.3](#)). Finally, the utility of this representation for the robot is demonstrated in an avoidance as well as a catching scenario ([Chapter 9](#)).

8.2 REPRESENTATION OF SPACE AROUND THE BODY

We have chosen a distributed representation in which every taxel is learning a collection of probabilities regarding the likelihood of its own body parts or objects from the environment coming into contact with that particular taxel. Loosely inspired by neurobiological findings, we decided to consider two key variables: (i) distance from the taxel D ; (ii) time to contact TTC . The latter is estimated from current distance and velocity of oncoming objects. Both variables are in the reference frame of each taxel. This is possible due to the existing skin calibration of the robot (Del Prete et al. [18]) and a full model of the robot’s kinematics – including head and eye (Pattacini [63]). For objects perceived visually, additional processing involving stereo vision is required. Eventually, every object can be mapped into the root reference frame of the robot and then transformed to the reference frames of individual taxels. However, the models as well as the perceived quantities from the environment (position and velocity of oncoming objects) are subject to errors, which will be detailed later in [Section 8.5](#). For example, it can happen that oncoming objects will seemingly penetrate the robot’s skin – based on our model and measurements, not in reality – and will thus have negative distance w.r.t. the taxel normal. Conversely, if the errors bring about an offset in the opposite direction, an actual contact on the robot’s skin may correspond to a positive distance perceived in our model. Therefore, our data will be affected by that and the learning method will thus have to account for it.

8.2.1 DATA COLLECTION FOR LEARNING

As briefly outlined above, two distinct scenarios were considered where either the robot's own body parts or external objects were approaching individual skin parts. However, the basic principle is the same in both and is realized in a local, distributed, event-driven manner. An illustration is depicted in [Figure 15](#); a schematics of the geometry of the setup is presented in [Figure 16](#).

A volume was chosen to demarcate a theoretical spatial receptive field around every taxel². It is cone-shaped and grows out of every taxel along the normal to the local surface and extends to maximum 20cm away from the taxel (green region in [Figure 16](#)). This is again loosely inspired by neurobiological findings. Once an object enters such a volume, we mark the onset of a potentially interesting event. From this time on, the position and velocity of the object w.r.t the taxel is recorded so as the distance D and time to contact TTC are computed.

The distance, D, is calculated as follows:

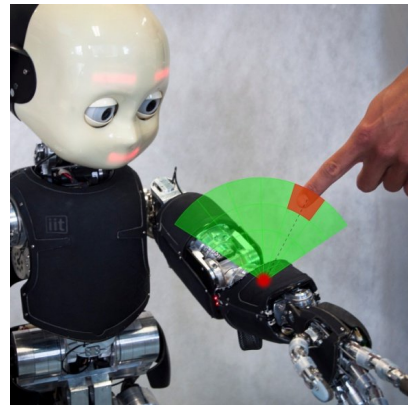
$$D = \text{sgn}(\vec{d} \cdot \vec{z}) \|\vec{d}\| , \quad (9)$$

where:

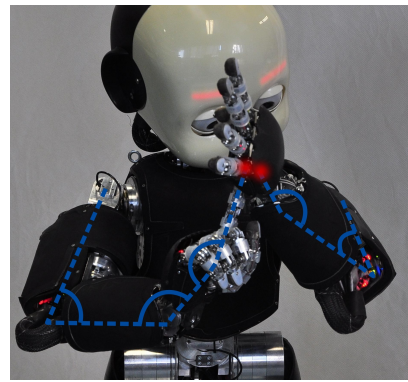
- \vec{d} is the displacement vector pointing from the taxel to the event (center of the oncoming object);
- \vec{z} is the z-axis of the reference frame centered on the taxel and pointing outward (coincident with the normal to the skin surface at the taxel position).

The sign of their dot product is thus positive if the angle between them is lower than 180° , that is if the object is belonging to the positive hemisphere extending from the taxel. Hence, according to our definition, the distance, D, will preserve the information about the relationship of the event w.r.t. the taxel normal. In this way, objects apparently "beneath" the skin surface will acquire negative distances, distinguishing them clearly

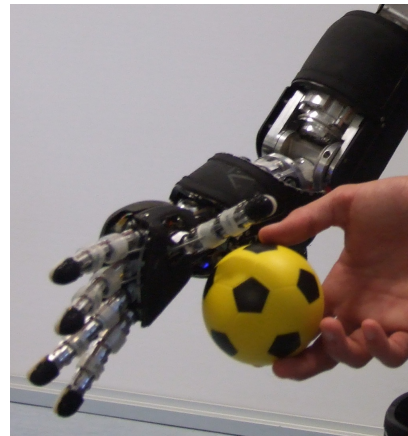
² We will use this notion of *receptive field* from now on. However, unlike in biology where receptive fields of individual neurons are tied to a particular sensory modality and response properties of the neuron, our receptive field is a theoretical construct – a volume of space around the taxel relying on the robot's kinematic model. In what follows, all objects coming toward the robot's body – note that these can be the robot's own body parts whose position is also available in motor or proprioceptive coordinates or they can be external visually detected objects – will be remapped into the taxel's reference frame and thus potentially enter its receptive field.



(a) Depiction of the receptive field belonging to one of the left forearm taxels.



(b) iCub performing a double touch behavior. A simplified schematic of the kinematics and joint angles is superimposed on top of the robot.



(c) An external object approaching the right palm during the scenario that involves learning with external objects (cf. [Section 4.3.3](#)).

Figure 15: Illustration of the experimental setup during different scenarios.

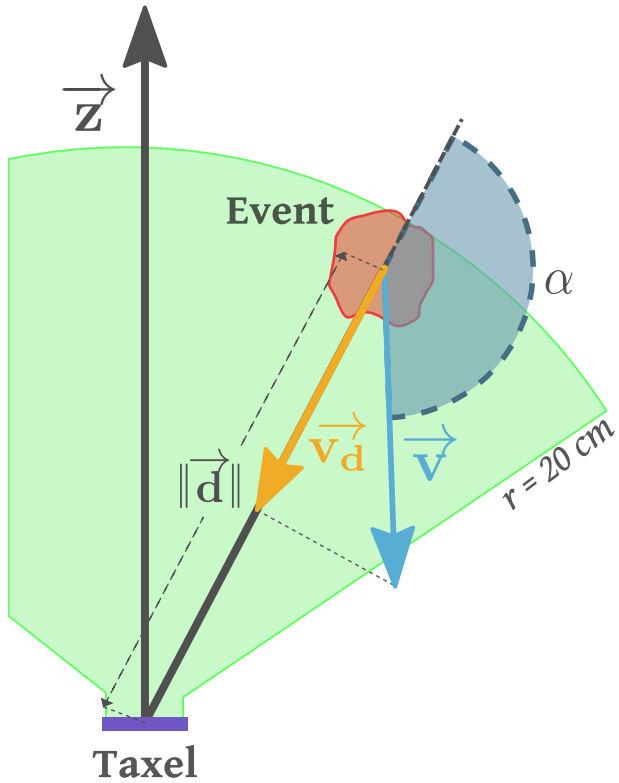


Figure 16: *Receptive field of a taxel and approaching object (event).* The taxel is schematically depicted as a flat 2D area (purple rectangle), whereas its receptive field is cone-shaped and represented in green. The red object portrays a generic event (either arm or external object); in the moment in which it enters the RF, its distance \vec{d} as well as its velocity \vec{v} w.r.t. the taxel's FoR are recorded with a 20Hz frequency. These quantities are later used in order to compute the variables our visuo-tactile representation is built upon (i.e. D and TTC, see text for details).

from their counterparts in the positive hemisphere (green area in Figure 16). Then, the time to contact, TTC, is defined as follows:

$$\text{TTC} = -\text{sgn}(\vec{d} \cdot \vec{v}) \frac{\|\vec{d}\|}{\|\vec{v}_d\|} = -\text{sgn}(\vec{d} \cdot \vec{v}) \frac{\|\vec{d}\|}{\|\vec{v} \cdot \cos(\alpha)\|}, \quad (10)$$

where:

- \vec{d} is again the displacement vector pointing from the taxel to the event;
- \vec{v} is the object's velocity vector;
- \vec{v}_d is the projection of the object's velocity \vec{v} onto the displacement \vec{d} , given by the product of \vec{v} and $\cos(\alpha)$;

- α is the angle between \vec{d} and \vec{v} , as depicted in [Figure 16](#).

Similarly to the formula for distance above, the sgn term stands for the direction of motion of the approaching object. That is, for objects coming from the “positive hemisphere” toward the taxel, the dot product will be negative (and will have opposite directions) and the final time to contact will be positive. The opposite will hold for objects going away from the taxel or the special case where they have already “penetrated” the skin according to the estimation. Finally, the second term accounts for the magnitude of the TTC, that is simply time as distance over speed (norms of the respective vectors, \vec{d} and $\vec{v_d}$).

Please note that this procedure – logging of D and TTC of approaching objects – proceeds in parallel for every taxel whose receptive field has been penetrated. This data is buffered for 3 seconds and it is used for learning only if the object eventually contacts the skin and is perceived by at least one taxel. In this case, a learning iteration is triggered that proceeds as follows:

- For all the taxels that experienced contact, the buffer of object positions in their local FoR is traversed back in time with time steps of 50 ms. While the object is still in their respective receptive fields, the distance and time to contact at every time step are recorded as positive examples in every taxel’s “memory”.
- For all the other taxels on the same body part, the procedure is analogous, but negative examples are appended to their respective memories.

Thus, objects that pass close to but never touch the body never enter the representations. This decision has been made by design on our side in order to reduce the necessary computation and memory. However, taking into account all events that come sufficiently close to the body would be an equally valid approach.

8.2.2 INTERNAL REPRESENTATION

Every taxel stores and continuously updates a record of the count of positive and negative examples it has encountered for every combination of distance and time to contact. We defined the range of D as $[-10, 20]$ cm and TTC as $[0, 3]$ s. The variables were discretized into 8 equally sized bins for the distance and 4

bins for the time to contact respectively; the asymmetry comes from the fact that the TTC required a velocity estimation of the approaching object and gave rise to more noisy estimates. There were 32 combinations and hence 32 items, $[n_{\text{positive}}, n_{\text{negative}}]$, in every taxel's memory. The main advantage of this representation is its simplicity and ease of incremental updating – with new positive or negative examples, the respective count in the memory is simply incremented.

However, most relevant for the agent is an estimation of the probability of an object hitting a particular part of the skin, which can be used to trigger avoidance responses, for example. For every oncoming object, its “coordinates” w.r.t. every taxel (i.e. distance, time to contact) can be discretized in the manner described above and a frequentist probability estimate obtained simply as:

$$P(D, \text{TTC}) \approx f(D, \text{TTC}) = \frac{n_{\text{positive}}(D, \text{TTC})}{n_{\text{positive}}(D, \text{TTC}) + n_{\text{negative}}(D, \text{TTC})} \quad (11)$$

Such an approach – discretized representation and querying – would constitute the simplest solution. Nonetheless, it may give rise to unstable performance, in particular in the case when the state space is undersampled. Therefore, it is desirable to obtain a continuous function f which can be sampled at any real values of $[D, \text{TTC}]$ and is capable of smoothing out the global discretized landscape³. This can be achieved by adapting the Parzen-Window density estimation algorithm [61] to our situation – by employing it as a data interpolation technique. In a 1-dimensional case, the interpolated value $p(x)$ for any x is given by:

$$p(x) = \frac{1}{n} \sum_{i=1}^n \frac{1}{h^2} \Phi \left(\frac{x_i - x}{h} \right) \quad , \quad (12)$$

where:

- x_i are the data points in the discrete input space

³ It is worth noting that only the original discretized $[D, \text{TTC}]$ combinations have estimates of a probability function associated with them, each pair $[D_i, \text{TTC}_j]$ independently from others. However, the whole “landscape” arising from $f(D, \text{TTC})$ cannot be interpreted as a probability mass function (in discrete case) or probability density function (in continuous case), because the overall probability for the whole space of D and TTC combinations can take any values and does not sum up to 1.

- Φ is the window function or kernel
- h is the bandwidth parameter, which is responsible for weighting the contributions of the neighbors of the point x .

We used a Gaussian function, hence we have:

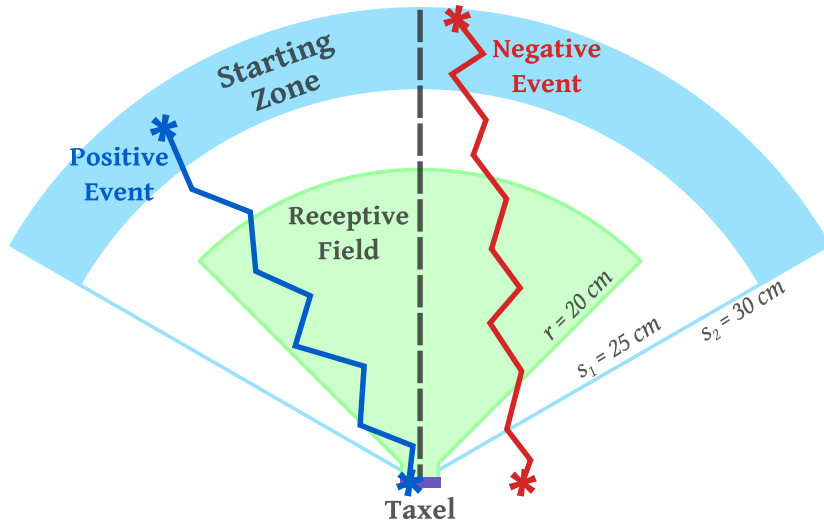
$$p(x) = \frac{1}{n} \sum_{i=1}^n \frac{1}{\sqrt{2\pi}\sigma} \exp\left(-\frac{(x_i - x)^2}{2\sigma^2}\right) . \quad (13)$$

In our case, which is 2-dimensional (with $x = [D, TTC]$ as the input variables), we specified the standard deviation vector σ equal to the width of the single bin in each dimension of the input space. Hence, for any value of $D = d$ and $TTC = ttc$, the final interpolated value – i.e. $p(d, ttc)$ – represents the probability of an object at distance d and time to contact ttc hitting the specific taxel under consideration.

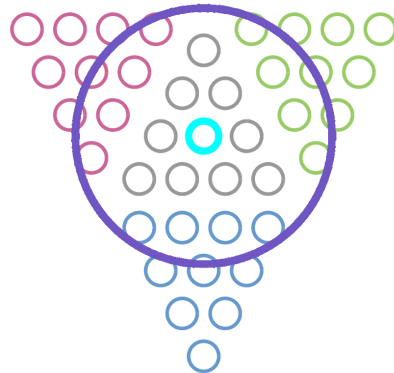
8.3 MONTE CARLO SIMULATION OF A SINGLE TAXEL MODEL

In order to investigate the behavior of the representation proposed in [Section 8.2](#), a Monte Carlo simulation was designed and carried out. In particular, we wanted to study the properties of the acquired representation in an ideal world – with sufficient samples available and with control over noise – and investigate the effect of different parameters (such as number of bins for discretization, parameters defining the cone, range of object speeds, etc.). To this end, a 3-dimensional model of a single taxel and its surroundings with oncoming simulated objects was set up – see [Figure 17](#) for a schematics of a 2D projection of the setup.

The model parameters were chosen to mimic the real robot setup as close as possible. The simulated taxel itself has a radius of 0.235 cm, which mimics the radius of the real iCub taxels. However, objects landing within 2 cm from the taxel's center (violet areas in [Figure 17b](#)) are still considered positive, resembling the size of a triangular module that is composed of 10 taxels – the basic building block of the iCub skin (see [Figure 18a](#) for a comparison with the real iCub's skin). These “virtual taxels” will be used also in the real setup. The taxel's cone-shaped receptive field is depicted in green. In addition, the oncoming objects were also simulated. Since the nature of



(a) Side view of the simulated taxel with oncoming objects.



(b) Top view of the simulated taxel.

Figure 17: Schematics of single taxel model. [Figure 17a](#)) Side view of the simulated taxel with oncoming objects. The violet line at the bottom represents a virtual taxel; green sector is a projection of the taxel's cone-shaped receptive field. The light blue region marks the area from which objects are shot toward the taxel. Examples of a positive (blue line) and a negative (red line) event are depicted. [Figure 17b](#)) Top view of the taxel. A single taxel is the light blue circle in the middle. The violet circle marks the area of a virtual, bigger taxel in simulation. See text for details.

our data collection and learning method requires positive examples (objects contacting the virtual taxel) as well as negative examples (objects contacting neighbouring taxels), we simulated additionally 3 neighbouring virtual taxels ([Figure 17b](#)). We implemented a stochastic “shower” of objects with their starting points uniformly distributed in the blue region (“starting zone” in [Figure 17a](#)) and their landing points following a Gaussian distribution centered on the simulated taxel ($\mu = 0$; $\sigma = 5$ cm). The velocity of the object is a vector directed from the starting point to the landing point, whose speed is uniformly distributed between 5 cm/s and 15 cm/s (but constant over the time). With the object’s trajectory thus defined, its position and velocity is then sampled at 50 ms, similarly to what happens in the real setup. In a second step, in order to simulate noise in the acquisition, additional Gaussian noise is added to the measurement of its position as well as velocity. The Monte Carlo simulation was implemented in the Matlab environment.

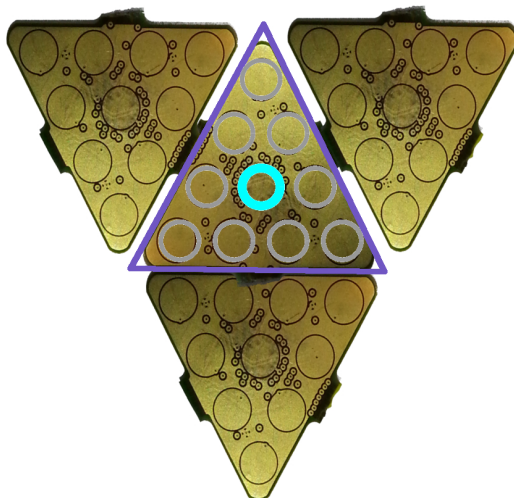
8.4 ICUB HUMANOID ROBOT AND KEY MODULES

The iCub platform used in this work has been described in [Chapter 3](#). Nonetheless, for the purposes of this work, further details are needed. Specifically, [Section 8.4.1](#) will provide more information about how the artificial skin of the iCub has been exploited for the purposes of this work.

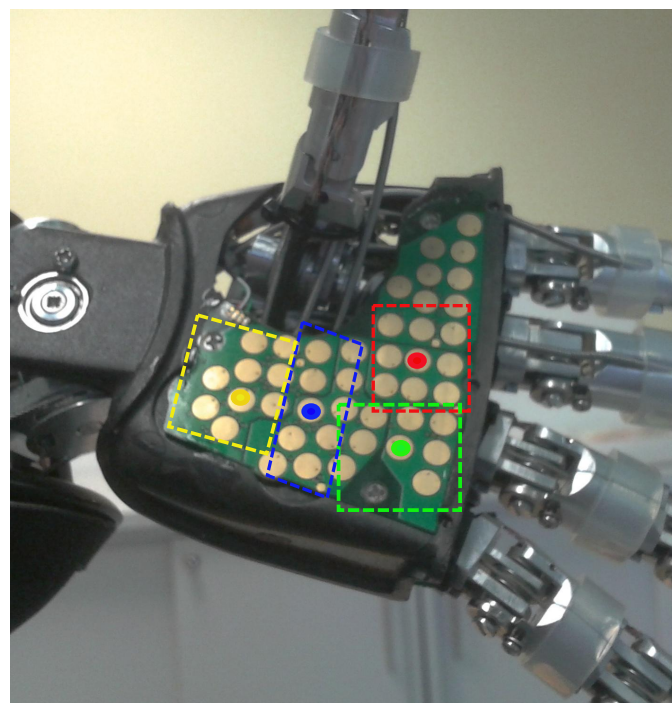
8.4.1 ARTIFICIAL SKIN

The artificial skin the iCub was recently equipped with has been detailed in [Section 3.1.3](#). With the exception of the palm, the skin covering all body parts consists of patches with triangular modules of 10 taxels each (Fig. [18a](#)). There are in total 23 modules on the forearm in two patches and hence 230 taxels. Without loss of generality, for the purposes of this study – spatial receptive fields around body parts – it would be an unnecessarily high resolution to consider every taxel independently. Therefore, in what follows, every triangular module acts as single virtual taxel. That is, the taxel in the center of the module acts as a representative of the whole module and an activation of any of the module’s taxels is represented as a signal coming from this virtual (*representative*) taxel.

The palm features a different design (see Fig. [18b](#)), composed of an array of 43 taxels. In order to mimic a similar resolution to the other body parts, we have artificially split the palm’s



(a) Four triangular modules with 10 taxels each.



(b) Exposed skin of the palm with virtual taxels highlighted.

Figure 18: Pressure-sensitive skin of the iCub.

skin into 4 regions of 8 to 10 taxels, forming “virtual taxels” of the palm. These are depicted in [Figure 18b](#), with the center taxels marked with full circles. The region enclosed between the thumb and the fingers is not considered, since it is very hard to be touched by oncoming objects.

A spatial calibration of the skin of the forearm has been performed in Del Prete et al. [[18](#)]. Using data from the CAD model, we have added calibration of the palm. Therefore, the poses of all taxels (position and orientation) as well as the virtual taxels in local reference frames of the robot are known.

8.4.2 KINEMATIC MODEL AND COORDINATE TRANSFORMATIONS

Each of the sensory modalities described above senses different physical quantities and also operates in different FoRs. Establishing a common ground between these rich but diverse sources of information is an important capacity that is attributed to the body and peripersonal space representations. As we described in [Section 8.2](#), coordinate transformations (such as between eye-centered and body-part-centered FoRs) are one necessary component and different mechanisms how they can be supported by the brain were put forth. In our case, we specifically need two types of transformations:

- *Purely kinematic transformations.* For the first scenario where the robot learns about the space around its body in the absence of visual information (cf. [Section 4.3.1](#)), the taxel positions need to be brought to a common FoR with the body parts touching them (like skin on the forearm being touched by the tip of the contralateral index finger – [Figure 15b](#)). We chose the FoR of the individual taxels to act as the common FoR here.
- *Visual-kinematic transformations.* In the subsequent scenarios (i.e. [Section 4.3.2](#), [Section 4.3.3](#), and [Section 4.3.4](#)), visual information was added. There were two variants of the experiment: first, the double touch scenario with visual tracking of the finger approaching the contralateral arm. Second, external objects were approaching and contacting the robot’s skin. In both cases, transformations involving the image (retina) frames are necessary. We chose to exploit binocular disparity in order to obtain a 3D position of the object in the head FoR and then following a coordinate transformation sequence to eventually reach the FoR of individual taxels.

Learning these transformations was not the goal of this work; therefore, we have employed the existing kinematic model of the iCub that is based on the Denavit-Hartenberg convention and embedded in the *iKin* software library (cf. [Figure 4](#)). Using this and setting current joint positions as obtained from the encoders, any kinematic chain of the robot (such as from tip of finger to wrist of contralateral arm or from eye/head to the wrist) can be traversed in either direction by employing an appropriate sequence of roto-translation matrix multiplications. In fact, kinematic representations of individual chains in *iKin* start/end in the root FoR of the robot (around waist) and this is employed as an intermediary to connect individual subchains. Finally, the last transformation to individual taxels comes from the skin calibration (cf. [Section 3.1.3](#)).

However, these composite transformations are subject to numerous errors that include (i) mismatch between the robot model based on the mechanical design specifications (CAD model) and the actual physical robot; (ii) inaccuracies in joint sensor calibration and measurements; (iii) unobserved variables from the sensed configuration coming from joint backlash or mechanical elasticity; (iv) inaccuracies in taxel pose calibration; (v) additional errors in visual perception coming from inaccurate camera calibration etc. As a whole, these errors can amount to a total of several cm. However, in the approach adopted here, they will be automatically compensated for by the representations that every taxel will learn regarding its surrounding space.

8.4.3 VISUAL PROCESSING AND GAZE CONTROL

For the scenario involving external objects approaching the robot's body, additional processing steps are needed to obtain their position and velocity: moving objects need to be detected, segmented out of the background and their position tracked. We prepared two modifications of the same experiment:

1. *Tracking of fingertip with colored marker.* In the first scenario, we implemented a color segmentation module able to track a green marker placed on the iCub's index fingertip and to project its position into the Root FoR.
2. *Tracking of arbitrary objects.* In this case, we developed a pipeline that allowed us to track general objects under some assumptions on the availability of visual features and limits on their velocity and size.

In both cases, a gaze controller was employed in order for the eyes and head to smoothly follow the tracked object in space.

The details of the gaze controller can be found in [63], whereas [Section 8.4.3.1](#) and [Section 8.4.3.2](#) will describe the implementation of the trackers we developed.

8.4.3.1 *Tracking of fingertip with colored marker*

The fingertip tracking task was achieved by means of a color segmentation algorithm. We used a hue thresholding in the HSV (Hue, Saturation, Value) color space in order to detect the green marker placed on the robot's fingertip ($40 < H < 80$). A depiction of this algorithm can be seen in [Figure 19](#).



(a) Index fingertip of the right iCub's hand performing a double touch as seen from the robot's point of view. It is covered by a green marker.
 (b) Filtered image with the HSV segmentation algorithm. The tracked fingertip is depicted in dark blue, whereas the brown dot is placed at the center of the fingertip.

[Figure 19: Tracking of fingertip with colored marker.](#) The center of the fingertip is retrieved for both the right and left image, and a triangulation algorithm converts this information into a 3D point. See text for details.

The segmentation algorithm was applied to the right and left image, in order to compute the center of the fingertip in both the image planes (cf. [Figure 19b](#)). Thanks to the kinematic model of the iCub, a triangulation was then applied to this binocular information in order to estimate the 3D coordinates of the fingertip in the robot's Root FoR.

8.4.3.2 *Tracking of arbitrary objects*

The scenarios involving the tracking of arbitrary objects needed the implementation of a more sophisticated software module, able to feature a reliable 3D tracking of any moving object in the robot's workspace.

The software architecture is composed of several interconnected modules, some of which were already available in the iCub software repository, and are described in [Section 3.2.3](#).

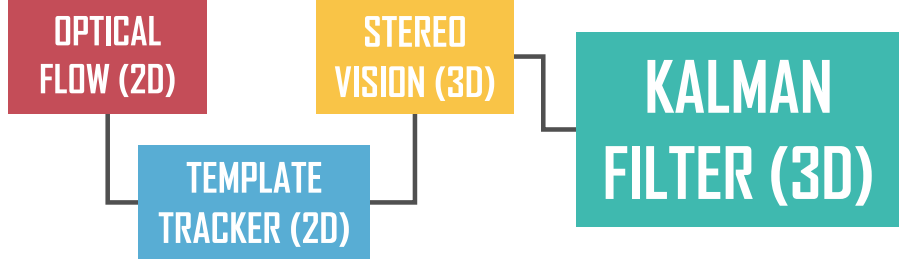


Figure 20: *Tracking of arbitrary objects* schematics. See text for details.

The framework is schematically depicted in Figure 20, whereas the outcome of each step is presented in Figure 21.

The first module computes a 2D Optical Flow (Ciliberto et al. [9]) to detect motion in the image plane. If the computed motion is consistent with the presence of an object coming in the nearby space of the robot⁴, it triggers a pipeline composed by three interconnected modules:

- a 2D particle filter (Tikhanoff et al. [83]) able to track the object in the image plane based on its color properties;
- a 3D stereo disparity module (Fanello et al. [23]), able to convert the 2D planar information related to the incoming event (namely, the centroid of the object and an estimation of its size) into 3D coordinates;
- a Kalman filter that receives 3D coordinates from the stereo vision module and improves the robustness of the estimation. It employs a fourth order dynamic model of the object motion.

The result coming out from the Kalman filter is an estimation of both the 3D position and the 3D velocity of the incoming object with respect to the robot’s Root FoR.

8.5 RESULTS

Results from four different experimental scenarios are reported. First, the behavior of the proposed representation is studied in a single taxel model (cf. Section 8.5.1). Second, we demonstrate how the robot can learn about the extent of its body and potential self-collisions in the absence of vision: through tactile-motor associations in a double touch scenario (cf. Section 8.5.2). Third, the motor information about the oncoming body part is

⁴ To this regard, a check on the stability of the detected motion has been implemented, in order to possibly avoid any outlier.

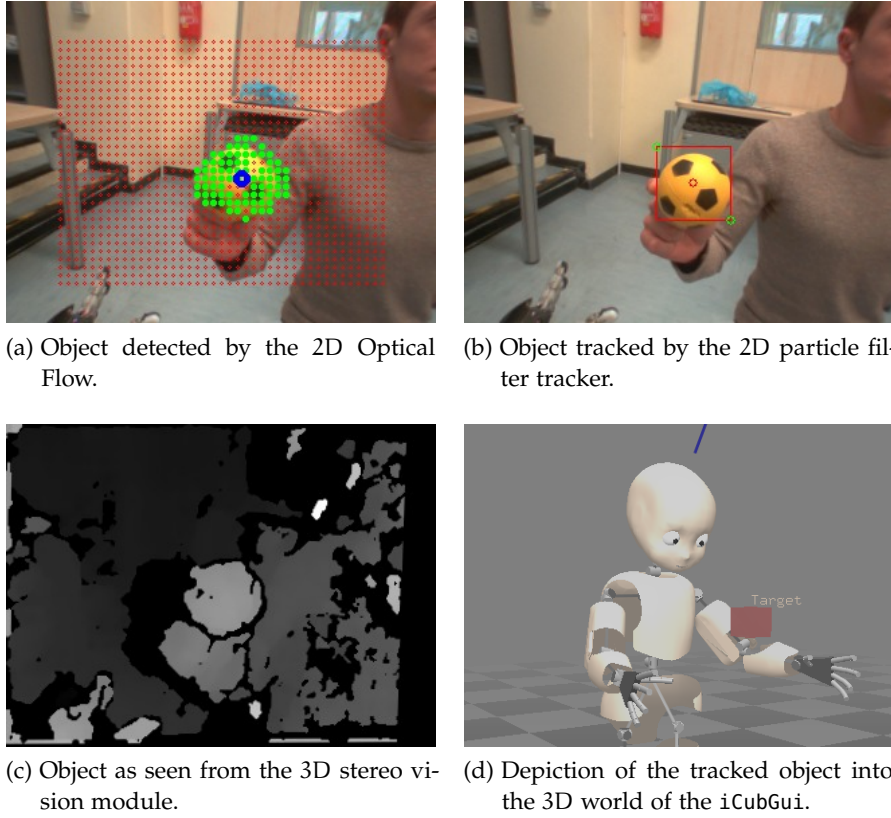


Figure 21: *Tracking of arbitrary objects pipeline*. Each figure shows one of the four modules involved in the 3D optical flow pipeline. See text for details.

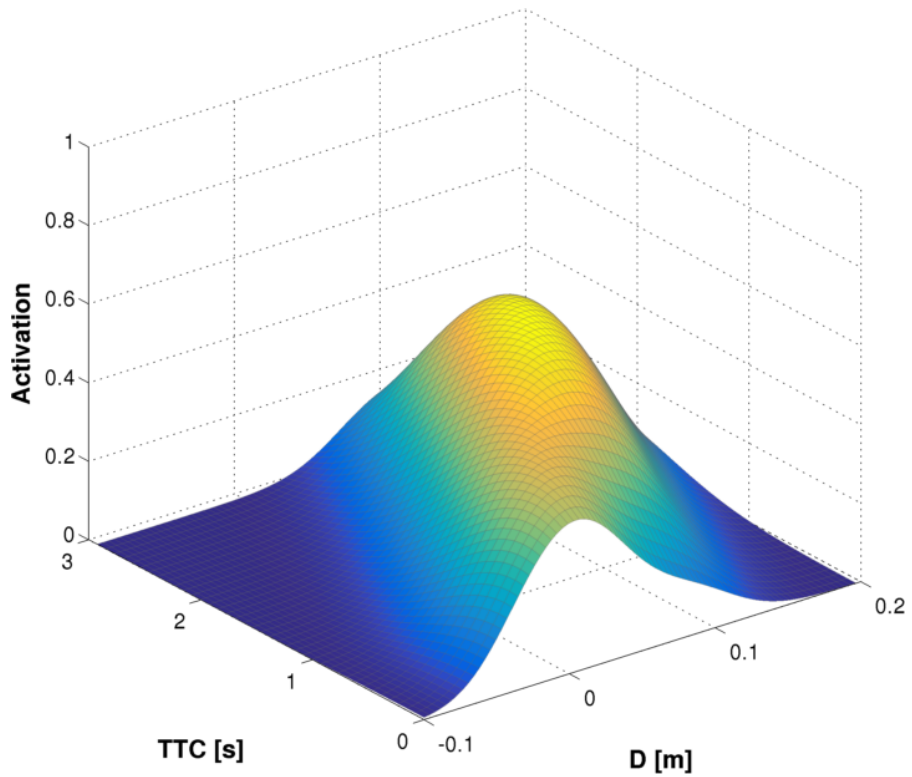
substituted by visual information and hence, first tactile-visual associations can be learned (cf. [Section 8.5.3.1](#)). Fourth, this scenario is extended by tracking arbitrary objects rather than the robot’s own body parts in the visual field as they near its skin (cf. [Section 8.5.3.2](#)).

8.5.1 LEARNING IN A SINGLE TAXEL MODEL

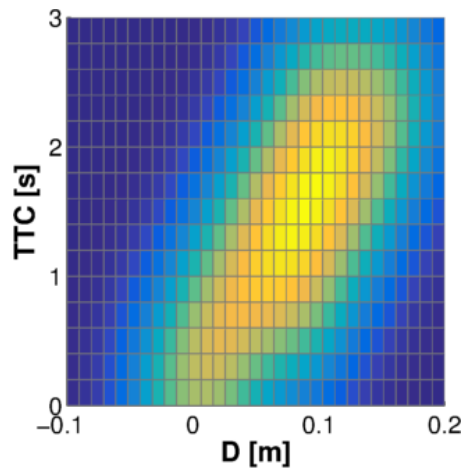
The properties of the learning procedure as well as the proposed representation ([Section 8.2](#)) were investigated in a single taxel model ([Section 8.3](#)). Two independent Monte Carlo simulations have been performed; the results from 500 iterations – 500 objects being fired toward the taxel – are depicted in [Figure 22](#) and [Figure 23](#). They both show the representation after learning and smoothing using the adapted Parzen Window method: the full landscape on the top and its projection into 2D with color coding the third dimension (the probability of contact) on the bottom.

The first stage (cf. [Figure 22](#)) was performed with a theoretically perfect model of the robotic setup: the measurement of position and velocity of the incoming event was without noise, and the simulated kinematic error was 0. A clear “ridge” can be seen in both plots which corresponds to the trajectories of objects as they approach the taxel and both D and TTC are decreasing. The contact with the taxel occurs at both D and TTC equal to 0.

In the second step, in order to come closer to the situation in the real robot, two additional features were added to the model. First, Gaussian noise was added to the measurement of position and velocity (and hence D and TTC). Second, we had to account for the fact that the object position and velocity measurements in the real robot are subject not only to random, but also to systematic errors. In particular, in both tactile-motor (double touch) and tactile-visual scenarios, the coordinate transformations needed to map the approaching object to the FoR of individual taxels rely on the model of the robot kinematic structure and its visual apparatus (see [Section 8.4.2](#)). These errors can sum up to a couple of centimeters. For example, imagine an object is just contacting a particular taxel – that is its real distance from it is 0. However, the position of the object as perceived through the robot’s eyes and then projected into the taxel’s FoR may give a result of 5 cm or even -5 cm. To clearly demonstrate the effect of this on the representation, we have introduced such a systematic offset into the model. The results for this configuration – noise and systematic error – can be seen in [Figure 23](#), in which we used an error of -10 cm. The Gaussian noise results in an overall less sharp profile of the activation landscape. The offset can be clearly seen in the distance axis, with the “ridge” of high activations cutting the x-axis in the negative domain. Furthermore, when compared with the previous experiment, it is clear how much the effect of the noise is shaping the representation: instead of having a well defined function (such as the one in [Figure 22](#)), the representation is here more spread in the whole domain of [D, TTC]. This is because, in such a noisy and uncertain environment, the simulated taxel is not able to discern which event will eventually contact the taxel: its output is approximatively 0.5 (i.e. 50%) for most of the domain as a result of this uncertainty.

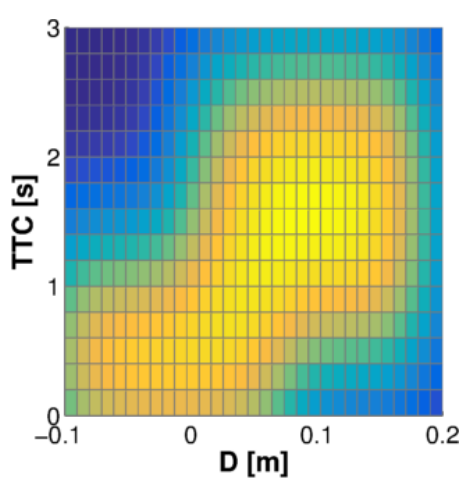
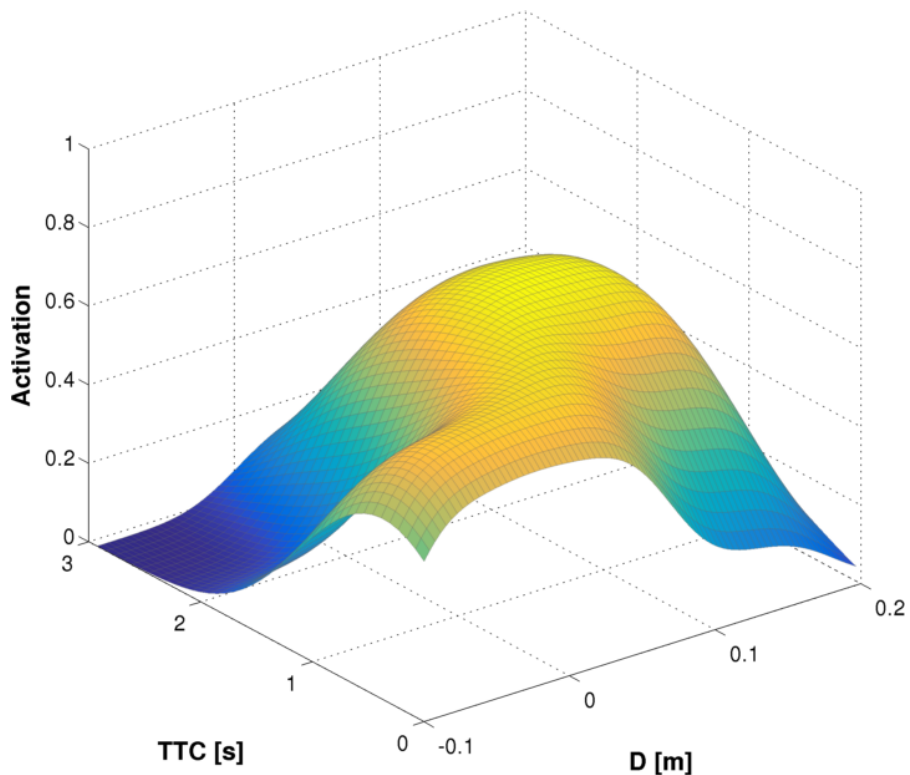


(a) 3D Parzen Window smoothing.



(b) 2D projection of the Parzen estimation.

Figure 22: Representation learned in single taxel model. D is the distance of object from taxel; TTC is the time to contact estimated from distance and velocity of the object. [Figure 22a](#)) Full 3D graph of the representation. The z -axis is given by the activation – estimate of the probability of object eventually landing on the taxel. [Figure 22b](#)) 2D projection; third dimension preserved in color map.



(b) 2D projection of the Parzen estimation.

Figure 23: Representation learned in single taxel model with noise and systematic error (-10 cm offset). The noise makes the representation more spread throughout the input domain; further, the response is shifted toward the negative domain, as an effect of the systematic error. Figure 23a) 3D Parzen Window smoothing after learning of the visuo-tactile representation. Figure 23b) 2D projection; third dimension preserved in color map.

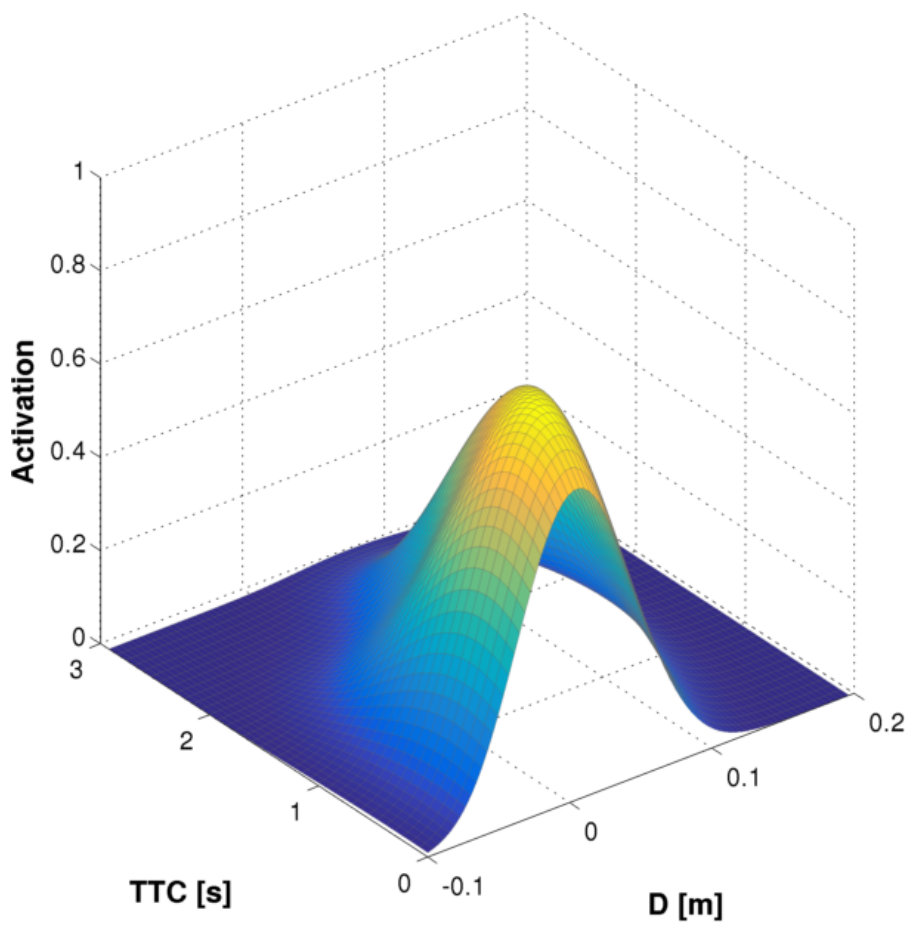
8.5.2 TACTILE-MOTOR LEARNING: DOUBLE TOUCH

In this experiment, we reused the scenario developed in [Part II](#): double touch. The robot is stimulated on the skin of a body part (specifically, the forearm); then a modified inverse kinematics solver and controller is used to command the contralateral fingertip to reach to the stimulated taxel (note that the taxel eventually touched by the robot may differ from the one that was stimulated initially); see [Figure 15b](#) for a schematic illustration. After a successful double-touch event (i.e. two skin parts activated with sufficient spatial and temporal congruency), a buffer is used for data collection and learning as explained in [Section 8.2.1](#). That is, the kinematic model and the values of the joint angles at every time step are used to convert the position of the tip of the index finger (the active, touching body part) to the FoRs of the taxels on the passive, touched part. Unfortunately, it is not feasible to touch the whole sensorized surface of the forearm since some configurations are kinematically not possible or unsafe; therefore, we selected 8 virtual taxels on the inner part of the forearm for which the double touch was triggered and these 8 taxels were learning in parallel from the distance and expected time to contact as the contralateral finger was approaching.

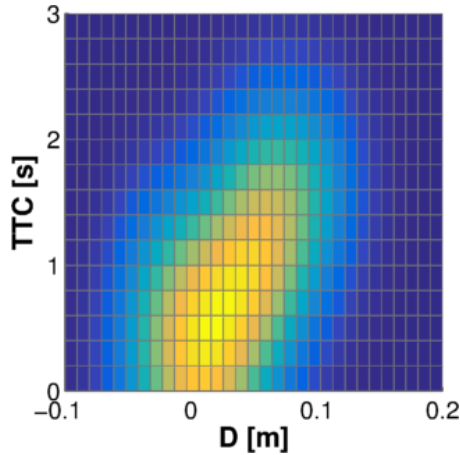
There were 107 successful double touch trials performed. That is, there were 107 trajectories sampled at 20 Hz that resulted in contact with the selected area of the skin – the actual number of data points was much larger. All the taxels whose receptive fields were penetrated were learning in parallel. From the 8 taxels subject to learning, only 6 were actually touched at least once by the contralateral index finger. In all of these, the results after learning were qualitatively similar and matched the predictions of our model. The results for one of the taxels with most training samples (taxel nr. 2; 1625 samples) are shown in [Figure 24](#) and demonstrate how the robot could learn what one could call a tactile-motor margin of safety: a way to predict self-collisions in the absence of visual input. No offset in the position as well as little noise is reflected in the learned representation, indicating that the model of the kinematic loop connecting the two arms was reasonably accurate in this case.

8.5.3 TACTILE-VISUAL LEARNING

In this section, two types of experiment were performed. First, the double touch scenario was repeated, but this time, visual



(a) 3D Parzen Window smoothing.



(b) 2D projection of the Parzen estimation.

Figure 24: *Tactile-motor representation learned in the double touch scenario. Results for taxel nr. 2 on the inner part of the left forearm. See text for details.*

rather than “motor” coordinates of the active arm were considered. Second, external objects were nearing the robot’s body. In both cases, the own body part / external objects were detected, tracked and their trajectory prior to contact was recorded and later used for learning of the representation of nearby space in corresponding taxels. Note that to know the passive arm as well as the head and neck configuration, proprioceptive signals were also considered in order to compute the necessary FoR transformations with the help of the kinematic model.

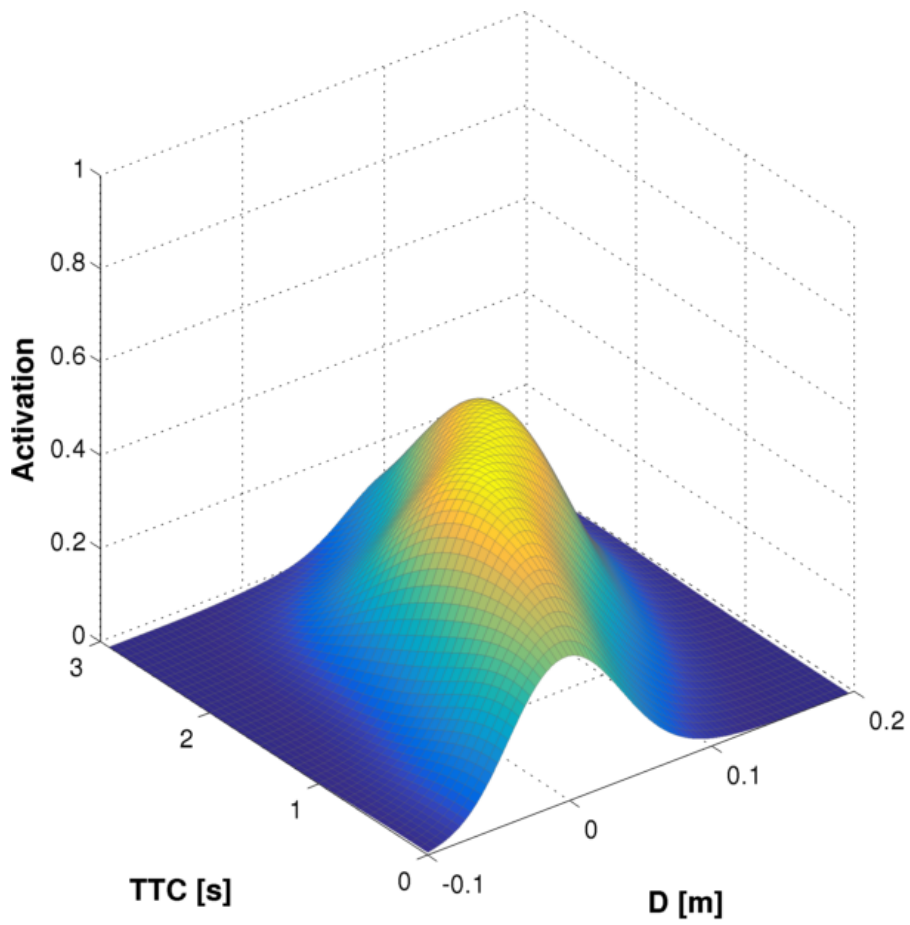
8.5.3.1 *Tactile-visual learning from double touch*

For this variant of the scenario – double touch but with the touching arm perceived visually – we added a small colored marker to the fingertip that was commanded to execute the double touch configurations. The method to extract the finger’s coordinates is described in [Section 8.4.3.1](#). Then, the learning procedure was exactly the same as in the previous double-touch scenario. We performed 45 trials. The results show a similar pattern to the previous scenario – the same taxel (nr. 2; 376 samples) on the inner forearm is picked for demonstration in [Figure 25](#).

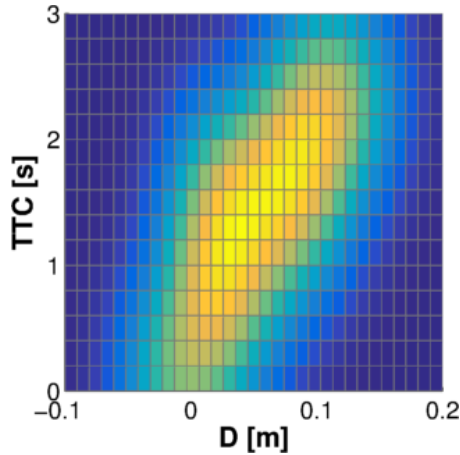
8.5.3.2 *Tactile-visual learning using external objects*

After the tactile-visual association have been learned using own body in the double touch scenario, the representation acquired can be generalized and applied to external (i.e. not self-generated) stimuli as well – objects coming onto the skin. The visual processing pipeline from previous experiment was adapted and replaced by a more general one that uses motion detection based on optic flow, visual template tracking, stereo vision, and a minimum-jerk model for the movement of objects – as explained in [Section 8.4.3.2](#). This setup was validated using two objects – a cube and a small football (see [Figure 26](#)) – approaching the virtual taxels on the robot’s body. Importantly, we were not limited to parts of the skin that can be activated in self-touch configurations anymore. Therefore, to demonstrate the generality of our approach, we have extended the learning to the outer part of the left forearm as well as the palm of the right hand.

On the inner part of the left forearm, the same 8 taxels as in the previous scenarios were subject to learning. Additionally, 4 taxels on the outer part of the forearm were added. Finally, 4 virtual taxels of the right palm (see [Figure 18b](#)) were also subject to learning. We conducted a total of 53 trials for the inner



(a) 3D Parzen Window smoothing.



(b) 2D projection of the Parzen estimation.

Figure 25: *Tactile-visual representation learned in double touch scenario. Results for taxel nr. 2 on the inner part of the left forearm. See text for details.*

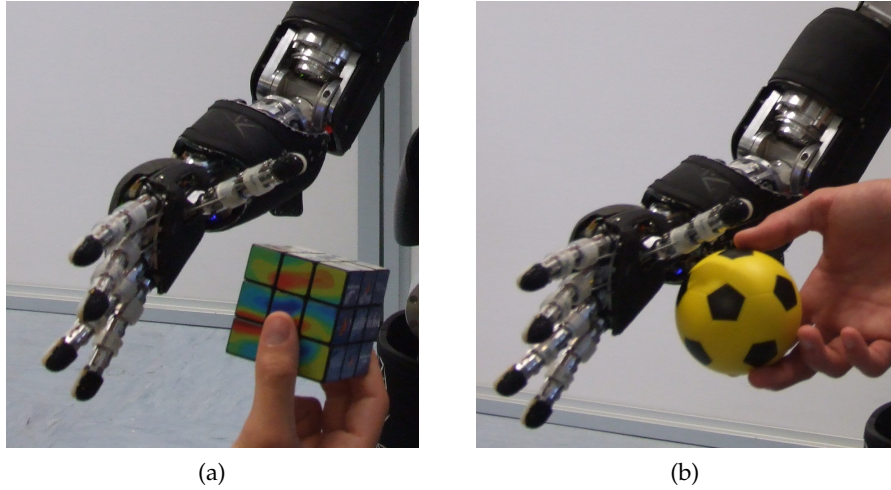
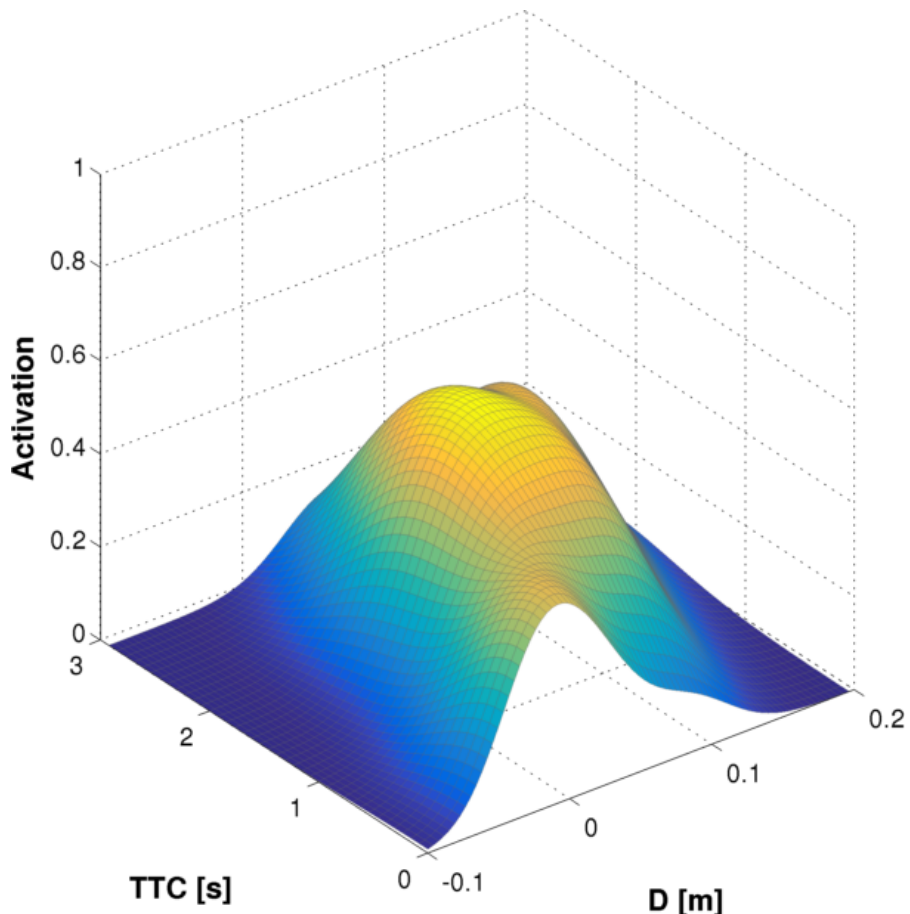


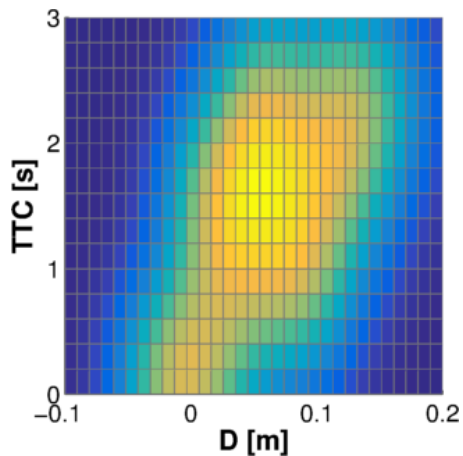
Figure 26: *Unmodeled objects approaching the right palm. (left) Cube. (right) Small football.*

part of the left forearm (events from both objects together), 34 trials for the outer part of the forearm, and 77 trials for the right hand. The results are shown in [Figure 27](#) for the inner part of the left forearm (627 samples, taxel nr. 2). The outer part of the forearm (451 samples; taxel nr. 8), and the right hand (944 samples; virtual taxel nr. 2; taxel marked in red in [Figure 2](#) right) are instead depicted in [Figure 28](#) and [Figure 29](#) respectively.

The representation learned for the inner part of the left forearm is in accordance with previous results for the same skin part. Interestingly, the other skin parts reveal a small systematic error in the models that the learned representation was relying on. Concretely, for the outer part of the forearm (cf. [Figure 28](#)), the ridge of maximum activation seems to cross the distance axis at a negative offset of around 3 cm; conversely, in the case of the right palm, the plot is suggestive of a positive offset of a similar magnitude. Importantly, the learned representation automatically compensates for this error, which will be demonstrated in [Chapter 9](#). Collectively, the representations learned by means of the interaction with external objects present another significant similarity, that is the effect of a bigger noise w.r.t. the representation learned at previous stages. This comes as a consequence of two motivations: (i) the experimental setups our representation was learning from are fundamentally different; the learning with external objects scenario involved the presence of an external human experimenter, whereas the double touch scenario (either with or without vision) was a more controlled setup; (ii) the amount of noise and errors coming from the visual system is intrinsically higher.

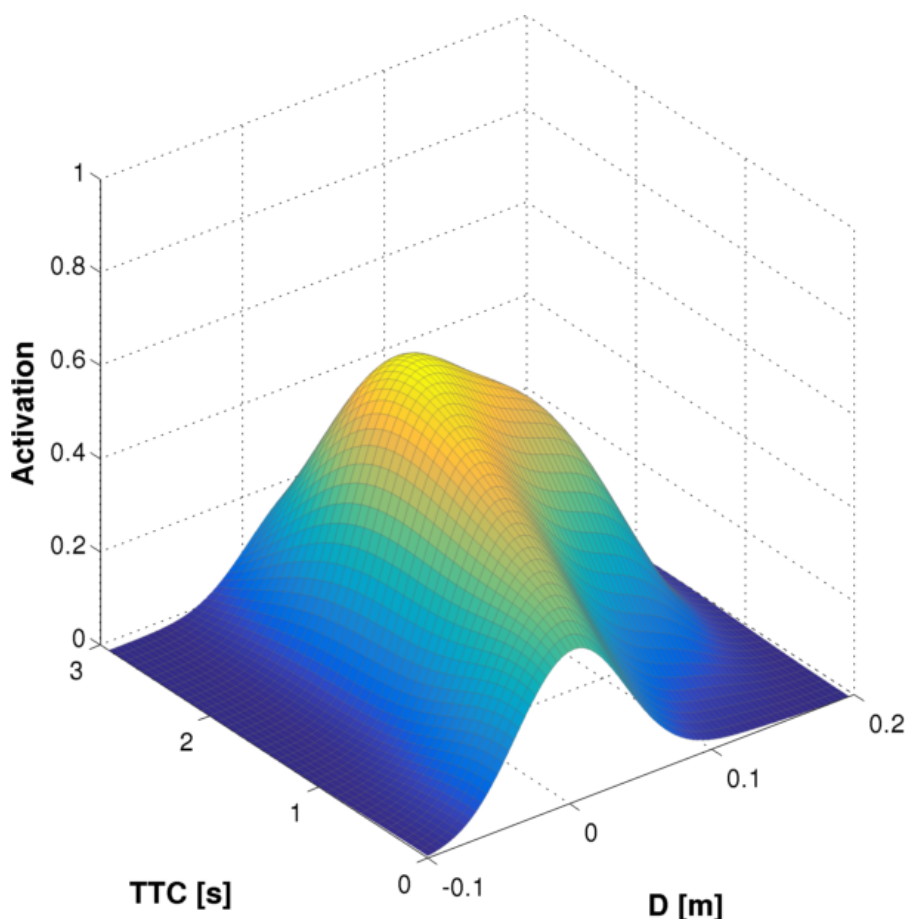


(a) 3D Parzen Window smoothing.

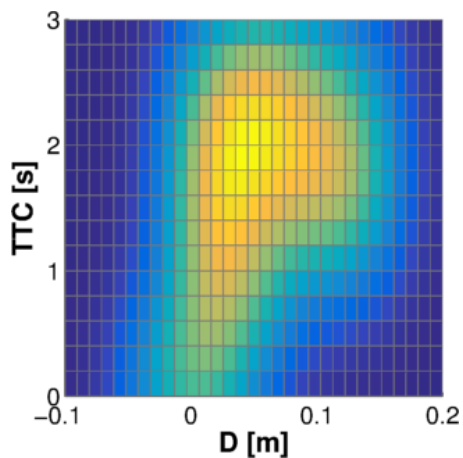


(b) 2D projection of the Parzen estimation.

Figure 27: *Tactile-visual representation learned from oncoming objects.* Results for taxel nr. 2 on the inner part of the left forearm. See text for details.

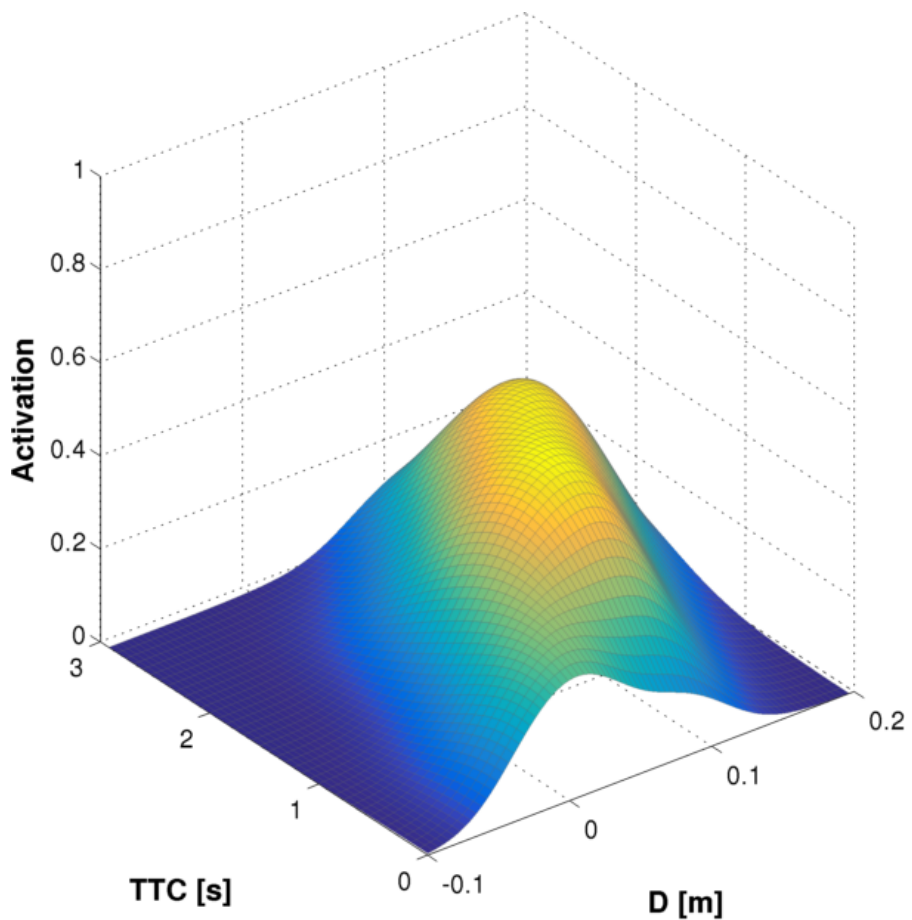


(a) 3D Parzen Window smoothing.

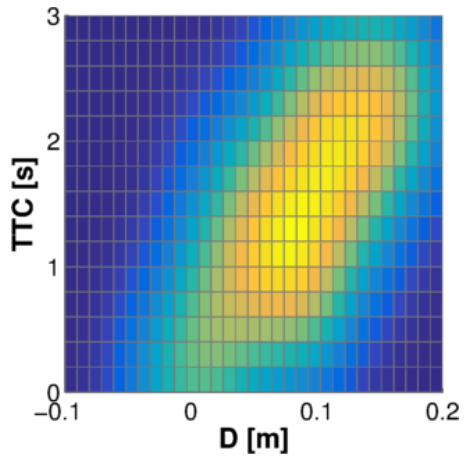


(b) 2D projection of the Parzen estimation.

Figure 28: *Tactile-visual representation learned from oncoming objects.* Results for taxel nr. 8 on the outer part of the left forearm. See text for details.



(a) 3D Parzen Window smoothing.



(b) 2D projection of the Parzen estimation.

Figure 29: *Tactile-visual representation learned from oncoming objects.* Results for taxel nr. 2 on the right hand. See text for details.

APPLICATIONS OF THE MARGIN OF SAFETY IMPLEMENTATION: AVOIDANCE AND CATCHING BEHAVIORS

9.1 INTRODUCTION

[Chapter 8](#) dealt with the construction of a tactile-visual integrated representations of the nearby space and, consequently, a margin of safety around the robot's body. To our knowledge, this is the first implementation of a visuo-tactile-proprioceptive association in a real robot, which effectively creates a margin of safety around all the body parts of the robot that were subject to the training procedure.

In the following, this distributed, decentralized information is put under testing by means of an experimental scenario that will feature an equally distributed motor controller. As illustrated in [Section 4.3](#), the utility of the proposed architecture has been tested in an avoidance and catching scenario that capitalizes on the tactile-visual representations acquired previously. The robot was able to exploit the model in order to either avoid or catch an incoming object with any of the skin parts that have been trained. In this context, the distributed information stored in every taxel's representation led to a similarly distributed response in the interaction with the environment. The experiments were conducted by presenting the robot with a series of objects detected through the optical flow tracker (cf. [Section 8.4.3](#)), similarly to the learning stage presented in [Section 8.5.3.2](#). Any oncoming object thus triggered an activation in each taxel given by the taxel's previous experience with such objects events (in terms of [D, TCC]). Consequently, this gave rise to a distribution of activations throughout the skin.

9.2 AVOIDANCE AND CATCHING CONTROLLER

In order to achieve the desired behavior, we implemented a velocity controller able to move any point of either the left or the right kinematic chain in a desired direction. During an avoidance task, the motion should be directed away from the point of maximum activation, along the normal to the local surface in that point. For the catching behavior, the desired movement vector is the same, only in opposite direction. For this reason, we computed a weighted average for both the position of the avoidance/catching behavior and its direction of motion:

$$\begin{aligned} \mathbf{P}(t) &= \frac{1}{k} \sum_{i=1}^k [a_i(t) \cdot \mathbf{p}_i(t)] \\ \mathbf{N}(t) &= \frac{1}{k} \sum_{i=1}^k [a_i(t) \cdot \mathbf{n}_i(t)] \end{aligned} \quad (14)$$

where:

- $\mathbf{P}(t)$ and $\mathbf{N}(t)$ are the desired position and direction of motion in the robot's root reference frame respectively;
- $\mathbf{p}_i(t)$ and $\mathbf{n}_i(t)$ are the individual taxels' positions and normals;
- $a_i(t)$ are the activations weights of the corresponding taxels.

The weighted average is computed by cycling through all the taxels whose activation is bigger than a predefined threshold at any given time. Therefore, the resultant position and the direction of motion of the avoidance/catching behavior were proportional to the activation of the taxels' representations and changed dynamically as the activation levels of different taxels varied. The velocity control loop employed a cartesian controller [63] whose reference speed was fixed to 10cm/s.

9.3 EXPLOITATION OF THE LEARNED ASSOCIATIONS

Using the representations developed at previous stages and the controller described in [Section 9.2](#), we validated our setup with two distinct experimental sessions. The iCub was presented

with an unknown object that has not been used at the learning stage (a pink octopus, [Figure 30](#)). It was used by the experimenter to perform a series of approaching behaviors toward the robot's body parts that had previously learned their models (left forearm and right hand). Also, the visual processing pipeline used was identical. However, here, the taxels' activations – given by the previously learned representations – were exploited by the robot to either avoid or catch the incoming object with any of the body parts used during the learning. As specified in [Section 9.2](#), only taxels with activation above a certain threshold contributed to the resultant movement vector that was executed by the controller. This threshold was empirically set to 0.4, corresponding to a 40% chance of that taxel being contacted by the oncoming object (according to the model it learned).

9.3.1 MARGIN OF SAFETY: AVOIDANCE BEHAVIOR DEMONSTRATION

To demonstrate the performance of the avoidance behavior, we conducted an experimental session of roughly 20 min. duration in which the experimenter performed a series of approaching movements, alternating between the body parts and varying the approaching direction. Here we restrict ourselves to a qualitative assessment only. In short, the avoidance behavior was successfully triggered in all cases. A snapshot illustrating typical behavior in a 15 s window for the left forearm ([Figure 31](#) left) and a 20 s window for the right palm ([Figure 31](#) right) is shown – with two approaching events each plot. In total, 9 taxels of the left forearm (6 on the inner part; 3 on the outer part) and 3 taxels of the right palm were considered: from the 12 (left forearm) and 4 (right hand) taxels that have been trained in [Section 8.5](#), two were left out because they did not experience a sufficient amount of training samples in order to show a significant response. The top plots of [Figure 31](#) depict the distance of the approaching object from the individual taxels (in their respective FoR). The bottom plots show the activations of the learned representations for each taxel¹. As the object comes closer, there is an onset of activation in the representations of the “most threatened” taxels (bottom plots). Once the activation level exceeds a predefined threshold (0.4 in this case – horizontal line in bottom plots), the avoidance behavior is triggered.

¹ Note that this representation uses a two-dimensional domain of D, TTC. However, to demonstrate the behavioral performance, we restrict ourselves to showing distance only in the upper plot.

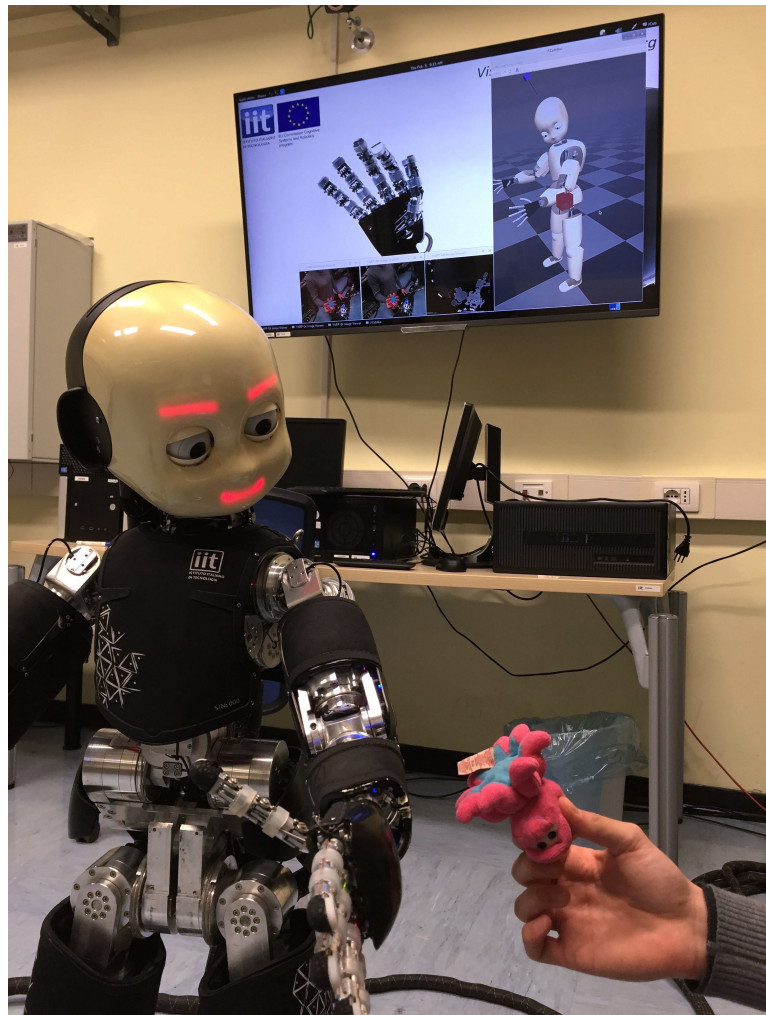


Figure 30: *Unknown object used during the avoidance/catching scenario.* The experimenter is approaching the outer part of the left forearm with a pink octopus, that was not experienced by the robot during the learning stage. The screen in the background shows the pipeline – motionCUT, particle filter tracker, stereo vision, kalman filter – that has been set up in order to track arbitrary objects (cf. [Figure 21](#)). See text for details.

This is illustrated in the top plots with the shaded violet area that marks the velocity of the respective body part (left forearm in the top left plot, right hand in the top right plot). To facilitate understanding, the first taxel responding has been highlighted in the corresponding upper and lower plots. The upper plots clearly demonstrate that the avoidance behavior was effective – a safety margin was always preserved.

9.3.2 “CATCHING” WITH ARBITRARY BODY PARTS

In a similar fashion, we probed the “catching” controller in a roughly 10-min. session. A snapshot illustrating the performance while approaching the inner part of left forearm is shown in [Figure 32](#). The graphical illustration is the same as in the avoidance case. The spatial representations pertaining to the taxels get activated (bottom plot) and trigger the movement (violet shaded area in top plot), which is approaching the object this time. In addition, the bottom plot illustrates also the physical skin activation (green shaded area). Importantly, contact is generated in both cases – as the skin activation testifies. The fact that the distance is greater than zero in the first event of the object approaching can be attributed to the systematic error (either incorrect visual perception of the object or offsets in the kinematic transformations). In spite of this, as demonstrated in [Section 8.2](#), the proposed model was able to successfully compensate for this error and achieve the task.

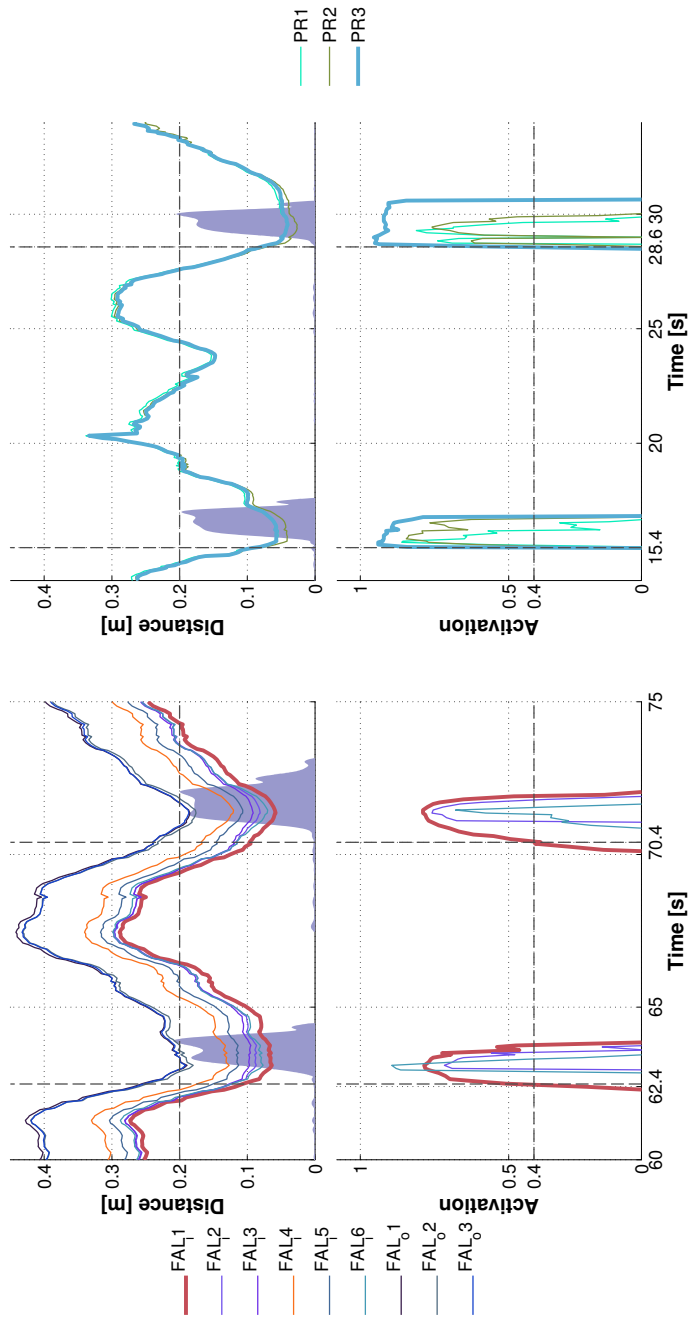


Figure 31: *Avoidance demonstration.* (Left) Object coming onto left forearm. 9 taxels of the left forearm (6 on the inner part; 3 on the outer part) were considered in the experiment. Top plot shows the distance of the object from the taxels in their individual ForRs. The shaded violet area marks the velocity of the body part (common to all taxels; maximum activation corresponding to 10 cm/s). Bottom plot depicts the activations of the forearm taxels' spatial representations. (Right) Object coming onto the right palm. There were 3 taxels considered. Interpretation of the plots is congruent with what presented for the left forearm.

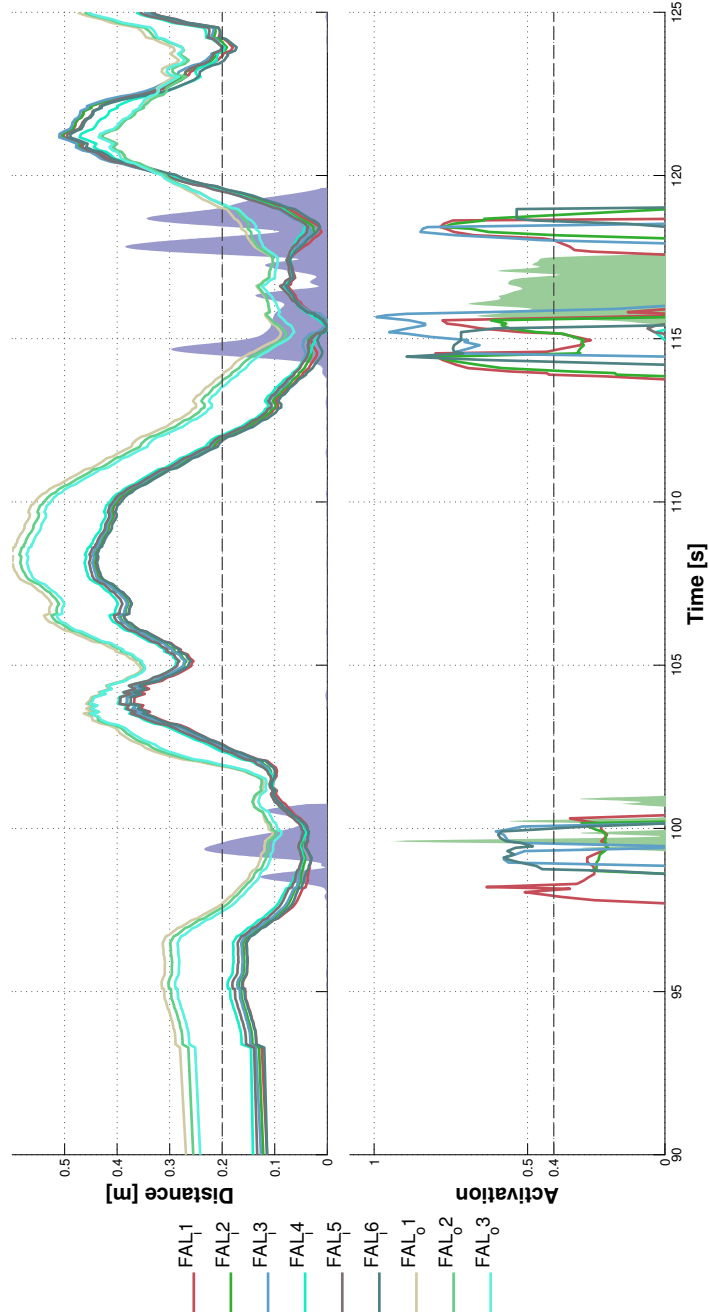


Figure 32: “Catching” with arbitrary body part demonstration. Object coming onto left forearm. 9 taxels of the left forearm (6 on the inner part; 3 on the outer part) were considered in the experiment. Top plot shows the distance of the object from the taxels in their individual FoRs. The shaded violet area marks the velocity of the body part. Bottom plot depicts the activations of the forearm taxels. The green shaded area marks physical contact with the robot’s skin – aggregated activation of all taxels contacted on the body part.

PART III: DISCUSSION AND CONCLUSIONS

In [Chapter 8](#) and [Chapter 9](#), we presented a novel methodology that lets a robot autonomously build up a representation of the space around its body through interaction with the self and the nearby space. More specifically, every taxel has a spatial receptive field extending into 20 cm along the normal to the skin surface. In this space, motor/proprioceptive events (in case of self-touching behaviors) or visual events (if external objects are considered) are recorded. If they eventually result in physical contact with the skin, the activated taxels update their representation tracing back the oncoming object and increasing the stored probability that such an event – in terms of distance and time to contact – is likely to contact the particular taxel. Other taxels on the body part that were not physically contacted also update their representations with negative examples. The spatial receptive field around every taxel is mediated by an initial kinematic model of the robot; however, it is adapted from experience, thus automatically compensating for errors in the model as well as incorporating the statistical properties of the oncoming objects. Furthermore, we devised a simple avoidance controller that is triggered by this representation, thus endowing a robot with a “margin of safety” around its body. Finally, simply reversing the sign in the controller we used gives rise to “catching” or approaching the oncoming objects.

An important asset of the proposed architecture is that learning is fast, proceeds in parallel for the whole body, and is incremental. That is, minutes of experience with objects coming toward a body part give already rise to a reasonable representation in the corresponding taxels that is manifested in the predictive activations – prior to contact – as well as avoidance behavior. The smoothing approach used (Parzen windows applied to the discrete representation) specifically contributes to this effect in the case of undersampled spaces.

One possible practical limitation of the presented architecture could be its computational and memory requirements. The distributed and parallel nature of the representation has many advantages. At the same time, the complexity grows linearly with

the number of taxels – each of them monitoring its spatial receptive field and possibly updating the representation. However, we are convinced that this is in line with the nature of brain computation. Furthermore, the spatial resolution regarding the taxels we have chosen (with “virtual taxels” of around 2 cm in diameter on the skin surface) is likely unnecessarily high – the body-part-centered receptive fields of neurons in the parietal-frontal network are typically much larger (e.g. spanning a whole upper arm, as presented by Fogassi et al. [25]). Also, lower resolution may still suffice to support the margin of safety behavior. Such a modification would be straightforward in our setup – requiring only a redefinition of the “virtual taxel” concept.

Part IV

CONCLUSIONS AND FUTURE WORK

CONCLUSIONS AND FUTURE WORK

In this thesis, we presented to our knowledge the first robot that learns a distributed representation of the space around its body by exploiting a whole-body artificial skin and through physical contact with itself and the environment. This representation naturally serves the purpose of predicting contacts with the whole body of the robot, which is of clear behavioral relevance. [Part I](#) described the proposed architecture, whereas [Part II](#) dealt with the double touch paradigm, which was preparatory for the implementation presented in [Part III](#).

11.1 SUMMARY

[Part I](#) leveraged on insights from cognitive psychology and neuroscience (cf. [Chapter 2](#)) in order to propose a plausible mechanism of development of peripersonal space representations in biological agents. It assumes the availability of some basic – “innate” – behaviors; they let the subject follow a gradual developmental path in order to build up complex tactile-visual models of the self and the nearby space. Further, it presented a set of four comparable stages throughout which any robotic platform – assuming it is provided with a whole-body artificial skin, such as the iCub humanoid robot used in this thesis – can undergo in order to grow a set of perceptual and motor capabilities comparable to what showcased by primates.

The subsequent chapters dealt with the implementation of these aforementioned stages. [Chapter 5](#) presented the theoretical and empirical foundations of a novel approach that let the iCub autonomously perform a double-touch: a reformulation of the reaching task was proven to be a key point in the achievement of such a constrained behavior. As a follow-up, [Chapter 6](#) described an application of this framework in the context of autonomous self-calibration for humanoid robots: an optimization of the kinematic model of the upper limbs of the iCub was carried out in the context of a closed-loop calibration that did not rely on any external metrology system as ground truth.

Finally, Chapters 8 and 9 detailed the development of tactile visual representations on the iCub robot. Specifically, Chapter 8 dealt with the proposed architecture, that consists in a series of a spatial, cone-shaped receptive fields extending from every taxel the iCub’s arms and hands are provided with. They equipped the robot with the ability to extend its tactile domain toward the nearby space: by integrating either motor (in case of self-touch) or visual (when external objects are involved) information with the physical activation of the skin, they enclosed a prior-to-contact representation of incoming events onto the skin. Crucial to the development of this representation was the fact that the robot was able to experience a temporal and spatial congruency in both the visual (or motor/proprioceptive) and the tactile systems: that is, if an event is successful in the activation of a specific taxel, that same taxel updates its probability of being touched by this particular event (encoded in terms of distance and time to contact w.r.t. the taxel). Furthermore, this representation was intrinsically compensating for both the noise in the acquisition and the systematic errors in the model. We have then capitalized this framework in Chapter 9: an avoidance and catching controller leveraged the representation learned at previous stages in order to set up an experimental scenario in which the robot was able to either prevent contact with or catch incoming objects. The movement was distributed and decentralized on the skin parts that were firing. This behavior endowed the robot with two capabilities: a “margin of safety” around the body, and a “reaching with arbitrary body parts” behavior. All these behaviors take automatically the whole body surface (or skin surface) into consideration.

11.2 DISCUSSION AND FUTURE WORK

This section deals with the potential impact of this thesis for the scientific community, pointing out possible applications and future developments of the proposed approach. The architecture presented in this thesis is, to our knowledge, the first attempt at creating a decentralized, multisensory representation of a robot and its nearby space by means of a distributed artificial skin and the interaction with the self and the surrounding environment. In our view, this method can be employed for life-long incremental learning in the robot, automatically incorporating robot’s new experiences or changes to its body or sensory apparatus. The robot can profit from this representation in that it provides a prediction of contacts with the skin prior to the actual contact.

Importantly, the architecture presented in this thesis is not attempting at modeling a particular brain network. Casting it into the vocabulary common in the neurosciences, one could say that the representation associated with every taxel that was learned in this work would correspond to a spatial receptive field of a neuron that is centered on that particular taxel (hence body-part centered coordinates). The RF has a spatial, modality-independent, nature, as we demonstrated by entering it and eliciting the “neural” response by motor/proprioceptive as well as visual targets. However, note that this “neuron” does not have a tactile RF – tactile sensations were used in the learning/adaptation of this RF only. Nonetheless, it would be easy to extend our representation by constructing a bimodal visuo-tactile or, more precisely, tactile-spatial neuron whose activation would be the sum of the “spatial” and tactile inputs. The reference frame transformations are in our case mediated by the kinematic model of the robot and use the “root reference frame” of the iCub, located in its waist, as common ground connecting all kinematic and visual chains. This is unlikely to be the case in the brain; however, other common reference frames (e.g., eye-centered, Cohen and Andersen [10]) have been proposed to act in the posterior parietal cortex. In summary, the architecture presented is a first implementation that supports the relevant behaviors. However, since the scenarios as well as the sensory modalities available to the robot parallel the biological situation (at a certain abstraction level), it is open to be further grounded in putative brain mechanisms.

The “demonstrators” – avoidance and catching – are also only first steps in this direction. They are simply exploiting the Cartesian solver and controller to generate movements of a virtual point that is a result of voting of taxels activated by an oncoming object. Avoidance differs from catching in the direction of this movement vector only. This could be further differentiated and developed, leading to simple reflexive as well as complex whole-body avoidance mechanisms such as those reported in monkeys [33]; an implementation in the iCub relying on force/torque feedback has been presented in Shimizu et al. [81]. Finally, the catching is a simple mechanism that results in approaching of an oncoming object with the skin part that was most likely to be contacted by the object. This is very simple and clearly very different from reaching – another key component of peripersonal space representations (especially in the peripersonal space interpretations as *space within reach*).

Future work can proceed along several directions. First, the architecture can be refined and better grounded in concrete mechanisms that are assumed to operate in primate brains, giving rise to first complete, physically embodied instantiations of the mechanisms. This would provide an invaluable tool to test the theories and crucially advance the computational modeling efforts. Second, the full kinematic model of the robot that was taken for granted in the current approach could be dropped and the learning problem expanded to full complexity dealing with the emergence of spatial representations from motor, proprioceptive, tactile and visual inputs. Third, the architecture proposed is prone to impact on practical applications. Whole-body tactile sensing together with a virtual margin of safety around the robot's body dramatically increases the robot's own safety as well as safety as humans that share the environment with the robot. The proposed architecture will have to be tested in such setups and possibly enhanced also by force/torque sensing that is already available on the robot to guarantee robustness in all situations. Finally, with the advent of robotic skin technologies (see Dahiya and Valle [15] for a review), frameworks similar to the one proposed can find applications in diverse robotic platforms and are by no means restricted to the iCub humanoid robot.

Part V

APPENDIX

A

THE KINEMATIC PROBLEM AND THE DENAVIT–HARTENBERG CONVENTION

The Denavit–Hartenberg (DH) convention has been introduced by Jacques Denavit and Richard S. Hartenberg in 1955 [19]. It has been since considered the prevailing notation to generically express a kinematic model of a robot.

The following sections will detail the kinematic problem as well as the DH convention, with an explicit reference to the robotic platform used in this thesis, best modeled by a set of independent serial kinematic chains composed by revolute joints (i.e. a set of joints whose single degree of freedom is a rotation along one axis).

A.1 DIRECT AND INVERSE KINEMATICS OF A SERIAL ROBOTIC ARM

Kinematics pertains to the motion of bodies in a robotic plant without dealing with their dynamical component, i.e. the forces and the torques that cause the motion. It is the most foundational aspect of the robotics field, and for this reason a number of different conventions has been developed in order to solve kinematics problems.

In the following, a brief contextualization of the problem of the direct and inverse kinematics of a serial robot arm composed by revolute joints only (i.e. the one of interest for this thesis) will be provided.

A.1.1 KINEMATIC MODEL OF A ROBOT

The kinematic model of a robot composed by n –joints is the analytical description of the relationships between:

- the joint configuration vector $\mathbf{q} \in \Re^n$

- the *pose* $\mathbf{x} \in \Re^m$ of a specific component of the robot structure. We are typically referring to the *end-effector* of the robot.

Usually, and particularly in the case of a serial manipulator, the end-effector is placed at the very end of the kinematic chain, whereas its *base* is fixed w.r.t. the world reference frame. The end-effector *pose* is usually defined by a set of $m = 6$ parameters that translate into an homogeneous roto-translation matrix T_n w.r.t. the world FoR¹:

$$T_n = \begin{bmatrix} \dots & & p_n^x \\ & R_n & p_n^y \\ & & \dots & p_n^z \\ 0 & 0 & 0 & 1 \end{bmatrix}, \quad (15)$$

where R_n is the rotation matrix that describes the orientation of the end-effector, and p_n^x , p_n^y and p_n^z are the three components of its position about the x , y , and z axis respectively.

DIRECT KINEMATIC PROBLEM The direct kinematic problem (also referred to as *forward kinematics*) deals with the identification of the pose of the end-effector given a specific joint configuration $\hat{\mathbf{q}}$. Mathematically, it reduces to finding the *direct kinematic mapping* $\Lambda(\hat{\mathbf{q}})$:

$$\mathbf{x} = \Lambda(\hat{\mathbf{q}}) \quad (16)$$

Λ can be computed by either a geometric (i.e. by manually inspecting the kinematic chain in order to explicitly find the relations between every link and its subsequent) or a systematic approach (namely, by assigning frames attached to the robot joints and using homogeneous transformation matrices). The DH notation is one of the systematic methodologies that have been devised in order to solve this problem. It will be detailed in [Section A.2](#).

INVERSE KINEMATIC PROBLEM The *inverse kinematics* is the inverse problem w.r.t. what detailed in the previous paragraph,

¹ It is worth noting that, in general, this approach holds for any reference frame considered. In this appendix, we will always implicitly refer to the absolute (or world) frame of reference. For this reason, any vector will be referred to the world FoR, if not explicitly indicated.

that is finding the set of joint angles suitable for the robot to fulfill a desired end-effector pose. It is typically a nonlinear problem, with no guarantee of either the existence or the uniqueness of the final solution (it is dependent on the redundancy of the robot w.r.t. the assigned kinematic task).

Two types of approaches are commonly used in this case as well: (i) an analytical method, namely an algebraic approach that leads to the formulation of a – solvable – set of polynomial equations; (ii) or a numerical, iterative technique, that uses the (analytical) *Jacobian matrix* $\mathbf{J}(\mathbf{q})$ of the direct kinematic map:

$$\mathbf{J}(\mathbf{q}) = \frac{\delta \Lambda(\mathbf{q})}{\delta \mathbf{q}} \quad (17)$$

This last method is generally slower and computationally expensive, but is needed especially in the case of redundant manipulators or configurations close to singularities. In this thesis, we used such an approach in order to implement the inverse kinematics solver needed for the solution of the double touch task (cf. [Section 5.4.2](#)).

A.1.2 KINEMATICS OF A SERIAL ROBOTIC ARM

A serial robotic arm is modeled by an open kinematic chain. In the general case useful for the pursuit of the goals of this thesis, we will further assume the following: (i) the end-effector space has $m = 6$ DoF, i.e. $\mathbf{x} \in \Re^6$; (ii) the chain under evaluation is redundant, and it is thus composed by n joints such that $n > m$.

In order to compute the kinematic model of the arm under consideration, the following rules apply:

- Every joint of the robot is equipped with a frame of reference that characterize its configuration;
- A set of homogeneous transform matrices are used in order to describe the relation between each joint and its subsequent;
- The pose of each joint w.r.t. the base reference frame is defined by the composition of the aforementioned matrices from the base up to the joint under consideration;

The DH notation deals with specifying a convention in order to set these rules systematically. In the following section, an analysis of this technique will be provided.

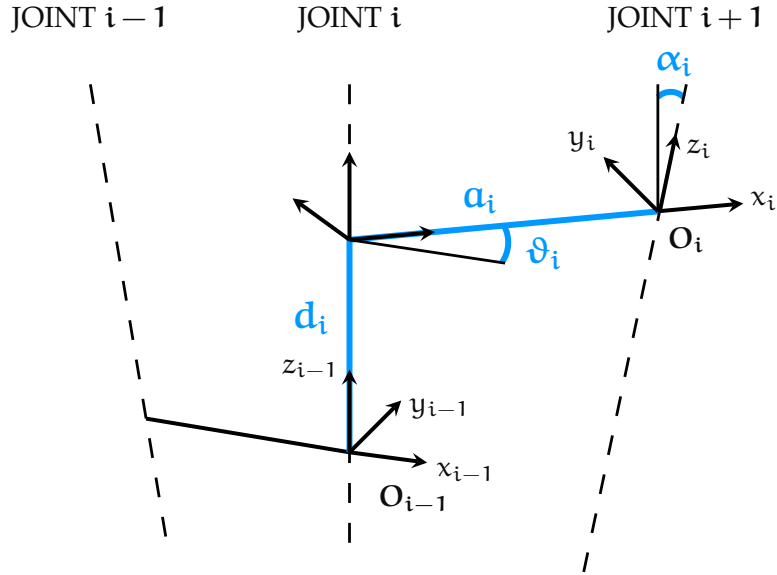


Figure 33: Denavit-Hartenberg convention for a generic link l_i . The homogeneous rototranslation matrix between the two frames of reference O_{i-1} and O_i is defined by a set of four parameters $\Phi_i = \{a_i, d_i, \alpha_i, \vartheta_i\}$.

A.2 THE DENAVIT-HARTENBERG NOTATION

The Denavit-Hartenberg notation provides us with a set of rules in order to standardize the process of iteratively constructing a kinematic model of a robot manipulator. By referring to [Figure 33](#), it is defined by a set of rules:

- Each link is numbered from 0 to n , starting from the base and up to the end-effector. Accordingly, since each manipulator with $n + 1$ links is composed by n joints, they will be numbered from 1 to n . Hence, link l_i will connect joint j_i with j_{i+1} .
- For each link l_i , a reference frame O_i is attached to the correspondent joint j_{i+1} , i.e. the terminal joint belonging to the link. Its z -axis is set to be parallel to the joint axis. For a revolute joint, this means that the z -axis is parallel to the axis of rotation.

Given the joint axis J_i and J_{i+1} , the reference frames O_{i-1} and O_i can still be placed in an arbitrary way; we need 6 parameters in order to describe the rototranslation between them. Five of them are purely geometric measures, where the last one is the joint variable. For this reason, the Denavit-Hartenberg convention further provides a set of rules to accomplish this

task. It defines a set of 4 parameters suitable for both revolute and prismatic joints – a subset of the 6 needed to describe any possible homogeneous transformation between two reference frames. These parameters are usually referred to as $\Phi_i = \{a_i, d_i, \alpha_i, \vartheta_i\}$; three of them are still dependent from the geometry of the link, whereas the last one is still the joint variable. They are depicted in [Figure 33](#), and defined by the following rules:

- the unit vector z_i is placed along the axis of joint j_{i+1} ;
- the unit vector x_i is put along the common normal to joint i and $i + 1$ axes;
- a_i is defined as the distance between an intermediate reference frame \hat{O}_i and O_i ; it is constant, and usually referred to as the *length* of the link l_i ;
- d_i is the distance between O_{i-1} and \hat{O}_i . It is the joint variable for a prismatic joint;
- α_i is the (constant) *twist* angle between z_{i-1} and z_i around x_i .
- ϑ_i is the angle between x_{i-1} and x_i about z_{i-1} . It is the joint variable for a revolute joint.

This final set of rules univocally defines the rototranslation between every FoR in the chain. There still are some ambiguities, though:

- the origin and the x -axis of the first reference frame are arbitrary;
- the z axis z_n of the last reference frame is not specified;
- when z_{i-1} and z_i are parallel, there is no unique definition of the common normal between the two;
- when z_{i-1} and z_i are incident, the determination of x_i is discretionary.

Finally, the homogeneous transformation matrix between two successive DH frames O_{i-1} and O_i is thus defined by a rototranslation about and along axis z_{i-1} and a subsequent rototranslation about and along axis x_i . They are given by Equa-

tions 18 and 19 respectively (with the omission of the “*i*” subscript in the matrix):

$${}^{i-1}DH^{\hat{i}}(q_i) = \begin{bmatrix} c_{\vartheta} & -s_{\vartheta} & 0 & 0 \\ s_{\vartheta} & c_{\vartheta} & 0 & 0 \\ 0 & 0 & 1 & d \\ 0 & 0 & 0 & 1 \end{bmatrix} \quad (18)$$

$$\hat{i}DH^i = \begin{bmatrix} 1 & 0 & 0 & a \\ 0 & c_{\alpha} & -s_{\alpha} & 0 \\ 0 & s_{\alpha} & c_{\alpha} & 0 \\ 0 & 0 & 0 & 1 \end{bmatrix} \quad (19)$$

Please note that the first transformation is dependent from the joint variable, whereas the second one is always a constant matrix. The composition of these two matrices lead to the standard *Denavit-Hartenberg matrix*:

$${}^{i-1}DH^i(q_i) = {}^{i-1}DH^{\hat{i}}(q_i) * {}^{\hat{i}}DH^i = \begin{bmatrix} c_{\vartheta} & -s_{\vartheta}c_{\alpha} & s_{\vartheta}s_{\alpha} & ac_{\vartheta} \\ s_{\vartheta} & c_{\vartheta}c_{\alpha} & -c_{\vartheta}s_{\alpha} & as_{\vartheta} \\ 0 & s_{\alpha} & c_{\alpha} & d \\ 0 & 0 & 0 & 1 \end{bmatrix} \quad (20)$$

By applying this technique to extract the full set of transform matrices for each of the *n* links of the chain, it is then possible to compute the pose of the end-effector as a sequence of rototranslations from the base to the terminal element of the chain.

BIBLIOGRAPHY

- [1] A. Albu-Schaffer, O. Eiberger, M. Grebenstein, S. Hadadin, C. Ott, T. Wimbock, S. Wolf, and G. Hirzinger. Soft robotics. *Robotics Automation Magazine, IEEE*, 15(3):20–30, september 2008. ISSN 1070-9932. doi: 10.1109/MRA.2008.927979.
- [2] Marco Antonelli, Beata J. Grzyb, Vicente Castelló, and Angel P. Del Pobil. Plastic representation of the reachable space for a humanoid robot. In *From Animals to Animats 12*, pages 167–176. Springer, 2012.
- [3] Marie Avillac, Sophie Deneve, Etienne Olivier, Alexandre Pouget, and Jean-René Duhamel. Reference frames for representing visual and tactile locations in parietal cortex. *Nature neuroscience*, 8(7):941–949, 2005.
- [4] Michela Bassolino, Andrea Serino, S. Ubaldi, and Elisabetta Ládavas. Everyday use of the computer mouse extends peripersonal space representation. *Neuropsychologia*, 48(3):803–811, 2010.
- [5] Nadja Berberovic and Jason B. Mattingley. Effects of prismatic adaptation on judgements of spatial extent in peripersonal and extrapersonal space. *Neuropsychologia*, 41(4):493–503, 2003.
- [6] M. B. Berkinblit, A. G. Feldman, and O. I. Fukson. Adaptability of innate motor patterns and motor control mechanisms. *Behavioral and Brain Sciences*, 9:585–599, 1986.
- [7] Frank Bremmer, Anja Schlack, N. Jon Shah, Oliver Zafiris, Michael Kubischik, Klaus-Peter Hoffmann, Karl Zilles, and Gereon R. Fink. Polymodal motion processing in posterior parietal and premotor cortex: a human fmri study strongly implies equivalencies between humans and monkeys. *Neuron*, 29(1):287–296, 2001.
- [8] Lewis Carroll. *Alice's Adventures in Wonderland*. Macmillan, November 1865.
- [9] Carlo Ciliberto, Ugo Pattacini, Lorenzo Natale, Francesco Nori, and Giorgio Metta. Reexamining Lucas-Kanade

- method for real-time independent motion detection: Application to the iCub humanoid robot. In *Intelligent Robots and Systems (IROS), 2011 IEEE/RSJ International Conference on*, pages 4154–4160. IEEE, 2011.
- [10] Y.E. Cohen and R.A. Andersen. A common reference frame for movement plans in the posterior parietal cortex. *Nature Reviews Neuroscience*, 3(7):553–562, 2002.
 - [11] C. L. Colby, J. R. Duhamel, and M. E. Goldberg. Ventral intraparietal area of the macaque: Anatomic location and visual response properties. *Journal of Neurophysiology*, 69: 902–914, 1993.
 - [12] Dylan F. Cooke, Charlotte S. R. Taylor, Tirin Moore, and Michael S. A. Graziano. Complex movements evoked by microstimulation of the ventral intraparietal area. *Proceedings of the National Academy of Sciences of the United States of America*, 100(10):6163–6168, May 2003.
 - [13] H. B. Coslett and E. Lie. Bare hands and attention: Evidence for a tactile representation of the human body. *Neuropsychologia*, 42:1865–1876, 2004.
 - [14] Marcello Costantini and Patrick Haggard. The rubber hand illusion: Sensitivity and reference frame for body ownership. *Consciousness and Cognition*, 16(2):229 – 240, 2007. ISSN 1053-8100. doi: <http://dx.doi.org/10.1016/j.concog.2007.01.001>.
 - [15] Ravinder S. Dahiya and Maurizio Valle. *Robotic Tactile Sensing*. Springer, 2013.
 - [16] Ravinder S. Dahiya, Giorgio Metta, Maurizio Valle, and Giulio Sandini. Tactile sensing - from humans to humanoids. *Robotics, IEEE Transactions on*, 26(1):1–20, 2010.
 - [17] Alessandro De Luca, Alin Albu-Schaffer, Sami Haddadin, and Gerd Hirzinger. Collision detection and safe reaction with the DLR-III lightweight manipulator arm. In *Intelligent Robots and Systems (IROS), 2006 IEEE/RSJ International Conference on*, pages 1623–1630. IEEE, 2006.
 - [18] A. Del Prete, S. Denei, Lorenzo Natale, Fulvio M., F. Nori, G. Cannata, and Giorgio Metta. Skin spatial calibration using force/torque measurements. In *Intelligent Robots and Systems (IROS), 2011 IEEE/RSJ International Conference on*, pages 3694 –3700, 2011.

- [19] Jacques Denavit. A kinematic notation for lower-pair mechanisms based on matrices. *Trans. of the ASME. Journal of Applied Mechanics*, 22:215–221, 1955.
- [20] Giuseppe di Pellegrino and Elisabetta Ládavas. Peripersonal space in the brain. *Neuropsychologia*, 66(0):126 – 133, 2015. ISSN 0028-3932.
- [21] Giuseppe di Pellegrino, Elisabetta Ládavas, and Alessandro Farné. Seeing where your hands are. *Nature*, 388:730, 1997.
- [22] J. R. Duhamel, C. L. Colby, and M. E. Goldberg. Ventral intraparietal area of the macaque: Congruent visual and somatic response properties. *Journal of Neurophysiology*, 79: 126–136, 1998.
- [23] Sean Ryan Fanello, Ugo Pattacini, Ilaria Gori, Vadim Tikhanoff, Marco Randazzo, Alessandro Roncone, Francesca Odone, and Giorgio Metta. 3D stereo estimation and fully automated learning of eye-hand coordination in humanoid robots. In *2014 IEEE-RAS Int. Conf. on Humanoid Robots - HUMANOIDS '14*, 2014.
- [24] Paul Fitzpatrick, Giorgio Metta, and Lorenzo Natale. Towards long-lived robot genes. *Robot. Auton. Syst.*, 56(1): 29–45, January 2008. ISSN 0921-8890. doi: 10.1016/j.robot.2007.09.014. URL <http://dx.doi.org/10.1016/j.robot.2007.09.014>.
- [25] L. Fogassi, V. Gallese, L. Fadiga, G. Luppino, M. Matelli, and G. Rizzolatti. Coding of peripersonal space in inferior premotor cortex (area F4). *Journal of Neurophysiology*, 76(1): 141–157, 1996. URL <http://jn.physiology.org/content/76/1/141>.
- [26] S. Fuke, M. Ogino, and M. Asada. Acquisition of the head-centered peri-personal spatial representation found in VIP neuron. *IEEE Trans. Autonomous Mental Development*, 1(2): 131–140, 2009.
- [27] O. I. Fukson, M. B. Berkinblit, and A. G. Feldman. The spinal frog takes into account the scheme of its body during the wiping reflex. *Science*, 209:1261–1263, 1980.
- [28] C. Gatla, R. Lumia, J. Wood, and G. Starr. An automated method to calibrate industrial robots using a virtual closed kinematic chain. *IEEE Transactions on Robotics*, 23 (6):1105–1116, 2007.

- [29] Maurizio Gentilucci, Leonardo Fogassi, Giuseppe Lupino, Massimo Matelli, Rosolino Camarda, and Giacomo Rizzolatti. Functional organization of inferior area 6 in the macaque monkey. *Experimental brain research*, 71(3):475–490, 1988.
- [30] M. S. A. Graziano, G. S. Yap, and C. G. Gross. Coding of visual space by premotor neurons. *Science*, 266:1054–1057, 1994.
- [31] M. S. A. Graziano, X. T. Hu, and C. G. Gross. Visuospatial properties of ventral premotor cortex. *Journal of Neurophysiology*, 77:2268–2292, 1997.
- [32] Michael S. A. Graziano and M. M. Botvinick. How the brain represents the body: insights from neurophysiology and psychology. *Common Mechanisms in Perception and Action: Attention and Performance*, 19:136–157, 2002.
- [33] Michael S. A. Graziano and Dylan F. Cooke. Parieto-frontal interactions, personal space and defensive behavior. *Neuropsychologia*, 44:845–859, 2006.
- [34] Michael S. A. Graziano and S. Gandhi. Location of the polysensory zone in the precentral gyrus of anesthetized monkeys. *Experimental Brain Research*, 135(2):259–266, 2000. ISSN 0014-4819. doi: 10.1007/s002210000518. URL <http://dx.doi.org/10.1007/s002210000518>.
- [35] Michael S. A. Graziano and Charles G. Gross. A bimodal map of space: somatosensory receptive fields in the macaque putamen with corresponding visual receptive fields. *Experimental Brain Research*, 97(1):96–109, 1993.
- [36] Edward T. Hall. *The Hidden Dimension*. Anchor, October 1966.
- [37] M. Hersch, E. Sauser, and A. Billard. Online learning of the body schema. *International Journal of Humanoid Robotics*, 5: 161–181, 2008.
- [38] M. Hikita, S. Fuke, M. Ogino, T. Minato, and M. Asada. Visual attention by saliency leads cross-modal body representation. In *7th Int. Conf. Develop. Learn. (ICDL)*, 2009.
- [39] Heiko Hirschmüller. Accurate and efficient stereo processing by semi-global matching and mutual information. In *In Proc. CVRP*, pages 807–814. IEEE Computer Society, 2005.

- [40] Matej Hoffmann, H. Marques, A. Hernandez Arieta, H. Sumioka, M. Lungarella, and R. Pfeifer. Body schema in robotics: a review. *IEEE Trans. Auton. Mental Develop.*, 2(4):304–324, 2010.
- [41] Matej Hoffmann, Alessandro Roncone, and Giorgio Metta. Modeling the development of human body representations. Submitted to the SMLC ’13 Workshop on Synthetic Modeling of Life and Cognition: Open questions, 2013.
- [42] J. Hollerbach, W. Khalil, and M. Gautier. Model identification. In B. Siciliano and O. Khatib, editors, *Handbook of robotics*, pages 321–343. Springer, 2008.
- [43] J. M. Hollerbach and C. W. Wampler. The calibration index and taxonomy for robotic kinematic calibration methods. *International Journal of Robotics Research*, 15(6):573–591, 1996.
- [44] N. P. Holmes and C. Spence. The body schema and the multisensory representation(s) of peripersonal space. *Cogn Process*, 5(2):94–105, Jun 2004.
- [45] Jwu-Sheng Hu, Jyun-Ji Wang, and Yung-Jung Chang. Kinematic calibration of manipulator using single laser pointer. In *Intelligent Robots and Systems (IROS), 2012 IEEE/RSJ International Conference on*, pages 426–430. IEEE, 2012.
- [46] Atsushi Iriki, M. Tanaka, and Y. Iwamura. Coding of modified body schema during tool use by macaque postcentral neurons. *Neuroreport*, 7(14):2325–30, 1996.
- [47] Advait Jain, Marc Daniel Killpack, Aaron Edsinger, and Charles C Kemp. Reaching in clutter with whole-arm tactile sensing. *The International Journal of Robotics Research*, page 0278364912471865, 2013.
- [48] Elisabetta Ládavas and Andrea Serino. Action-dependent plasticity in peripersonal space representations. *Cogn. Neuropsychology*, 25:1099–1113, 2008.
- [49] Bruce D. Lucas and Takeo Kanade. An iterative image registration technique with an application to stereo vision. In *Proceedings of the 7th International Joint Conference on Artificial Intelligence - Volume 2*, IJCAI’81, pages 674–679, San Francisco, CA, USA, 1981. Morgan Kaufmann Publishers Inc.

- [50] M. MacKay-Lyons. Central pattern generation of locomotion: a review of the evidence. *Physical Therapy*, 82:69–83, 2002.
- [51] Elisa Magosso, Melissa Zavaglia, Andrea Serino, Giuseppe Di Pellegrino, and Mauro Ursino. Visuotactile representation of peripersonal space: a neural network study. *Neural computation*, 22(1):190–243, 2010.
- [52] Perla Maiolino, Marco Maggiali, Giorgio Cannata, Giorgio Metta, and Lorenzo Natale. A flexible and robust large scale capacitive tactile system for robots. *Sensors Journal, IEEE*, 13(10):3910–3917, 2013.
- [53] T. R. Makin, N. P. Holmes, and E. Zohary. Is That Near My Hand? Multisensory Representation of Peripersonal Space in Human Intraparietal Sulcus. *Journal of Neuroscience*, 27:731–740, 2007.
- [54] R. Martinez-Cantin, M. Lopes, and L. Montesano. Body schema acquisition through active learning. In *Proc. Int. Conf. on Robotics and Automation (ICRA)*, 2010.
- [55] Giorgio Metta, Lorenzo Natale, F. Nori, G. Sandini, D. Vernon, Luciano Fadiga, C. von Hofsten, K. Rosander, M. Lopes, José Santos-Victor, A. Bernardino, and L. Montesano. The iCub humanoid robot: An open-systems platform for research in cognitive development. *Neural Networks*, 23(8-9):1125–1134, 2010. ISSN 0893-6080.
- [56] Philipp Mittendorfer and Gordon Cheng. Humanoid multimodal tactile-sensing modules. *Robotics, IEEE Transactions on*, 27(3):401–410, 2011.
- [57] Philipp Mittendorfer and Gordon Cheng. Self-organizing sensory-motor map for low-level touch reactions. In *Humanoid Robots (Humanoids), 2011 11th IEEE-RAS International Conference on*, pages 59–66. IEEE, 2011.
- [58] Philipp Mittendorfer and Gordon Cheng. Open-loop self-calibration of articulated robots with artificial skins. In *Robotics and Automation (ICRA), 2012 IEEE International Conference on*, pages 4539–4545. IEEE, 2012.
- [59] Alberto Parmiggiani, Marco Randazzo, Lorenzo Natale, Giorgio Metta, and Giulio Sandini. Joint torque sensing for the upper-body of the iCub humanoid robot. In *Humanoid Robots, 2009. Humanoids 2009. 9th IEEE-RAS International Conference on*, pages 15–20. IEEE, 2009.

- [60] Alberto Parmiggiani, Marco Maggiali, Lorenzo Natale, Francesco Nori, Alexander Schmitz, Nikos Tsagarakis, José Santos-Victor, Francesco Becchi, Giulio Sandini, and Giorgio Metta. The design of the iCub humanoid robot. *International Journal of Humanoid Robotics*, 9(04), 2012.
- [61] Emanuel Parzen. On Estimation of a Probability Density Function and Mode. *The Annals of Mathematical Statistics*, 33(3):1065–1076, 1962.
- [62] U. Pattacini, F. Nori, L. Natale, G. Metta, and G. Sandini. An experimental evaluation of a novel minimum-jerk cartesian controller for humanoid robots. In *Intelligent Robots and Systems (IROS), 2010 IEEE/RSJ International Conference on*, 2010.
- [63] Ugo Pattacini. *Modular cartesian controllers for humanoid robots: Design and implementation on the iCub*. PhD thesis, RBCS, Italian Institute of Technology, Genova, 2011.
- [64] Steven Pinker. *The Language Instinct*. Harper Perennial Modern Classics, New York, 1994. This is the complete quote of what I put in the introduction: “*The main lesson of thirty-five years of AI research is that the hard problems are easy and the easy problems are hard. The mental abilities of a four-year-old that we take for granted – recognizing a face, lifting a pencil, walking across a room, answering a question – in fact solve some of the hardest engineering problems ever conceived. [...] As the new generation of intelligent devices appears, it will be the stock analysts and petrochemical engineers and parole board members who are in danger of being replaced by machines. The gardeners, receptionists, and cooks are secure in their jobs for decades to come.*”.
- [65] Alexandre Pouget and Terrence Sejnowski. Spatial transformations in the parietal cortex using basis functions. *Cognitive Neuroscience, Journal of*, 9(2):222–237, 1997.
- [66] Giacomo Rizzolatti, C. Scandolara, M. Matelli, and M. Gentilucci. Afferent properties of periarcuate neurons in macaque monkeys. II Visual responses. *Behavioral Brain Research*, 2:147–163, 1981.
- [67] Giacomo Rizzolatti, Luciano Fadiga, Leonardo Fogassi, and Vittorio Gallese. The space around us. *Science*, 277 (5323):190–191, 1997. doi: 10.1126/science.277.5323.190.
- [68] Giacomo Rizzolatti, G. Luppino, and M. Matelli. The organization of the cortical motor system: new concepts. *Elec-*

- troencephalography and Clinical Neurophysiology*, 106(4):283–296, 1998.
- [69] P. Rochat. Self-perception and action in infancy. *Exp Brain Res*, 123:102–109, 1998.
 - [70] Richard Rodgers and Oscar Hammerstein, 1945. Show tune introduced in the 1945 musical *Carousel*.
 - [71] Daniel Roetenberg, Henk Luinge, and Per Slycke. Xsens mvn: full 6DOF human motion tracking using miniature inertial sensors. *Xsens Motion Technologies BV, Tech. Rep*, 2009.
 - [72] Alessandro Roncone, Matej Hoffmann, Ugo Pattacini, and Giorgio Metta. Automatic kinematic chain calibration using artificial skin: self-touch in the iCub humanoid robot. In *Proc. IEEE Int. Conf. Robotics and Automation (ICRA)*, pages 2305–2312, 2014.
 - [73] Alessandro Roncone, Ugo Pattacini, Giorgio Metta, and Lorenzo Natale. Gaze stabilization for humanoid robots: a comprehensive framework. In *2014 IEEE-RAS Int. Conf. on Humanoid Robots - HUMANOIDS '14*, 2014.
 - [74] Alessandro Roncone, Matej Hoffmann, Ugo Pattacini, Luciano Fadiga, and Giorgio Metta. Peripersonal space and margin of safety around the body: learning tactile-visual associations in a humanoid robot with artificial skin. Manuscript, 2015.
 - [75] Alessandro Roncone, Matej Hoffmann, Ugo Pattacini, and Giorgio Metta. Learning peripersonal space representation through artificial skin for avoidance and reaching with whole body surface. Submitted to the 2015 IEEE/RSJ International Conference on Intelligent Robots and Systems (IROS), 2015.
 - [76] C. F. Sambo and B. Forster. An ERP investigation on visuo-tactile interactions in peripersonal and extrapersonal space: Evidence for the spatial rule. *Journal of Cognitive Neuroscience*, 21:1550–1559, 2009.
 - [77] R. A. Schmidt and T. D. Lee. *Motor control and learning : a behavioral emphasis*. Human Kinetics, 2005.
 - [78] S. Schutz-Bosbach, J. J. Musil, and P. Haggard. Touchant-touché: The role of self-touch in the representation of body structure. *Consciousness and Cognition*, 18(1):2–11, 2009. ISSN 1053-8100. doi: 10.1016/j.concog.2008.08.003.

- [79] Valentina Sclafani, Elizabeth A. Simpson, Stephen J. Suomi, and Pier Francesco Ferrari. Development of space perception in relation to the maturation of the motor system in infant rhesus macaques (*macaca mulatta*). *Neuropsychologia*, 2014. ISSN 0028-3932. doi: <http://dx.doi.org/10.1016/j.neuropsychologia.2014.12.002>.
- [80] Andrea Serino, Michela Bassolino, A. Farnè, and Elisabetta Ládavas. Extended multisensory space in blind cane users. *Psychological Science*, 18:642–648, 2007.
- [81] Toshihiko Shimizu, Ryo Saegusa, Shuhei Ikemoto, Hiroshi Ishiguro, and Giorgio Metta. Self-protective whole body motion for humanoid robots based on synergy of global reaction and local reflex. *Neural Networks*, 32:109–118, 2012.
- [82] C. Spence, F. Pavani, A. Maravita, and N. P. Holmes. Multisensory interactions. In M. C. Lin and M. A. Otaduy, editors, *Haptic rendering: Foundations, algorithms, and applications*, pages 21–52. Wellesley: AK Peters LTD, 2008.
- [83] Vadim Tikhanoff, Ugo Pattacini, Lorenzo Natale, and Giorgio Metta. Exploring affordances and tool use on the iCub. In *Humanoid Robots, 2013. Humanoids 2009. 13th IEEE-RAS International Conference on*. IEEE, 2013.
- [84] M. Valentini, U. Kischka, and P. W. Halligan. Residual haptic sensation following stroke using ipsilateral stimulation. *Journal of Neurology, Neurosurgery & Psychiatry*, 79:266–270, 2008.
- [85] Andreas Wächter and Lorenz T. Biegler. On the implementation of an interior-point filter line-search algorithm for large-scale nonlinear programming. *Mathematical programming*, 106(1):25–57, 2006.
- [86] L. Weiskrantz and D. Zhang. Residual tactile sensitivity with self-directed stimulation in hemianaesthesia. *Journal of Neurology, Neurosurgery & Psychiatry*, 50:632–634, 1987.
- [87] Jing Xing and R. Andersen. Models of the posterior parietal cortex which perform multimodal integration and represent space in several coordinate frames. *Cognitive Neuroscience, Journal of*, 12(4):601–614, 2000.